Quantitative Wear Particle Analysis for Osteoarthritis Assessment

By

Meizhai Guo

A thesis fulfilment of the requirements for the degree of

Master by Research

School of Mechanical and Manufacturing Engineering

Faculty of Engineering

The University of New South Wales, Sydney, Australia

March 2016

Thesis/Dissertation Sheet

Surname/Family Name	**:GUO**
Given Name/s	**:Meizhai**
Abbreviation for degree as give in the University calendar	**:PG**
Faculty	**:Engineering**
School	**:Mechanical and Manufacturing Eng**
Thesis Title	**:Quantiative wear particle analysis for osteoarthritis assessment**

Abstract 350 words maximum: (PLEASE TYPE)

Osteoarthritis is a degenerative joint disease that affects millions of people worldwide. The aims of this study were (1) to quantitatively characterise the boundary and surface features of wear particles present in the synovial fluid of patients, (2) to select key numerical parameters that describe distinctive particle features and enable osteoarthritis assessment and (3) to develop a model to assess osteoarthritis conditions using comprehensive wear debris information. Discriminant analysis was used to statistically group particles based on differences in their numerical parameters. The analysis methods agreed with the clinical osteoarthritis grades in 63%, 50% and 61% of particles for no osteoarthritis, mild osteoarthritis and severe osteoarthritis, respectively. This study has revealed particle features specific to different osteoarthritis grades and provided further understanding of the cartilage degradation process through wear particle analysis – the technique that has the potential to be developed as an objective and minimally invasive method for osteoarthritis diagnosis.

ORIGINALITY STATEMENT

'I hereby declare that this submission is my own work and to the best of my knowledge it contains no materials previously published or written by another person, or substantial proportions of material which have been accepted for the award of any other degree or diploma at UNSW or any other educational institution, except where due acknowledgement is made in the thesis. Any contribution made to the research by others, with whom I have worked at UNSW or elsewhere, is explicitly acknowledged in the thesis. I also declare that the intellectual content of this thesis is the product of my own work, except to the extent that assistance from others in the project's design and conception or in style, presentation and linguistic expression is acknowledged.'

Signed ……..

Date ……..

COPYRIGHT STATEMENT

Signed …….....

Date …….....

AUTHENTICITY STATEMENT

‘I certify that the Library deposit digital copy is a direct equivalent of the final officially approved version of my thesis.’

Signed …….....

Date …….....

INCLUSION OF PUBLICATIONS STATEMENT

UNSW is supportive of candidates publishing their research results during their candidature as detailed in the UNSW Thesis Examination Procedure.

Publications can be used in their thesis in lieu of a Chapter if:

- The candidate contributed greater than 50% of the content in the publication and is the "primary author", ie. the candidate was responsible primarily for the planning, execution and preparation of the work for publication
- The candidate has approval to include the publication in their thesis in lieu of a Chapter from their supervisor and Postgraduate Coordinator.
- The publication is not subject to any obligations or contractual agreements with a third party that would constrain its inclusion in the thesis

Please indicate whether this thesis contains published material or not:

☒ This thesis contains no publications, either published or submitted for publication
(if this box is checked, you may delete all the material on page 2)

☒ Some of the work described in this thesis has been published and it has been documented in the relevant Chapters with acknowledgement
(if this box is checked, you may delete all the material on page 2)

☐ This thesis has publications (either published or submitted for publication) incorporated into it in lieu of a chapter and the details are presented below

CANDIDATE'S DECLARATION

I declare that:

- I have complied with the UNSW Thesis Examination Procedure
- where I have used a publication in lieu of a Chapter, the listed publication(s) below meet(s) the requirements to be included in the thesis.

Candidate's Name	Signature	Date (dd/mm/yy)

Acknowledgements

Although the realization of this thesis tested my dedication, knowledge and creativity, this project lied in a stable base created by people and institutions who directly or indirectly, allowed me to successfully materialize it.

I sincerely thank A/Prof Zhongxiao Peng of the School of Mechanical and Manufacturing Engineering at the University of New South Wales, Australia, and Dr Megan Lord of the Graduate School of Biomedical Engineering at the University of New South Wales, Australia. Their guidance, advice and support through the whole project were essentials for its satisfactory completion.

Dr Ross Odell, Lecturer of Engineering Statistics and Experiment Design, Graduate School of Biomedical Engineering, UNSW, Australia, for his assistance with the statistical analysis

The author thanks Dr Meiling Wang for her help in collecting wear particles. The author would also like to acknowledge the Australian Research Council to provide research funds (DP1093975) to this project.

Abstract

Osteoarthritis (OA) is one of the most common joint diseases that can cause pain, swelling, stiffness, joint deformities, and can be extremely debilitating. The burden of OA is expected to increase exponentially in coming decades due to an aging and increasingly obese population, with prevalence expected to reach three million Australians by 2032. During the progression of OA, the cartilage experiences a continuous degradation and releases wear particles into the surrounding synovial fluid. The aims of the study were to: (i) quantitatively characterise the boundary and surface features of wear particles present in the synovial fluid of patients, to (ii) select key numerical parameters that describe distinctive particle features and enable OA assessment and to (iii) conduct correlation between particle and cartilage surface parameters and find the common features between them. The ultimate goal is to develop effective wear debris analysis techniques for OA diagnosis.

Laser scanning microscopy was used to capture 3-dimensional (3D) images of 263 human knee particles from 22 patients with clinically classified no OA, mild (grade 1-2) or severe (grade 3-4) OA. The 3D images were analysed using 29 numerical parameters including amplitude, spatial, functional, hybrid and shape descriptors. Correlation analyses were then carried out to identify correlated parameters that describe common trends during OA progress. After the correlation analysis, the uncorrelated parameters were further analysed using discriminant analysis to statistically group particles based on differences in their numerical parameters. The analysis methods agreed with the clinical OA grade in 63, 50 and 61% of particles for no OA, mild OA and severe OA, respectively. This study also has demonstrated that wear particle analysis has the

potential to be developed as an objective and minimally invasive method for OA diagnosis.

Table of Contents

List of Abbreviations

Abbreviations	Full name
OA	Osteoarthritis
LSM	Laser scanning microscope
AFM	Atomic force microscope
SEM	Scan electron microscope
PBS	Phosphate buffered saline
SD	Standard deviation
Sa	Roughness average
Sq	Root mean square
Ssk	Surface skewness
Sku	Surface kurtosis
S10z	Ten point height
Sp	Max peak height
Sv	Max valley depth
Ssc	Mean summit curvature
Sdr	Surface area ratio
Sbi	Surface bearing index
Svi	Valley fluid retention index
Spk	Reduced summit height
Sk	Core roughness depth
Svk	Reduced valley depth
Sds	Density of summits
Std	Texture direction

Stdi	Texture direction index
Scl20	Correlation length at 20%
Scl37	Correlation length at 37%
Str20	Texture aspect ratio at 20%
Str37	Texture aspect ratio at 20%
Smr1	Pear material ratio
Smr2	Valley material ratio
A	Area
L	Length
Mv	Material volume
Vv	Void volume
Nv	Net volume
R	Roundness
C	Convexity
FF	Form factor
E	Elongation
S	Solidity

List of Figures

List of Tables

Chapter 1 Introduction

1.1 Background

Osteoarthritis (OA) as the result of cartilage degradation causes pain and movement limitation and affected more than 8.4% of the Australians in 2013 [2]. More than 83% of males and 87% of females had radiological evidence of OA in the age range of 55–64. OA can develop at any age but tends to be more common in people aged over 40 years or those who have had joint injuries. The number of people suffering OA aged 40 years old or less has been increasing in recent years [3]. The progression of OA is not fully understood because different variables including mechanical behaviour, genetic propensity and ageing contribute to the wear process.

Due to the high social and economic impact of OA, understanding of the cartilage degradation process has become an important issue. Unfortunately, articular cartilage damage has been difficult to classify due to the lack of objective measurements. Different criteria have been used to evaluate OA severities. Two popularly used criteria to evaluate the OA grade are the International Cartilage Repair Society (ICRS) scale and Outer-bridge scaling system. The ICRS classification is based on the depth of the cartilage injury, and has four OA grades, being OA grades 1 and 2 for a partial cartilage loss, and grades 3 and 4 for nearly full or full-thickness defect. In comparison, the Outer-bridge classification [4], based on the size of the affected area, is used to describe the level of cartilage degradation in clinic.

The articular cartilage is composed of chondrocytes surrounded by an extracellular matrix rich in proteoglycans, collagen type II and hyaluronan [5]. OA is characterised by the loss of cartilage matrix due to its limited ability to repair [6]. In the clinic, the severity of OA is currently assessed by the observation of joint space narrowing and surface characteristics of the articular cartilage. The methods to detect OA include arthroscopic surgery, X-ray and magnetic resonance imaging which are not sensitive enough to detect early OA and they are rarely used to accurately predict the factors influencing the progression of cartilage degradation [7]. Therefore, new diagnostic and prognostic techniques are needed to be developed for objective and sensitive OA assessment.

Wear particles present in the synovial fluid as a result of cartilage degradation, are much easier to obtain than cartilage for clinical diagnosis. Furthermore, the wear particles carry valuable information. For example, the shape of wear particles has been reported to be related to different OA grades in human knee joints [8]. Leaf-like wear particles are commonly found in healthy knee joints while rod-shaped wear particles are most abundant in knee joints during early stages of OA [9]. Animal samples have been used for particle morphology [7] characterisation but very limited work has been conducted on human wear particles. Both shape and surface information of human wear particles need to be studied in order to advance wear particle analysis as an OA diagnostic tool [9].

To quantitatively characterise the wear particles found in human knee joints, laser scanning microscopy (LSM) [7] and atomic force microscopy (AFM) [9] have been used to capture 3D images of wear particles. Numerical parameters were then applied to

extract the shape and the surface information of particles from 3D images. Although AFM is able to capture 3D images of human wear particles in a nano-metre scale, it is limited by the working distance which is a major challenge to obtain the boundary information or the high peaks in the wear particles [9]. Also, it is very time-consuming to acquire particle images using AFM. By comparing the LSM with AFM for cartilage wear analysis [2], it was found that LSM is a more suitable technique to obtain surface features in 3D and a micro-scale for quantitative characterisation. Based on digital images, shape parameters in 2D, e.g. elongation and form factor, were used in a previous study [8]. Also, 3D shape parameters, e.g. material volume and void volume, were applied to describe the particle shapes (spherical, chunky and leaf-like particles). Recently, the surface parameters including amplitude, spatial, hybrid and functional parameters, were used to describe distinctive particle features [9].

Few studies have been conducted on human wear debris for OA assessment and the common features of the particles found in the same OA grade and distinct features between different OA grades have not been reported and need to be identified for OA diagnosis. In this study, a multi-parameter analysis, namely discriminant analysis, was used to identify the distinct parameters and classify the particles into different OA grades based on their surface and shape features.

1.2 Aims and objectives

The main purpose of this research project was to characterize the wear particles found in human knee joint with different OA grades. The wear particles were quantitatively characterised at a micro scale by using laser scanning microscopy (LSM) and numerical

parameters. To achieve the goal, four objectives of this project are specified below.

1. To acquire high resolution 3D images of wear particles present in OA synovial fluid.

2. To numerically analyse the 3D images of wear particles for wear characteristics.

3. To analyse correlations of particle results and cartilage analysis results.

4. To conduct a correlation study between the particle and cartilage surface parameters and identify their common features.

Chapter 2 Literature Review

This chapter presents the basic information related to the project. A better understanding of human knee structure can assist the understanding of load bearing during daily activity and the signs of osteoarthritis are also included. Articular cartilage is reviewed because the degree of cartilage degeneration can present different OA grade. However, it is much easier and less invasive to obtain synovial fluid samples from patient than cartilage samples. Wear debris analysis techniques, including particle separation, image acquisition and numerical characterisations have been reviewed.

2.1 The knee and osteoarthritis

2.1.1 Knee structure

The knee joint works like a hinge although in reality the motion at the knee joint is more complex than a simple hinge. In the case of the knee, the hinge connects the tibia to the femur. The normal range of motion of the knee is from full extension (straightening of the knee) at 0 degrees to about 130 degrees of flexion (bending of knee) [10]. The normal knee can bear vertical force of nearly 7 times' body weight, but it is vulnerable to horizontal force, especially lateral force to the extended knee [9, 11]. The top of the tibial surface is relatively flat and therefore is referred to as the tibial plateau (see Figure 2.1). The end of the femur is shaped like a 'W', with two rounded protrusions. The other bone that comprises the knee joint is the patella (also called knee cap). The patella sits in a groove on the front of the femur called trochlea. The trochlea guides the location of the patella through the full-range motion of the knee.

The contact areas of the tibia and femur that have relative motion against each other are all covered with articular cartilage [10]. There is an additional set of cartilages (see Figure 2.1) sited between the femur and the tibia called the meniscus (two of them). The meniscus shaped like a "C" act as a cradle to help create a better fit between the surfaces of the tibia and femur. The synovial membrane is around the margins of the articular surfaces and the superior and inferior outer layer of the meniscus. The synovial fluid, surrounded by the synovial membrane, lubricates the joint. The ligaments keep the knee joint together [10]. The knee joint is stabilized from lateral motion by the collateral ligaments. The cruciate ligaments are also important for stabilizing the knee in the front-to-back direction [9].

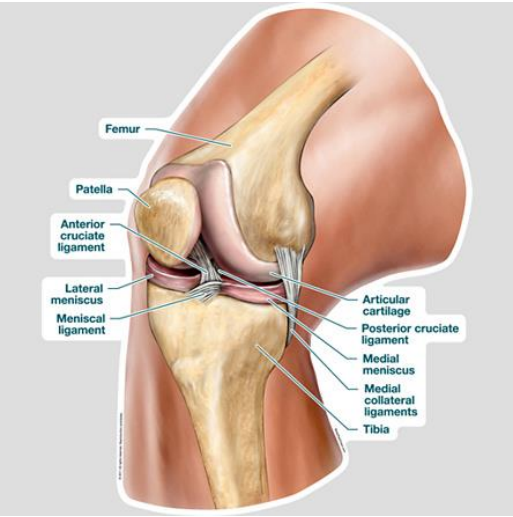

Figure 2.1 Anatomy of human knee [10].

2.1.2 Osteoarthritis (OA) and current diagnosis techniques

It has been reported that OA progression involves the entire joint [12]. OA involves biochemical, biomechanical, morphologic and molecular changes of matrix and cells which lead to a fibrillation, ulceration, softening, sclerosis of subchondral bone, subchondral cysts, osteophytes and loss of articular cartilage [12, 13] (see Figure 2.2).

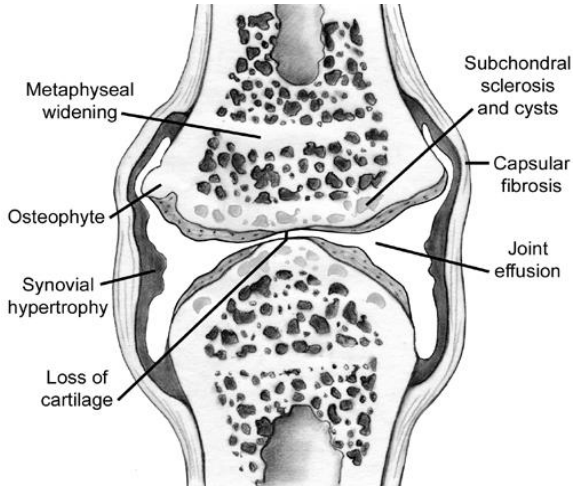

Figure 2.2 Gross pathologic changes observed in OA joints during years of degenerative change [12].

Normal adult articular cartilage is comprised of chondrocytes and extracellular matrix (proteoglycans, collagen and water) [14, 15].The collagen turnover rate is comparatively slow (over 100 years), whilst the turnover rate of proteoglycans is less slow; aggrecan, a major proteoglycan, its half-life is about 30 years. Due to the repair limitation of cartilage, the final pathway of the disease is the disruption of this homeostatic balance between the component synthesis and degradation [6]. This disruption in articular cartilage causes increased hydration and decreased proteoglycan and collagen content within the extracellular matrix and increased apoptosis of chondrocytes while interleukins promote the break-down of collagen [14, 15]. To some extent, OA is related to the degeneration and loss of some macromolecules due to risk factors at the molecular level. Table 2.1 shows the statistics about risk factors and their relation to OA.

The Outer-bridge classification [4] has been used to grade the severities of OA. Grade 0 represents healthy cartilage; cartilage with swelling and softening is classified as Grade

1; Grade 2 indicates that fissures have not extended to the subchondral bone with less than 1.5 cm of defect's diameter. Once the fissuring spreads to the level of the subchondral bone and the diameter is more than 1.5 cm, the cartilage is classified as Grade 3. Lastly, Grade 4 is classified as the articular cartilage which is injured resulting in the exposure of the subchondral born.

Table 2.1 Risk factors influencing OA

Risk factor	**Relation to OA**
Aging	Knee osteophyte development increased by 20% per 5-year age increase [12]
Gender	Women develop knee OA more frequently than men [12]
Occupational activity	Risk of later knee OA was highest in men whose jobs were classified as having at least medium physical demands [12]
No occupational physical activity	Athletics activities involving excessive activity acting on a vulnerable joint [12]
Bone mineral density (BMD)	Those without OA had 3% to 8% lower femoral neck BMD versus Those with knee OA [14]
Hormone status	Estrogen may have effects on bone and further influence OA development [14]
Injury	Injury increase OA risk [14]
Genetic factors	39% to 65% of the variance of hand and knee OA was attributed to genetic factors [14]
Obesity	Obesity antedates the progression and increases the risk of OA [9]
Muscle weakness	May increase the risk of OA progression [9]
Smoking	Smokers had a lower risk of knee OA than non-smokers [14]

The techniques that are used to diagnose knee OA include X-ray, magnetic resonance imaging (MRI) and arthroscopy [9]. X-ray is the most common imaging technique used

to diagnose OA and reveals anatomical changes including damage to bone in the form of subchondral sclerosis as well as damage to the cartilage indirectly through joint space narrowing. However, radiography findings are poorly correlated with severity of symptoms expressed by the subject due to the fact that the initiate changes of articular cartilage in early OA is in a nano-scale [16]. MRI can illustrate thickness changes in cartilage over time in healthy joints and joints with OA, but it is costly and rarely indicates in acute disease [17]. Arthroscopy can reach a greater portion of the synovium of the knee joint than that of traditional open synovectomy. However, the operation of arthroscopy could be technically difficult to perform and it is invasive [17]. A non-intrusive technique which is sensitive enough to detect early changes of the knee joints needs to be developed.

2.2 Articular cartilage and its properties

2.2.1 Composition and main structure of articular cartilage

Articular cartilage is avascular and is devoid of nerves [18]. Normal adult articular cartilage is comprised of chondrocytes and an extracellular matrix which consists primarily of collagen, hyaluronan and proteoglycans. The chondrocytes, making up around 10% of the wet weight of cartilage, are specialized metabolically active cells that contribute to the development of cartilage but exhibit a very limited repair capacity. The chondrocytes, even in the deepest layer of cartilage, are nourished by diffusion of synovial fluid [19]. Collagen makes up 10-30% of the wet weight of normal articular cartilage, while proteoglycans comprise only 3-10% [20]. The extracellular matrix contains additional, but quantitatively, minor glycoproteins and lipids. Water and

dissolved electrolytes comprise 60- 85% of the wet weight of normal cartilage. Consequently, when regarding the mechanical properties and function of cartilage, it must be considered as a two-phase material: a porous-permeable fibre-reinforced solid phase and a freely flowing fluid phase [21].

Articular cartilage has a highly ordered structure; typically, it consists of four distinct zones (Figure 2.3): superficial, middle, deep and the calcified cartilage zone. The superficial zone is the thinnest (only 10%-20% of overall cartilage) and forms the sliding surface of the joint. Also, elongated and inactive chondrocytes are interspersed with densely packed collagen fibres. The middle zone accounts for about 40%-60% of the cartilage. The chondrocytes in this zone are spherical, suggesting a matrix synthesis function [22]. The deep zone is thicker than the middle zone, with round chondrocytes arranged in columns. These cells appear to be very active in protein synthesis [22]. The calcified zone acts as an anchor between the subchondral bone and the cartilage. The cells in this zone are usually smaller and surrounded by a cartilaginous matrix.

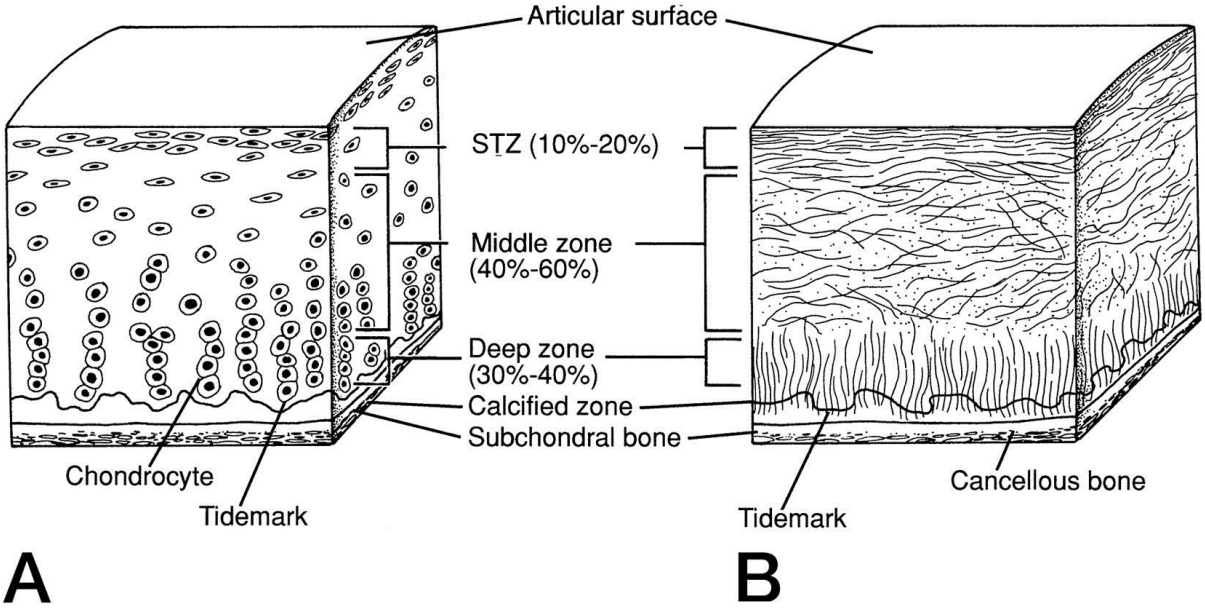

Figure 2.3 The structure of articular cartilage. A, the chondrocyte organization in zones; B, collagen fibre architecture [23].

The key compositions of articular cartilage are briefly introduced in the following sub-sections so that their importance to the functionality of the joint and wear processes can be appreciated.

2.2.1.1 Water

The cartilage is approximately 80% water which is concentrated at the articular surface and decreases in a near linear trend with the increasing of depth to the deep zone of a concentration of about 65% [24]. The water content does not change with aging and increases in OA cartilage [25]. The fluid contains numerous free mobile cations, including Na^{+}, K^{+} and Ca^{2+}, which greatly influence the physicochemical and mechanical behaviours of cartilage. A small percentage of water resides intracellularly, and approximately 30% is strongly related to the aggrecan and hyaluronan [24]. When loaded by a compressive force, approximately 70% of the water may be removed to

become solid phase to resist the force. This interstitial fluid movement plays an important role in controlling cartilage mechanical behaviour and joint lubrication [24].

2.2.1.2 Collagen

The dominant collagen type in articular cartilage, accounting for approximately 90-95% of total amount of collagen, is known as collagen type II, whilst types X, XI, IX and VI are found in minor concentrations. Collagen VI serves as a link for fibrous and globular proteins with chondrocytes; collagen IX may be involved in organizing or maintaining the 3-dimensional meshwork of collagen through interactions with fibrils of type II; collagen X bridges the spatial and temporal transition from cartilage to bone; collagen XI exhibits a firm binding to cartilage proteoglycans [26]. Collagen fibres (that easily buckled under compression), do not offer a large resistance to compression; in contrast, they are the primary component of cartilage to provide its tensile properties as they are very strong in tension [27]. Three distinct zones, with relatively different collagen orientations, are found in articular cartilage. In the superficial zone, the orientation of collagen fibrils is parallel to the cartilage surface, and owing to this, the superficial zone is primarily responsible for resisting shearing load [21] and contributes to the low permeability of cartilage [19]. In this layer, the matrix has considerably low proteoglycan content and superficial zone protein (SZP) has been reported to play an vital role in the either a protective or lubrication mechanism of articular cartilage surface [4]. The collagen fibres disperse in the middle zone with random directions and the proteoglycan content reaches its maximum in this zone. In the deep zone, the fibres are perpendicular to the cartilage surface and resist both shear and compressive forces [9] (Figure 2.3). The tidemark delineates the boundary between deep zone and the

calcified cartilage zone and also resists shear stress. The zone of calcified cartilage provides a transition in material properties between hyaline cartilage and bone and chondrocytes are produced in subchondral bone.

2.2.1.3 Hyaluronan

Hyaluronan (HA), a significant component of articular cartilage, is present as a coat around chondrocytes and exists in a high level in the normal cartilage matrix [28]. Aggrecan binds to HA and plays an essential role in stabilizing the matrix. HA has profound effects on the movement and distribution of water and plays a major role in water homeostasis as its osmotic activity is disproportionately high [28]. HA is also present in the synovial fluid [29]. When the joint is under load, the gap between joint surfaces gradually decreases. At a point of time, synovial fluid can easily be squeezed out sideways through the gap into the unload area. As the gap becomes narrower, some flow must take place through cartilage because the resistance to the fluid flowing through the gap increases. Pores of cartilages are too small to allow the molecules of HA to pass. Therefore, the solution in the gap becomes more and more concentrated in HA and eventually changes into a gel to keep balance with applied pressure [30].

2.2.1.4 Proteoglycans

Proteoglycans are comprised of a protein core, which is attached to polysaccharide chains known as glycosaminoglycans. There are two dominant polysaccharides in cartilage: chondroitin and keratan sulphate. The protein core contains several distinct globular and extended domains that are decorated with glycosaminoglycans. The prime

proteoglycan in articular cartilage is aggrecan, which consists of chondroitin, keratan sulphate and a protein core. When aggrecan binds to HA in the presence of link protein, aggregates will be negatively charged (see Figure 2.4). Because of the highly negative charge, the matrix imbibes water to maintain tissue equilibrium. The elastic restraint of the collagen network keeps balance with the swelling [21]. It is apparent that the loss of proteoglycans may result in a lack of fluid pressurisation, and refers to distortion of mechanical function [31]. Abnormal fluid pressure weakening and even damaging the collagen network, influences the ability of cartilage to bear load [21].

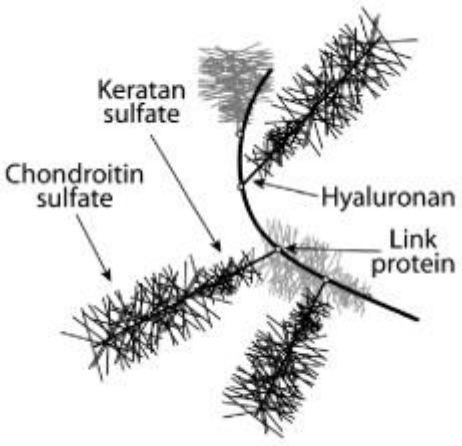

Figure 2.4 The negatively charged keratan and chondroitin sulphate repel each other [32].

The proteoglycans and collagen form a strong, porous-permeable, fibre-reinforced network (see Figure 2.5). Due to tight packing arrangement of the network, these groups are negatively charged when they are placed in the fluid and cause a high fixed charge density within the articular cartilage. Then the dense concentration of negatively charged proteoglycans exerts a large swelling pressure which is also a tensile stress to the surrounding collagen network. This swelling pressure further provides the mechanism for maintaining the normally high degree of hydration in articular cartilage.

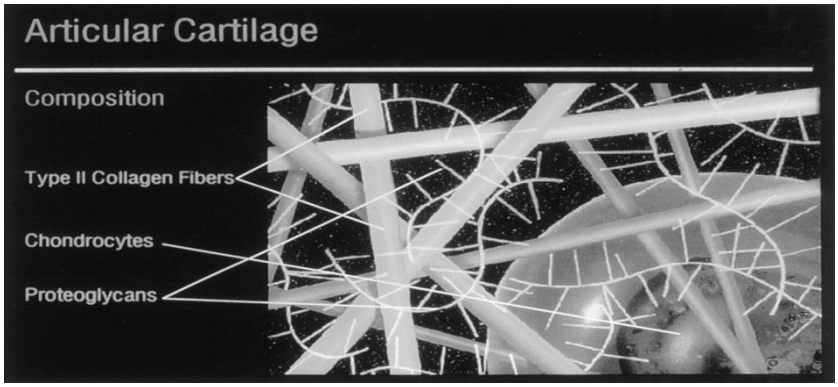

Figure 2.5 This representation of articular cartilage extracellular matrix shows how the collagen network traps the proteoglycan aggregate to form a fibre-reinforced composite [33].

2.2.1.5 Lubricin

Lubricin is a gene product of *PRG4*. It is a major component of synovial fluid and contributes to the boundary lubrication (this part is described in 2.3.1). Also, this gene encodes SZP by the expression of superficial zone chondrocytes but not by chondrocytes in the middle or deep zone [34]. Some of the SZP accumulates in the cartilage superficial matrix to demarcate the cartilage surface with the synovial cavity of articulating joints [23, 35]. Unlike the aggrecan, SZP is not maintained in the extracellular matrix, but mostly permeates into synovial fluid and functions as a boundary lubricant [23].

2.2.2 Biomechanical properties of articular cartilage

Articular cartilage consists of fluid (mostly water with free mobile cations) and a solid, porous-permeable matrix. This biphasic nature of articular cartilage has profound implications on its ability to bear load. When a pressure gradient (either hydraulic or osmotic) acts on articular cartilage, it causes water and ions to flow through the

porous-permeable solid phase and exerts a large frictional drag on the solid matrix.

Fluid flow has long been recognized as a pivotal function of articular cartilage [21]. Permeability is a measurement of the ability of fluid to flow through the cartilage matrix, and it is inversely proportional to the frictional drag exerted by the interstitial fluid. The average permeability of normal human knee cartilage has been shown to a range from 1.14 - 2.17 × 10^{15} m^4/Ns [36]. For cartilage with porosity of 0.75, a pressure differential of 7.5 MPa is required to move a 1 mm column of fluid through the tissue at a speed of approximately 15 μm/s. Therefore, very large drag forces are exerted on the solid matrix even for very small flow speeds. This resisting drag force related to interstitial fluid flow appears to be the major mechanism of load support in the joint [21, 36]. Additionally, articular cartilage has been shown to exhibit a nonlinear permeability response at high pressure and strain, that is, permeability decreases to a stable minimum with the increasing of compressive strain and hydraulic pressure. This decrease results from the decreased pore size due to the compressed solid matrix, and causing increased frictional resistance to the fluid flow. This suggests a protective mechanical feedback system which stiffens the cartilage by limiting rapid fluid flow rate that may occur in sports-related or other high joint-loading situations [37].

Viscoelasticity is defined as the time-dependent response of a material that has been subjected to a constant load or deformation and two characteristic responses of a viscoelastic material are creep and stress relaxation. Fluid flow through the cartilage solid matrix has been thought to be the primary factor responsible for the viscoelastic behaviours observed in articular cartilage [21]. Creep occurs when the articular cartilage undergoes constant loading. The articular cartilage responds with a rapid initial

deformation and then much slower deformation over time. This time-dependent deformation lasts until the equilibrium is reached. When the cartilage undergoes constant deformation, it typically responds with a high initial stress which progressively decreases over time, until equilibrium is reached, here the stress is zero. This time-dependent stress response is called stress relaxation [38] .

Experimental results on the material properties of articular cartilage were reported [21].The biphasic indentation theory indicated that fluid flow plays the primary role in the stress-relaxation and creep behaviour of normal cartilage. The collagen network in the extracellular matrix is the primary determinant of the tensile behaviour of these tissues, and thus the orientation of the collagen network influences their tensile behaviours. The swelling pressure contributes minimally to cartilage stiffness, which in shear is directly proportional to the amount of collagen present in the tissue [21]. Furthermore, it has been shown that proteoglycans do not provide much resistance to shear, that is, they have a low shear modulus [9, 39]. It also has been reported that the compressive stiffness of the deep zone is six times that of the superficial zone under a compressive equilibrium load [5]. This behaviour has been attributed almost entirely to osmotic and structural contributions from proteoglycans. There are regional and zonal variations in the tensile stiffness. The tensile modulus of the superficial zone can be as much as times greater than that of the deep zone. Tensile modulus is also significantly greater in low-weight-bearing region tissue compared with high-weight-bearing regions [5].

To fully characterize the biomechanical behaviour of isotropic material, elastic constants are needed. Cartilage is assumed to consist of a perfectly elastic and isotropic

solid matrix with homogeneously distributed fluid phase [40] . Poisson's ratio (ν) and Young's modulus (E) are two independent elastic constants to characterize the mechanical behaviour of cartilage. E only depends on the elastic stiffness of solid matrix, as suggested by the biphasic model [37]. Higher values of E for the cartilage have been studied in indentation geometry than in unconfined compression geometry, while the modulus values are highly related between measurement geometries. Larger values of E have systematically been reported for the deep layers than for the superficial layers. In addition, decrease of E has been found to strongly relate to the degeneration of cartilage [40].

2.2.3 Articular cartilage degeneration and OA

Significant changes occur in the articular cartilage with OA including decreased proteoglycan content in the superficial and middle zone, fibrillation of the superficial zone extending into the middle zone and the formation of blood vessels from subchondral bone Penetrating into the deep zone of the cartilage [13]. Two main factors strongly contributing to degeneration of articular cartilage are aging and unfavourable biomechanical grades. As there is little or no cell division or cell death in adult articular cartilage, chondrocytes are thought to be long-lived cells. However, chondrocytes can be accumulated to degenerated by age-related changes such as circulation system ageing [41]. As a consequence, chondrocyte functions are altered profoundly and further influence matrix structure and function. The other relations between articular cartilage degeneration and unfavourable biomechanical grades are shown in Table 2.2.

Table 2.2 The knee joints in unfavourable biomechanical grades and the mechanisms of relative overloading of the cartilage [15].

Unfavourable biomechanical grade	**Mechanism of relative cartilage overloading**
Malalignment	Shifting the pressure of the tibiofemoral force leads to irregular load distribution, causing locally increased stresses on the articular cartilage
Loss of meniscal tissue	Increased peak stresses on the articular cartilage results from the alteration in load transmission as partial loss of constraint to anteroposterior translation is unstable
Cartilage lesions	Increased exposure of subchondral bone due to the Increased stresses on the lesion rim of diameters greater than 10 mm, leading to endplate stiffening and micro cracks
Joint instability or ligament laxity	Accelerated chondrocyte senescence results from Cartilage damage due to oxidative stress of chondrocytes and traumatic impact per second
Trauma	Increased metabolic

OA is a result of an imbalance between synthesis and degradation of collagen and proteoglycans [9]. Functions of chondrocytes are influenced by many factors, including cytokines, growth factors, structural physical stimuli and the components of the matrix themselves [21]. Wear particles are produced even during the normal functioning of

articular cartilage. Trauma causing the abnormal wear and tear to the articular cartilage may induce the formation of wear particles. At the initial time, the generation of these particles prevails over the capability of the system to reduce and dispel them and stimulates the chondrocytes to release degrading enzymes. Synovial macrophages phagocytize molecules from breakdown of collagen and proteoglycans and release pro-inflammatory cytokines, including IL-6, IL-1 and TNFα, which can bind to receptors on the surface of chondrocytes resulting in further release of metalloproteinases that degrade collagens. At first, proliferation of chondrocytes in the deeper layer of the cartilage and increased synthesis of matrix molecules, are capable of maintaining the integrity of the articular cartilage, but eventually mechanical changes in extracellular matrix and loss of chondrocytes and OA develops [15, 21].

Changes in the morphology and biomechanical properties of articular cartilage can assist in detecting cartilage degeneration. When the cartilage with early OA is degenerated, the thickness of cartilage changes in nano-scale. The overall thickness of articular cartilage decreases with the severity of disease. It has been reported that the superficial zone in OA comprises a higher percentage of the full depth than that in healthy cartilage and thus may provide a protective layer with more resistant to load [42]. The stiffness of cartilage also changes due to the cartilage synthesis and degradation in the proteoglycan-collagen solid matrix, that is, the decrease of matrix synthesis results in a softening of the tissue [13]. The stiffness has been observed on both the millimetre and nanometre scales [9]. The normal articular cartilage has a smooth and firm surface and the earliest indication of degeneration visible in the articular is disruption of the most superficial layers or localized fibrillation [13]. With the disease process, the surface of cartilage becomes irregular and roughened and

fibrillation extends deeper through the cartilage until reaches the subchondral bone. [13].

2.3 Wear particles analysis techniques

Biological wear particles carry valuable information. The shape of wear particles has been reported to be related to different OA grades in human knee joints [43]. It has also been reported that the detection of wear particle surfaces can reflect the information of its wear process [37].

2.3.1 Wear debris generation mechanisms

The human knee joint can perform a large number of movements and adopt various postures. It has been reported that the highest knee joint loading occurs during the downhill walking [44]. The complexity of soft tissues makes the wear mechanisms difficult to be fully understood. Thus, conventional lubrication theories (which are described below) used in engineering are adopted to explain wear debris generation mechanisms in natural joint [45].

Wear is defined as the substance loss owing to mechanical interaction between two contacting surfaces [46]. Only asperities or a small area of the higher peaks contact when two surfaces are placed together under a load. In the individual contacts, atomic binding and electro-repulsive interact. Once the two surfaces slide a small distance to one another, the interactions are disrupted and then this disruption leads to the formation of particles [47].

Lubricin is the major component in the synovial fluid present in the superficial zone of the cartilage that lubricates the knee joint for low wear and low friction [48]. Synovial fluid offers a high level of lubrication which the sliding friction coefficient can be as low as 0.005 [44]. Therefore, hydrodynamic and elastohydrodynamic theories have been applied to explain the wear mechanism [49]. If the joint suffers a long loading time, the water drag out of the cartilage and the hardness of cartilage becomes larger compared to unloaded cartilage. In the same time, lubricating glycoproteins and hyaluronan in the synovial fluid can maintain a higher viscosity to prevent the cartilage surfaces from contacting each other [45, 49-51]. Also, it has long been observed that a thin lipid layer, covering the articular cartilage end, allows lubricin osmosis and works with hyaluronan to reduce load energy between interfaces [52, 53]. Wiping or rubbing can easily remove the coating of cartilage surface [53]. When this lipid layer becomes thinner or even removed, the underlying collagen meshwork is exposed and the wear and tear on cartilage is accelerated [54] which allows the accelerated formation of wear particles and leads to OA.

In short, OA is a very complex process primarily dominated by the wear of articular cartilage. Its wear mechanisms have not been well understood. It is hoped that through wear debris analysis, a better understanding of the process and its distinctive features can be achieved [55].

2.3.2 Preparation techniques of biological wear particles

The techniques used for preparing wear particles are essential in investigating the key

features of wear particles found in human knee joint. Ferrography, bio-ferrography and filtergram are three commonly used methods to acquire wear particles.

Ferrography [56] is a technique for wear analysis by means of separating wear particles with different magnetism. Consequently, smaller particles are differentially deposited along the flow path and larger particles are deposited near the entry end of the substrate [57]. This approach focuses on metal wear particles and is widely used in industry [58]. Bio-ferrography [59] has the similar theory as ferrography. Biological particles do not naturally possess magnetization; hence, wear particles found in human knee joints must be magnetized first to bio-ferrography. In this method a magnetization method, namely adsorption of the paramagnetic lanthanide cation is used. The test solution is mixed with a solution of erbium chloride ($ErCl_3$, 10 mM) in a proportion of 4:1 by volume [60]. However, this method might be influenced by the particle properties, especially their mechanical properties and most important particle overlapping is often a problem in this method [9].

Filtergram is a method using a filter membrane to separate from the solution and collect wear particles. The particle overlapping problem can be significantly minimised in the filtergram. However, the filter membrane may be ruptured due to a large applied force and the membrane may be blocked by randomly arranged wear particles [9]. Therefore, extreme caution is needed during the filter process. In addition, bio-particles won't be separated according to their sizes which bio-ferrography is able to do.

2.3.3 Image acquisition techniques of biological wear particles

Image acquisition techniques play a pivotal role in obtaining the surface topographic data of biological wear particles. Many imaging techniques such as scanning electron microscopy (SEM), transmission electron microscopy (TEM), atomic force microscopy (AFM), and laser scanning microscopy (LSM), are commonly used. Traditional TEM and SEM provide 2D images while AFM and LSM are able to acquire 3D surface data.

2.3.3.1 Overview of available imaging techniques

SEM generates images of a sample by scanning the surface with a focused beam of electrons. The quality of images depends on the electronic emitter, thus the resolution can fall between less than 1 nm and 20 nm which may cause significant error to the results [61]. The requirement of SEM for operating is in a vacuum, thus biological wear particles are required to be coated and then dehydrated, which may make particles shrink and alter their surface topography. Another disadvantage of SEM is that conventional SEM can only acquire 2D surface data of an object.

To overcome the limitations of the above technique, and more importantly to obtain 3D data for comprehensive analysis, AFM has become a popular imaging and analysis technique in recent years. The means of force-distance curves is applied to study the sample surface in AFM. When AFM scans a surface, it monitors the position of a sharpened tip, which is supported by a micro cantilever mounted on a piezo electric transducer. AFM with high force (1 pN) resolution, lateral (25 nm) and vertical (0.01 nm) [62] can image both conductive and non-conductive surfaces, and can be used in

liquid environment, therefore becoming the favoured instrument for biological investigation [63]. However, image artefacts could be induced by the sample itself or by an unsuitable tip. Due to the nature of AFM probes, AFM cannot measure overhangs or steep walls [64], which could be a disadvantage when imaging wear particles found in advanced OA.

LSM is a technique for obtaining high quality of images with depth selectivity. It is able to acquire high lateral resolution 3D images by receiving the reflection information from the surface of specimen through the optics system which contains a confocal aperture to reduce light from focal plane. It requires almost zero sample preparation and is able to detect steep angles. LSM has been used in the study of sheep wear particles, but not human wear particles [9]. Further information of LSM can be found below.

2.3.3.2 The principle of laser scanning confocal microscopy and image acquisition of biological samples using LSM

The laser microscope uses a laser light source and the confocal principle to measure surface morphology of the target. The system configuration is shown below (Figure 2.6). The images are subsequently stored and combined to a 3D image using computer media.

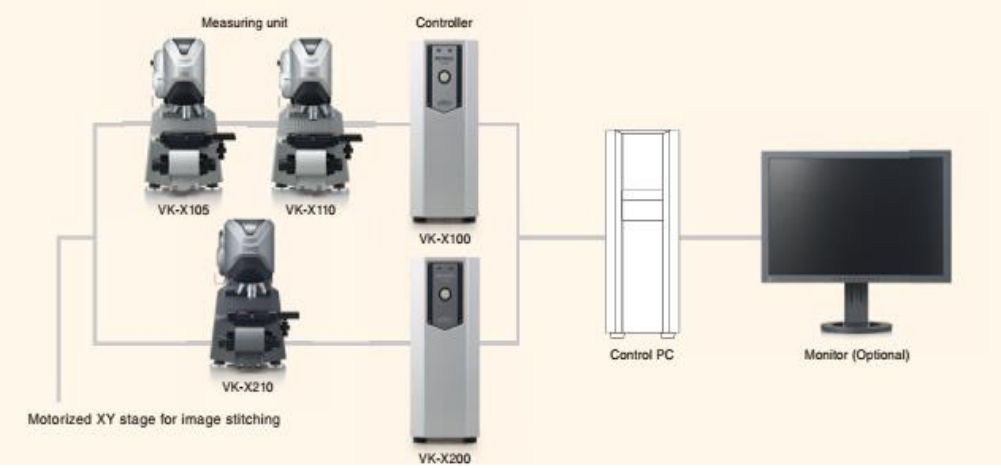

Figure 2.6 The measurement system [65].

The laser light is focused on the target via the XY scanning system and the objective lens. The focused beam spot performs a surface unevenness of the target within the observation field of 1024 × 768 pixels. The target is scanned, and then reflected light for each pixel is detected by the light receiving element. The objective lens is then driven in the Z-direction and surface scanning is repeated (see Figure 2.7).

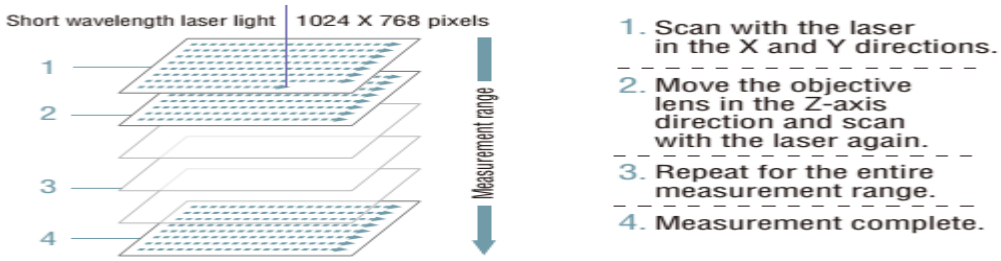

Figure 2.7 Diagram of the measurement principle [65].

Part of the light emitted from semiconductor laser passes through the half mirror and reaches the reference surface, while the rest of the light is reflected and reaches the targets surface (see Figure 2.8). Optical paths from the CCD to the reference surface and from the CCD to the target surface generate interference stripes and appear in the image formed on the CCD. In the confocal system with a pinhole, light is only detected when the target is on focus, creating very sharp images with high-resolution measurement

data (see Figure 2.9).

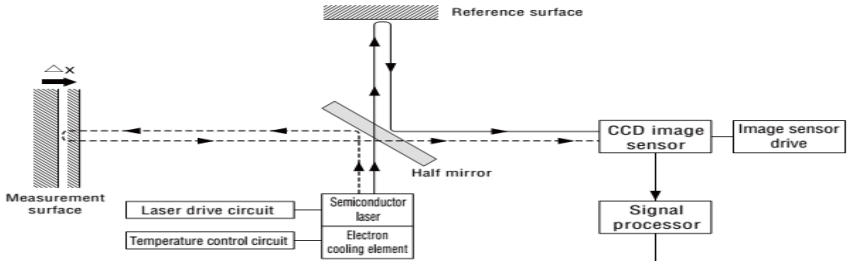

Figure 2.8 Structural diagram of a light interferometer [65].

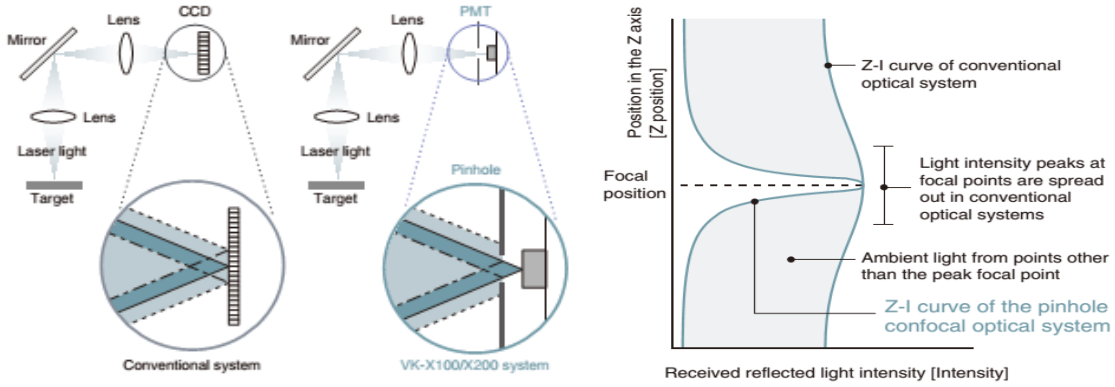

Figure 2.9 Pinhole confocal optical system (left) and Peak detection (focal point) comparison between a pinhole confocal system and conventional system (right) [65].

As shown in Figure 2.10, the interference stripes on a flat target (left) and inclined target (right) differ greatly. When observing the interference stripes of each target placed in front of a CCD at a distance, no interference stripes appear for the left case because a flat surface causes no difference in the optical path and the interference stripes appear for the inclined target (right) due to the different optical path.

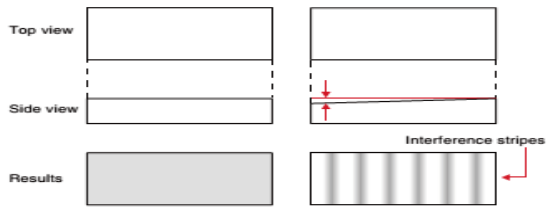

Figure 2.10 Interference stripes [65].

The height differences of a target can be measured from the number of interference stripes that appear at half-wavelength intervals (1/2λ). If the light source with a wavelength of 408 nm forms the interference pattern, the distance between the adjacent interference stripes is 0.204 μm. In this case, the distance from one peak to another can be divided into 20 segments and achieve a high resolution of 0.01 μm. The regular changes in interference stripe brightness due to height variables are measured by a light interferometer.

As shown in Figure 2.11, when using a single-wavelength light source, the interference patterns appear the same regardless of height differences of (1/2 + n) times the light source wavelength (λ) or the orientation of the inclination. To overcome this phenomenon, a white light source is used to capture four interference stripe patterns of the target by moving the objective lens in 1/8λ intervals. This method is called Phase Shift Interferometry (PSI).

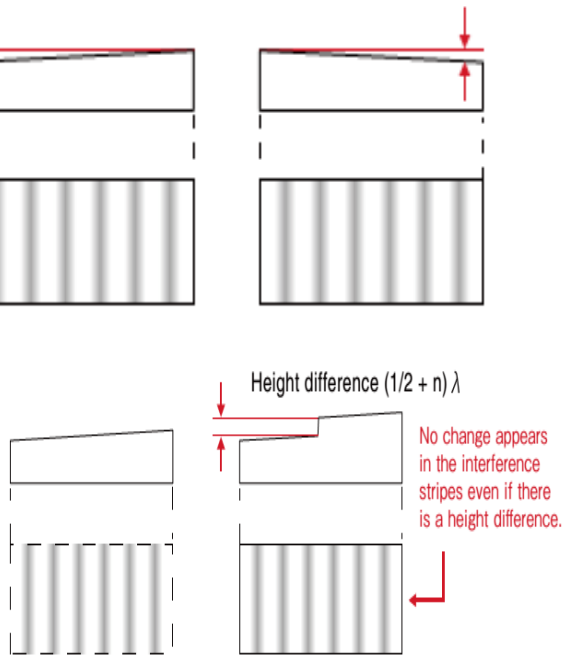

Figure 2.11 Same Interference stripes with different target surfaces [65].

2.3.4 Characterisation of biological wear particles

Visual inspection of a particle using microscopy image is commonly employed to analyze wear particles [42]. AFM has been used to confirm the size range and boundaries of wear particles [9, 54, 66] while LSM has been used to detected 3D surface morphology of wear particles [67]. Current studies on wear particles found in human knee joint focus on the size distribution of wear particles, their shape (2D analysis) and the relationship to inflammation and its surface morphology (3D analysis).

2.3.4.1 Size information vs OA severity

According to a current study by Wang *et al.* [68], the majority of the particles found in human knee joints were in a size range of 5–60 μm, and 80 % of them in all OA grades were smaller than 20 μm. The size of the most abundant wear particles was about 10 μm in all OA grades. The mean sizes of the wear particles increased from healthy joints to mild OA (OA 2), with OA 2 reaching the largest mean size. Then the particle sizes decreased in severe OA (OA 3–4). The particles were categorized into small (less than10 μm), medium (10 to 20 μm) and large groups (more than 20 μm) based on their sizes in the major dimension. The small particles formed the majority which accounted for approximately 40–50 % of the total particle number. The medium sized particles, with a mean size of 13.7 μm, comprised about 30–40 % of the total particles. The percentage and mean of the medium particles revealed marginal changes with increasing OA grade and the percentage and mean size of the large particles in osteoarthritic knee joints were larger than those in healthy joint. However, in this study, the size of wear particles less than 3 μm were not studied owing to the nature of AFM. It did not examine the

mechanical properties of wear particles. Only the size distribution could not reveal distinct features of wear particles in every OA grade. Human wear particles were studied to confirm if the shape of particles is related to OA grade [69]. In healthy people, wear particles with the length of 13.6-97.4 μm were examined; particles ranged 11.4-268.3 μm, 11.3- 228.0 μm, and 7.8-179.3 μm were extracted from OA grade 1, OA grade 2, and OA grade 3 patients, respectively.

2.3.4.2 Quantitative characterisation of boundary features in 2D

The general shape of wear particles also has been studied. Lamellar particles with a smooth surface morphology were normally generated in healthy joints while most abundant particles with rod shapes were present in joints with the early stages of OA, i.e. grade 1. It had been thought that the origin of chunky particles was from the deep zone of cartilage and osseous particles were generated from the subchondral bone which implied that in some places the subchondral bone was devoid of cartilage [8, 69]. However, this study did not take inflammation into consideration which is one of the main characteristics of OA, even in early OA. Although rod-shaped particles were abundant in early OA, they could also find this particle shape in other OA grades, i.e. grade 3. For diagnosis of OA, the shape study would be time-consuming to detect all wear particles.
According to Stachowiak's group [42], SEM stereoscopy was used to obtain the images of wear particles found in tribological systems. Boundary fractal dimension and spike parameter were used to characterize the angularity and the boundary of particles. However, this study focused on different types of abrasive grits rather than wear particles. The erosive or abrasive wear rates significantly increases with the increase of particle angularity [70].

2.3.4.3 Surface morphologic characterisation in 3D

The amplitude properties are characterized by 8 parameters, which depend on the height deviation [71]. These parameters are used to describe average ordinates, peaks and valleys of surface. The definition of the parameters is illustrated in Table 2.3.

Slope gradients are indicated by three hybrid parameters whose calculations are based on local z-slopes and based on both spatial and amplitude information [71].

The Mean Summit Curvature, *Ssc***,** is the arithmetic mean of the principal curvature of the local maximums on the surface. It is defined as:

$$Ssc = \frac{-1}{2n}\sum_{i=1}^{n}\left[\left(\frac{\delta^2 z(x,y)}{\delta x^2}\right) + \left(\frac{\delta^2 z(x,y)}{\delta y^2}\right)\right] ,$$

where δx and δy are the pixel separation distances , and z is the height of the corresponding point [72].

The Root Mean Square Gradient, *Sdq***,** is the root mean square of the surface slope within the sampling area and it is defined as:

$$Sdq = \sqrt{\frac{1}{(M-1)(N-1)}\sum_{k=0}^{M-1}\sum_{l=0}^{N-1}\left[\left(\frac{z(x_k,y_l)-z(x_{k-1},y_l)}{\delta x}\right)^2 + \left(\frac{z(x_k,y_l)-z(x_k,y_{l-1})}{\delta y}\right)^2\right]}.$$

Table 2.3 Definition of amplitude parameters.

Amplitude Parameters	Definition	Unit	3D reference
Sa (Roughness Average)	$Sa = \frac{1}{MN}\sum_{k=0}^{M-1}\sum_{l=0}^{N-1}\left\|z(x_{k,y_l})\right\|$	[nm]	ISO/DIS 25178-2 ASME B46.1
Sq (Root Mean Square)	$Sq = \sqrt{\frac{1}{MN}\sum_{k=0}^{M-1}\sum_{l=0}^{N-1}\left[z(x_{k,}y_l)\right]^2}$	[nm]	ISO/DIS 25178-2 ASME B46.1
Ssk (Surface Skewness)	$Ssk = \frac{1}{MNs_q^3}\sum_{k=0}^{M-1}\sum_{l=0}^{N-1}\left[z(x_{k,}y_l)\right]^3$		ISO/DIS 25178-2 ASME B46.1
Sku (Surface Kurtosis)	$Sku = \frac{1}{MNs_q^4}\sum_{k=0}^{M-1}\sum_{l=0}^{N-1}\left[z(x_{k,}y_l)\right]^4$		ISO/DIS 25178-2 ASME B46.1
Sz/St/Sy (Peak-Peak)	$Sz = St = Sy = Zmax - Zmin$	[nm]	ISO/DIS 25178-2
S10z (Ten Point Height)	$S10z = \frac{\sum_{i=1}^{5}\left\|z_{pi}\right\| + \sum_{i=1}^{5}\left\|z_{vi}\right\|}{5}$	[nm]	ISO/DIS 25178-2 ASME B46.1
Sv (Max Valley Depth)	The largest valley depth value		ISO/DIS 25178-2 ASME B46.1
Sp (Max Peak Height)	The largest peak height value		ISO/DIS 25178-2

			ASME B46.1

The Surfaces Area Ratio, *Sdr*, describes the increment of the interfacial surface area relative to the area of the projected x-y plane:

$$Sdr = \frac{\left(\sum_{k=0}^{M-2}\sum_{l=0}^{N-2} A_{kl}\right) - (M-1)(N-1)\delta x \delta y}{(M-1)(N-1)\delta x \delta y} 100\%,$$

$$A_{kl} =$$

$$\frac{1}{4}\left(\sqrt{\delta y^2 + \left(z(x_k, y_l) - z(x_k, y_{l+1})\right)^2} + \sqrt{\delta y^2 + \left(z(x_{k+1}, y_l) - z(x_{k+1}, y_{l+1})\right)^2}\right) \times$$

$$\left(\sqrt{\delta x^2 + \left(z(x_k, y_l) - z(x_{k+1}, y_l)\right)^2} + \sqrt{\delta x^2 + \left(z(x_k, y_{l+1}) - z(x_{k+1}, y_{l+1})\right)^2}\right).$$

For a totally flat surface, *Sdr* = 0 %.

Six functional parameters characterize fluid retention and bearing properties of material surface. The parameters are all defined from the bearing area ratio curve shown in Figure 2.14.

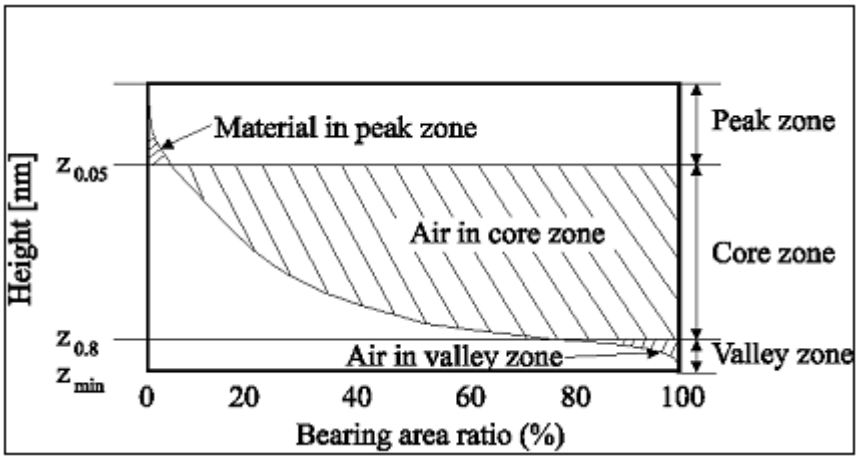

Figure 2.12 The surface Bearing area ratio curve [71].

The Surface Bearing Index, *Sbi*, is defined as:

$Sbi = \frac{s_q}{z_{0.05}}$,

For a Gaussian height distribution, s_{bi} reaches at 0.608. Large s_{bi} refers to a good bearing property.

The Core Fluid Retention Index, *Sci*, is defined as:

$Sci = \frac{v_v(z_{0.05}) - v_v(z_{0.80})}{(M-1)(N-1)\delta x \delta y} / s_q$, where *Vv*(*Zx*) is the void area under the horizontal line (*Zx*) over the bearing area ratio curve. Large *Sci* reveals the void volume in the core zone is large.

The Valley Fluid Retention Index, *Svi*, is defined as:

$Svi = \frac{v_v(z_{0.80})}{(M-1)(N-1)\delta x \delta y} / s_q$,

Large *Svi* indicates large void volumes in the valley zone.

The Reduced Summit Height, *Spk*, is the height of the upper left triangle.

The Reduced Valley Depth, *Svk*, is the height of the triangle drawn at 100%.

The Core Roughness Depth, *Sk*, is the height difference between the intersection points of the found least mean square line.

The spatial parameters, refer to the spatial properties of surfaces, are designed to access the peak density and texture strength. These parameters are the density of summits, the correlation length, and the texture aspect ratio.

The Density of Summits, *Sds*, is the number of local maximums per area:

$Sds = \frac{Number\ of\ summits}{(M-1)(N-1)\delta x \delta y}$.

The Correlation Length parameters, *Scl20* and *Scl37,* are defined as the horizontal distance of the areal auto-correlation function that has the fastest decay to 0.2 and 0.37 respectively.

The Texture Aspect Ratio Parameters, *Str20* **and** *Str37***,** are defined as the ratio of the fastest to slowest decay to correlation 0.2 and 0.37 of the auto-correlation function respectively.

Amplitude parameters including root-mean-square roughness (S_q), average roughness (S_a), and skewness (S_{sk}), were employed to describe the surface roughness of wear particles with OA process [73]. Representative boundary parameters were also carried out to examine the shape complexity of the wear particles. In this part, the parameters were length, area, roundness, aspect ratio, convexity, curl, fractal dimensions and form factor. Area and length could compare the size and dimension of the wear particles at the different OA grade; other parameters reveal the stability of formation of wear particles during the wear development [45]. Height related (amplitude), spatial, and hybrid parameters, have been implemented to be significant characterisation of the wear particles. Tian's study indicates that these parameters were able to indicate the wear changes of the sampled wear particles. 10 of these parameters have been chosen as key indicators [45]. However, these feature parameters are used for evaluating the surface morphology of the wear particles collected from sheep knee joints and whether these selected parameters can also be used to reveal distinct features of human wear particles is still unknown. Furthermore, the field parameters and functional parameters were used

in investigating articular cartilage but rarely selected to reveal morphology of the wear particles.

2.4 Summary

The knee joint is acting like a hinge in the walking process. It can absorb extremely large vertical forces but it is weak to horizontal forces. All bones in the knee joint are coated with articular cartilage which is comprised of chondrocytes and an extracellular matrix. Articular cartilage is considered as bi-phase material and the balance between synthesis and degradation of extracellular matrix components contributes to its ability to resist various forces including compression, tear and shear. Once chondrocytes fail to maintain the homeostasis, OA will occur. The Outer bridge classification has been used to rank the severity of OA from grade 0 (health joint) to grade 4 (advanced disease).

Wear particles, the by-products of the articular cartilage, may include valuable information in their surface morphology and mechanical properties for assisting in the understanding of OA. The filtergram particle separation methods and LSM were deemed the most appropriate particle preparation and analysis tools for this study. During the sample preparation, Phosphate-buffered saline (PBS) is important to keep wear particles hydrated and protect their mechanical properties. Boundary parameters, height related, spatial and hybrid parameters were determine to reveal the morphology features of wear particles. Statistical analysis methods were used to selected distinct parameters.

Existing studies focused on the animal particle analysis and human cartilage study. Although staining solutions can enhance reflexion of particles and be imaged in high magnification of optic microscopy, the nature of particles may in turn be influenced by the staining solution. Therefore, samples were not be stained in this project and were imaged using LSM with high resolution. Functional and field parameters, only used to indicate animal particles, were considered in numerical analysis of human wear particles.

Chapter 3 Methodology

3.1 Sample collection

Synovial fluid samples of knee joint were collected from 25 patients who underwent knee orthopaedic surgery at hospitals in Queensland, Australia. 14 female and 11 male patients had either total knee replacement surgeries or knee arthroscopic operations, and the corresponding OA grades are indicated in Table 3.1. The OA severities of the knee joints were graded according to the Outer-bridge classification system which has been described in section 2.1.2. The synovial fluid samples also contained fat and blood was separated from the viscous synovial fluid [9]. Firstly, the synovial fluid sample was centrifuged at 2500*g* and at 4 ℃ for 15 min using a centrifuge (HEART LABOFUGE 400R, Thermo Scientific) to separate the wear particles from the fat. The wear particles are heavier than the fat which was suspended on the top of the synovial fluid and was taken out using a pipette (Eppendorf). Secondly, the filtergram method was used to isolate and collect wear particles. The solution was passed through a 60 μm filter paper to remove tissue particles. 4-15 ml sterile distilled water was then mixed with the remaining solution and filtered through a 3 μm filter paper. The clean particles were finally collected from the viscous synovial fluid. After the extraction procedure, the wear particle samples from the same joint were placed onto an aldehyde functional plasma polymer described elsewhere [9, 74, 75]. Thirdly, the prepared particles were then stored in a freezer at -25 ℃ to minimise sample degradation and enable them to bind to the substrate for imaging. The steps above were performed by Wang *et al.* [9].

Table 3.1 Patient profiles and OA classification of the collected samples [9]

OA grade	Classification of OA grade	Number sex (M:F)	Mean age (range)
No OA	Normal cartilage	2 (1:1)	33 (16-49)
Mild OA	• Softening and swelling • Fragmentation and fissuring in an area 1/2 inch or less in diameter	11 (4:7)	60 (43-81)
Severe OA	• Fragmentation and fissuring in an area 1/2 inch or more in diameter • Erosion of cartilage is down to bone	11 (6:5)	61 (47-76)
No classification		1 (0:1)	45

3.2 Image acquisition using LSM

Compared to other imaging techniques, the LSM can acquire 3D images of human wear particles with high lateral resolution and resolution in X-Y axis and requires almost zero sample preparation [65]. The LSM (VK-X100, Japan) used in this project was equipped with 10×, 20×, 50× and 150× objective lens. Since the sheep knee joints particles have the similar features to the human knee joint particles, the sheep knee joint particles were tested using different objective lens to choose a suitable one for the project.

Sheep particles were first produced by scratching the cartilage of sheep knee with a knife. Samples were confirmed to have a good hydration state 10 to 17 minutes after

removal from the fridge (see Figure 3.1a), but after 17 minutes, the sample exhibited many wrinkles (Figure 3.1b). This test not only determined the time period that sheep particles would in a good grade to enable imaging of human particles, but also enabled comparison of hydrated and dry particles. Normally 10 minutes was taken to focus a particle using the 10× objective lens, but cannot obtain sufficient surface data of the wear particles. The objective lens of 20× (Figure 3.2a) and 50× (Figure 3.2b) with the corresponding smallest z-pitch were both used to capture the same sheep particle and suggested that the latter set up of microscopy is more suitable to capture the human knee particles as more surface information of particles was included under 50× objective lens. Normally, the height of particles was greater than 10 μm, therefore a lateral resolution of 0.01 μm provided enough image resolution to enable particle analysis. The imaging time for 50× objective lens was approximately 5 minutes. The 150× objective lens could not obtain high quality of images due to limited light reflexion of bio-materials.

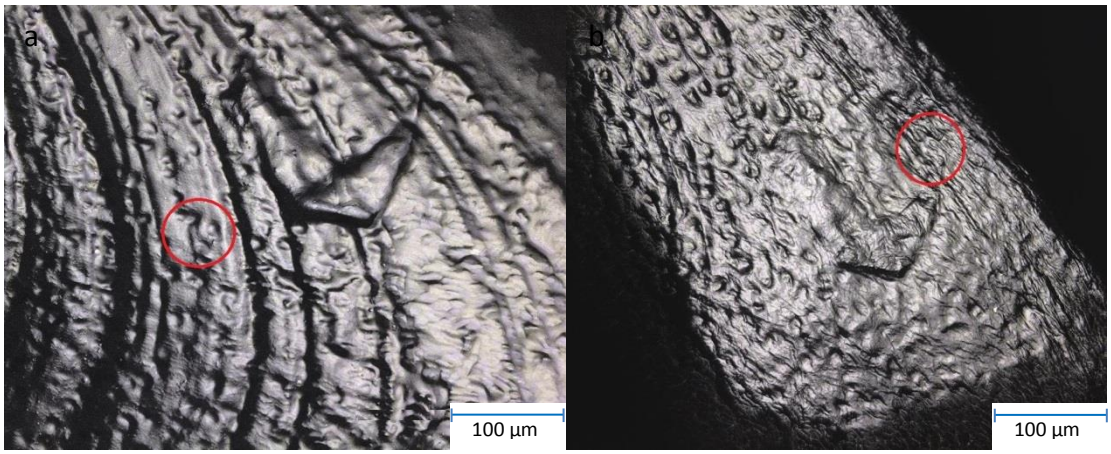

Figure 3.1 LSM Images of sheep joint wear particles. (a)The particle imaged in a good hydrated grade and the read circle indicates particle surface morphology; (b) the particle imaged in a dry grade and the read circle indicates dry-related wrinkles on the particle surface.

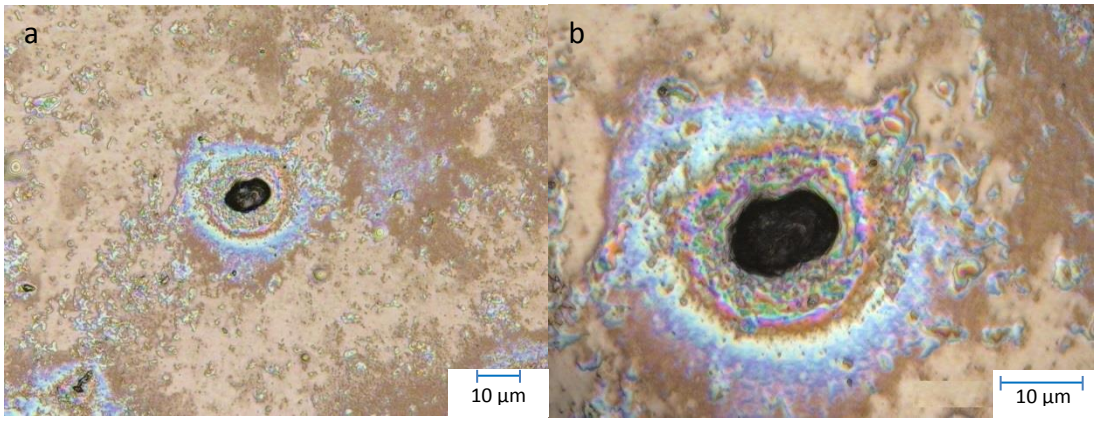

Figure 3.2 A sheep particle sample under different objective lens and z-pitch. (a) The objective lens of 20× with a step size of 0.05 µm (smallest) in z direction was used; (b) The objective lens of 50× with a step size of 0.01 µm (smallest) in z direction was used.

Before the image acquisition using LSM, the prepared samples were placed in a fridge for 24 hours to thaw them at 4 ℃ [9, 45, 76]. The long thaw period avoided the deformation of damaging ice crystals within the specimens and surface [77]. However, freeze/thaw cycles will increase damage to proteins in the samples, so that experiments only used samples that had undergone one freeze/thaw cycle [78]. The particles in nine different positions on each slide were captured using LSM. The layout of particles imaged are shown in Figure 3.3. To better understand the wear process, a variety of particles including small, large, smooth and very rough particles were imaged. A range of 7-18 particles were captured on a slide and a total of 387 wear particles from 25 spcimens were captured.

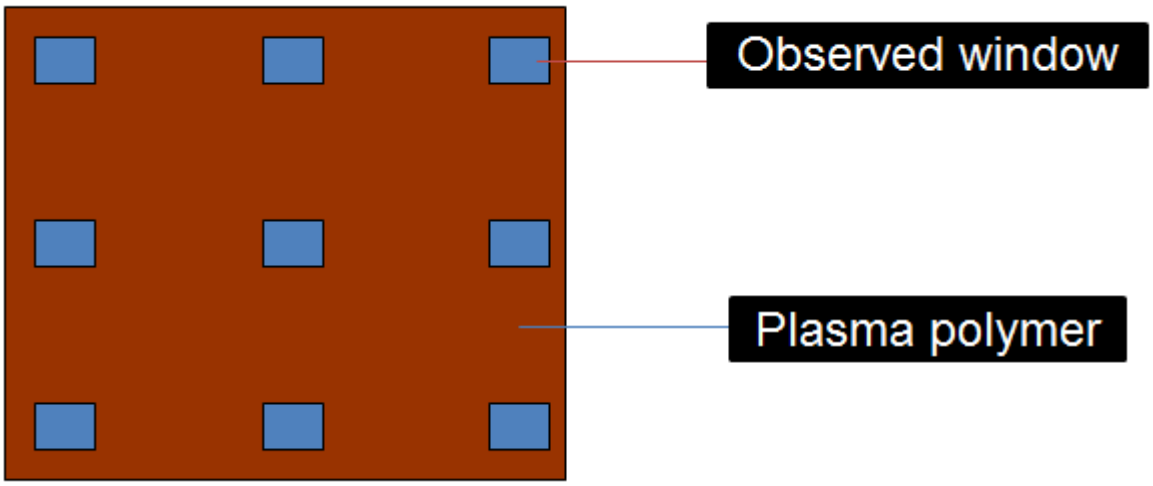

Figure 3.3 Wear particles randomly captured in nine positions of each slide.

3.3 Numerical characterisation and statistical analysis

Each particle was imaged two different ways. One image was a vk4 file which included 3D data; while the other one was jpg files which contained the laser intensity information. The topography image of thin particles was similar to the background, therefore, it was hard to find the boundary of these particles when using topography image. In contrast, the shape of particles was more easily detected in the intensity image and then copied over to topography image. All the steps above were performed using SPIP. However, the software could only calculate boundary parameters based on the whole particle. The surface morphological parameters were calculated based on the area of interest which was drawn by hand and close to the real particle boundary.

In order to describe distinct surface features of wear particles and to understand how the particle shapes and surfaces different with different OA grades, effective numerical parameters were selected. Average roughness (*Sa*), root-mean-square deviation of surface (*Sq*), ten point height (*Sz*), skewness of topography height distribution (*Ssk*),

kurtosis of topography height distribution (*Sku*), the maximum surface peak height (*Sp*), the lowest valley of the surface (*Sv*) were carried out to reveal the surface roughness and height distribution of wear particles [9]. In order to further describe texture strength of the particles, density of summits of the surface (*Sds*), the fastest decay auto-correlation length (*Scl*), texture aspect ratio of the surface (*Str*) were added into parameter groups. Developed interfacial area ratio (*Sdr*) reflects the hybrid property of surfaces which is related to amplitude or the spacing or both [79]. The stability of formation of wear particles and their functional topographical features were indicated by texture direction of the surface (*Std*), core roughness depth (*Sk*), reduced peak height (*Spk*), reduced valley height (*Svk*), peak/valley material component (*Smr1* and *Smr2*) [80]. Material volume, void volume, net volume, area, length, roundness, convexity, form factor, elongation and solidity were analysed to present the boundary information of particles [81].

In Figure 3.4, some of the 29 parameters were selected as distinct parameters to distinguish different OA grade particles. A correlation study was the first step to identify the correlated parameters that described common trends in particle features. Secondly, a one-way ANOVA was carried out to compare in a pairwise manner the differences between OA particles on each parameter and the parameters were not used further in the analysis if they showed no difference between all particles. Finally, discriminant analysis was used to establish linear combinations using multi-parameters based on known patients' information.

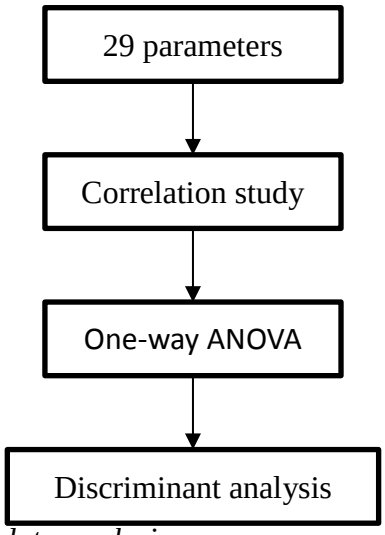

Figure 3.4 Diagram of data analysis.

3.4 Correlation of particle results and cartilage analysis results

Cartilage is the origin of wear particles. The correlation may explain some mechanical properties and assist in understanding OA process. However, comparing the particle and cartilage surface features would be nonsense to some extent as different set-up, amplification and image analysis may significantly influent the parameters obtained. Instead, a comparison of the main trend of each parameter by OA grade was used to study the correlation.

Chapter 4 Visual and numerical analysis results of particles

The morphology study of wear particle depends on the quality of the images obtained. In this project, 2D and 3D images with high resolution were captured using LSM. Visual analysis of particle images was essential to differentiate the shape or surface features of particles from different OA grades. The numerical characteristics were then extracted from particle images using SPIP and the results were analysed based on each OA grade.

As mentioned in Chapter 3, LSM was used to capture particles collected from 25 patients. The OA grade of 24 in 25 patients was clinically diagnosed. There were 2 synovial fluid samples from patients without OA symptoms, 11 mild OA and 11 severe OA patients. 387 particles with clear surface topography were obtained for visual inspection and quantitative numerical characterisation.

This Chapter presents the size distribution of particles since it has been identified that the size distribution was related to OA grade. The visual shape analysis of particles was presented because it has been reported that different OA grades contributed to the shape changes of particles [8]. The visual surface roughness inspection and quantitative surface characterisation results are presented below.

4.1 Particle sizes

The particle size was separated into small (< 10 μm), medium (10-20 μm) and large groups (> 20 μm) based on their length in the longest dimension. Figure 4.1a is a 3D

image of a small particle with the major dimension of 8.47 µm. A medium particle from a severe OA specimen is shown in Figure 4.1b. The length of this medium particle was found to be 10.51 µm. Figure 4.1c shows a large particle from a mild OA patient. The length of the large particle was 34.14 µm.

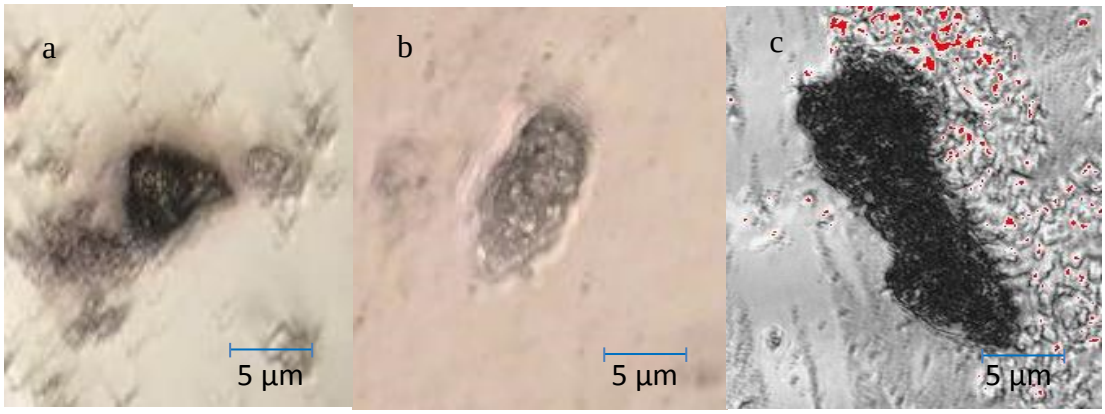

Figure 4.1 3D images of particles in different sizes: (a) a small particle with the length of 8.47 µm; (b) a medium particle with the length of 10.51 µm; (c) a large particle with the length of 34.14 µm.

The number of particles analysed in different OA grades was counted and the particle sizes were measured (Table 4.1). Around 80% of particles in all OA grades were smaller than 20 µm, while the majority of particles captured were in a size range 4-50 µm. The mean size of the wear particles increased from no OA to mild OA, with mild OA having the largest mean size. Then the particle size decreased in severe OA. This trend has been reported previously for human knee joint wear particles [9]. More specifically, the small particles for the majority of all particles and comprised approximately 43% of the total particle number. The medium sized particles accounted for 34-40 % of the total particles. The proportion of different particle sizes was also similar to that reported previously with 270 non-OA, 1219 mild OA and 2776 severe OA particles [9]. Even though the size distribution was related to the OA grades, the percentage of each particle size in different OA grades was similar. After analysis of the size distribution, the visual inspection of shape features and the corresponding numerical analysis of the particle

shapes was conducted and the key results are presented in next section.

Table 4.1 The number and mean of length in the major dimension and percentage of particles in each OA grade.

OA grade (the number of particles)		**No OA (93 particles)**		**Mild OA (123 particles)**		**Severe OA (115 particles)**		**Unsure OA (56 particles)**	
	Particle size (µm)	Percentage (%)	Mean (µm)	Percentage (%)	Mean (µm)	Percentage (%)	Mean (µm)	Percentage (%)	Mean (µm)
Small	<10	44.1	7.04	44.7	7.72	42.6	6.96	48.2	7.18
Medium	10-20	39.8	14.23	34.2	15.21	38.3	14.84	30.4	13.54
Large	>20	16.1	34.49	21.1	39.37	19.1	36.76	21.4	34.70
Mean ± SD (µm)		*14.33 ± 11.56*		*16.97 ± 14.05*		*15.69 ± 12.76*		*15.01 ± 11.45*	
Range (µm)		*4.74-71.96*		*3.79-90.37*		*4.46-74.49*		*4.39-44.61*	

4.2 Visual examination and numerical analysis of particle shape features

Visual shape analysis of wear particles found in human knee joints was performed to compare the distinct shape features in different OA grades. During the shape analysis, several types of particles were identified including spherical, chunky, leaf-like, rod-shaped and irregular shape. More particle images presented in Appendix A.

Spherical particles. Their shape was circular or elliptical. The circular particles were commonly found in healthy joint while the elliptical particles were found in the osteoarthritic joints.

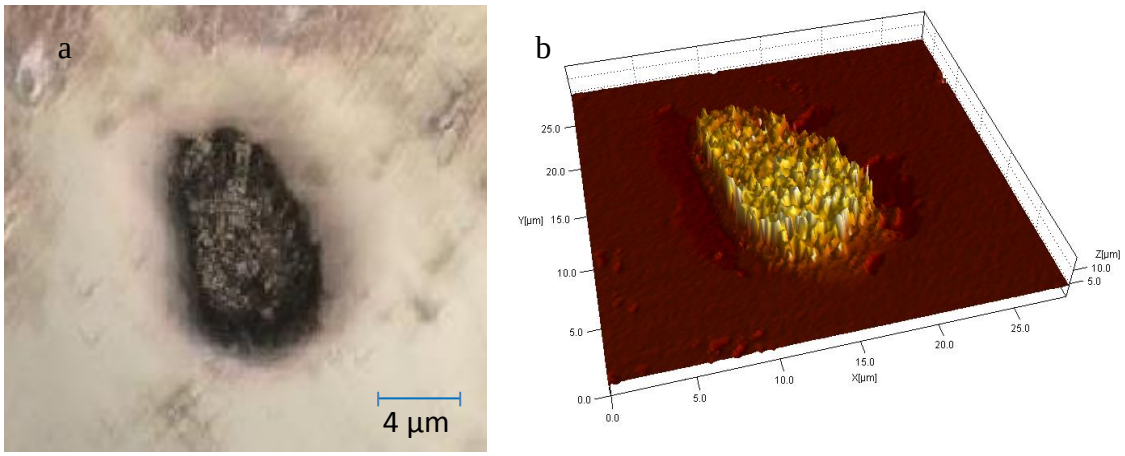

Figure 4.2 LSM images of a spherical wear particle. (a) Colour+larser intensity image of the particle; (b) 3D image of the particle.

Chunky particles. Distinct corners were detected on these particles. Most of them were observed from medium and large particles. They were performed with a cleavage (Figure 4.3b) or spongy type of surface. This type of particle is reported to originate from the deep zone and is commonly found in the OA joints [8]. In the samples, the chunky particle were deteted in the mild and severe OA joints.

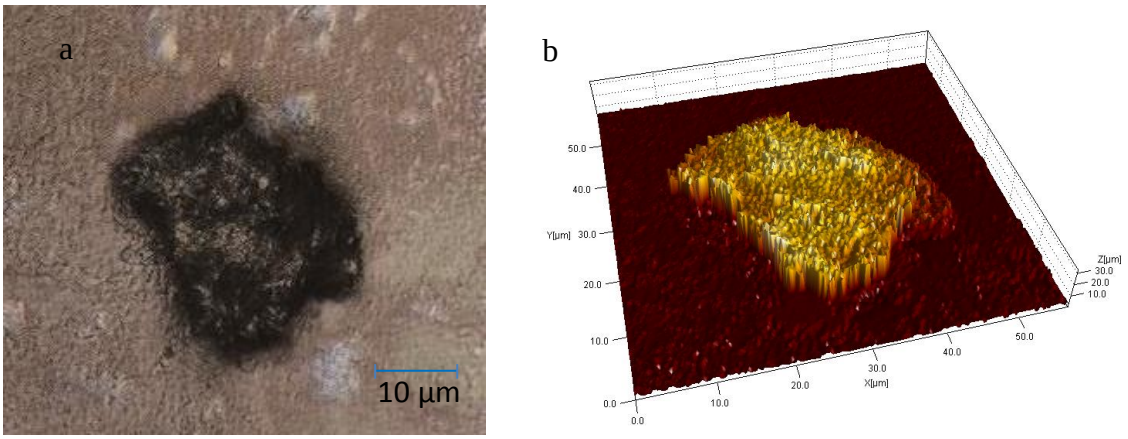

Figure 4.3 LSM images of a chunky wear particle. (a) Colour+larser intensity image of the particle; (b) 3D image of the particle.

Leaf-like particles. Their appearance was flat with a smooth surface topography. They were thought to be produced from the lamina splendens. In the samples, this type of

particles was commonly found in no OA.

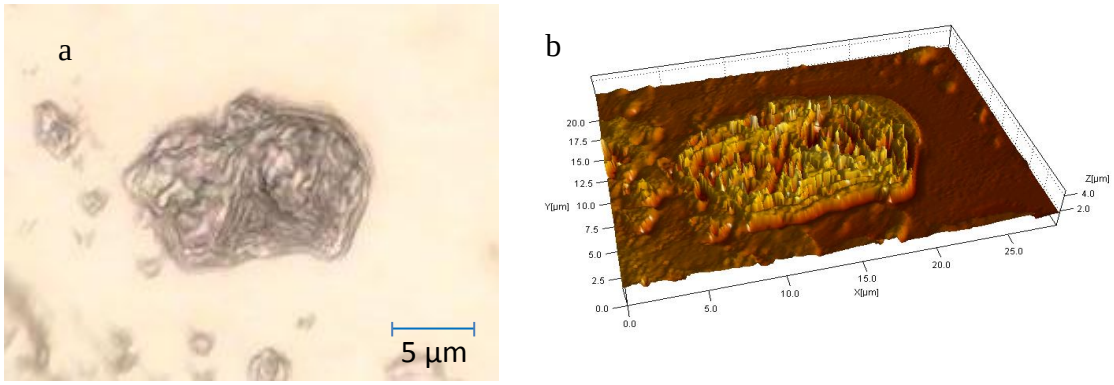

Figure 4.4 LSM images of a leaf-like wear particle. (a) Colour+larser intensity image of the particle; (b) 3D image of the particle.

Rod-shaped particles. They were elongated particles which was reported to originate from the individual collagen strends [68]. In the samples, this type of particles was most abundant in joints with mild OA.

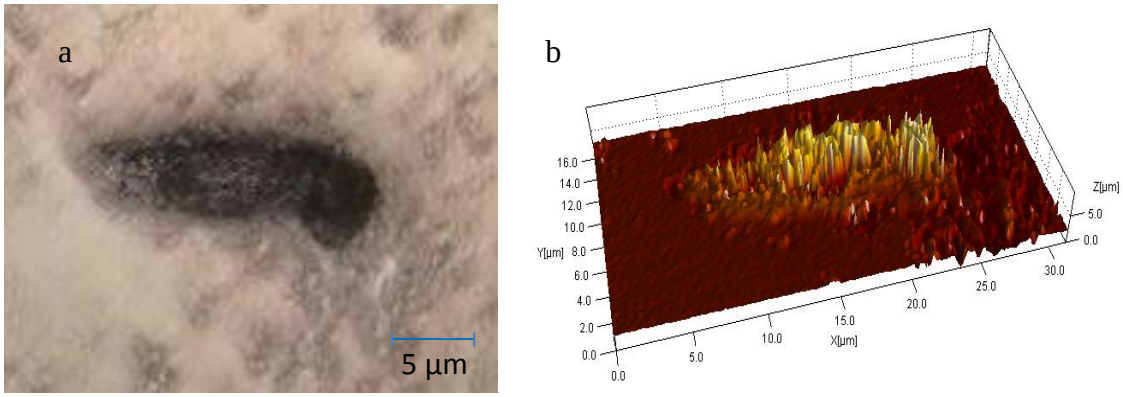

Figure 4.5 LSM images of a rod-shaped wear particle. (a) Colour+larser intensity image of the particle; (b) 3D image of the particle.

Irregular particles. They were irregularly shaped and the surface height was various as well. This type of particles was detected in the severe OA joints.

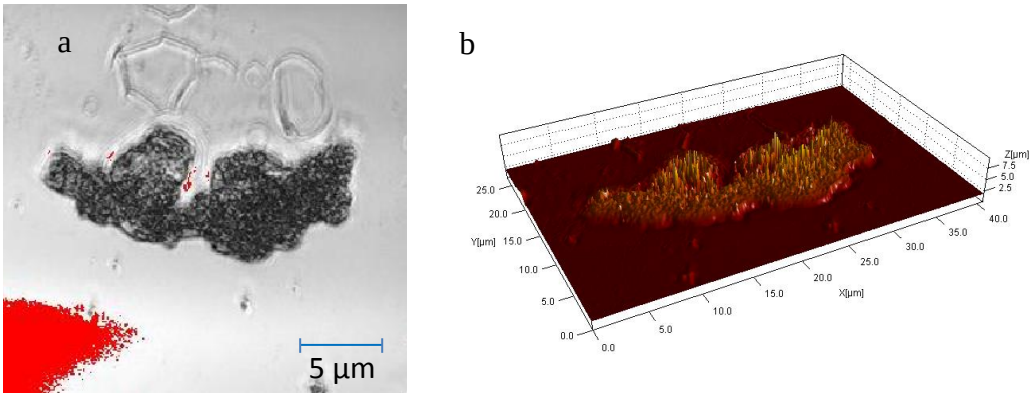

Figure 4.6 LSM images of an irregular wear particle. (a) larser intensity image of the particle; (b) 3D image of the particle.

The shape of particles was visually analysed and the number of each type of particle was counted in Table 4.2. In no OA, leaf-like and rod-shaped particles were the main types of particles, both accounted for 26.9% of the total particles found in non-OA synovial fluid. The leaf-like particles were thin with a maximum height less than 5 µm that mainly contributed to the roughness of the surface. The rod-shaped particles were from the superficial zone with the collagens horizontally oriented [68]. A similar proportion of chunky and spherical particles were present in the non-OA samples representing 19.4% and 16.1% of all particles analysed in the non-OA smaples). Chunky and spherical particles found in healthy joints may generate from fatigue wear. When the degradation continues to OA grade 2, the cartilage became rougher [2]. The distinct edges and cleavage surfaces of the chunky particles were modelled by the contact of the cartilages. This correlated with the increased proportion of chunky particles in mild OA, which accounted for 37.4% of total particles in the mild OA grade, compared to the non-OA samples analysed. When the fissures extended to deep zone with the collagens vertical directed, the wear broke the collagens and irregular particles with randomly shape produced [7]. At this stage, the wear mainly occurred in the deep zone of cartilage because the fissures in the deep zone were the narrowest [68].

Therefore, the percentage of irregular particles increased to the maximum of 17.4% of total particles analysed in the severe OA samples. The wear also happened in the middle zone of the cartilage and the percentage of chunky particles slightly decreased from 37.4 to 32.2%. From the percentage of each of the different shaped particles present in the sample collected from the patient without OA grade classification, it is possible that patient could have either mild or severe OA.

Table 4.2 The number of particles in each OA grade and the percentages of particles in several shapes.

	OA grade (the number of particles)			
Proportion of different shaped particles (%)	No OA (93)	Mild OA (123)	Severe OA (115)	No classification (56)
Spherical	16.1	23.6	19.1	16.1
Chunky	19.4	37.4	32.2	36.4
Leaf-like	26.9	16.3	21.7	22.4
Rod-shaped	26.9	10.6	9.6	12.5
Irregular	10.7	12.1	17.4	12.6

Table 4.3 shows the means of shape parameters in each OA grade. The value of Roundness, Formfactor and Elongation were the most related to the particle shapes. The rod-shaped particles accounted for the majority in non-OA grade, thus the largest mean of Elongation (0.33) was expected. Roundness describes the shape's resemblance to a circle and the Roundness will approach to 1 the closer the shape resembles a circle. Compared to other shapes, spherical and chunky shapes increased the mean value of Roundness. Due to this, the most spherical and chunky particles were detected in mild and severe OA grades (around 50-60% of total particles) which contributed to the mean Roundness of wear particles. Thus, the mean Roundness of mild OA was close to that of severe OA with the non-OA having the smallest mean Roundness. Formfactor was

defined as the ratio of area to perimeter. The elongated or irregular shapes increased the perimeter and further decreased the mean value of Formfactor. Therefore, the non-OA with around 37% of rod-shaped or irregular particles had the smallest mean of Formfactor.

Table 4.3 The means of shape parameters in each OA grade.

	Non-OA	**Mild OA**	**Severe OA**	**No classification**
	Mean ± SD	Mean ± SD	Mean ± SD	Mean ± SD
Area (μm^2)	136 ± 364	229 ± 572	166 ± 318	124 ± 179
Roundness	0.49 ± 0.14	0.57 ± 0.11	0.54 ± 0.12	0.52 ± 0.14
Formfactor	0.36 ± 0.14	0.49 ± 0.16	0.46 ± 0.19	0.47 ± 0.20
Convexity	1.71 ± 0.97	1.52 ± 0.71	1.69 ± 0.88	1.97 ± 1.01
Elongation	0.33 ± 0.16	0.29 ± 0.15	0.30 ± 0.15	0.30 ± 0.15
Solidity	0.88 ± 0.06	0.93 ± 0.03	0.91 ± 0.05	0.90 ± 0.07

4.3 Study of the surface morphologies of particles in each OA grade

The analysis of surface topography of particles was conducted and several roughness levels were identified. The particle surfaces were qualitatively classified as smooth, moderately rough, rough and very rough as shown in Figures 4.7-4.10. The numbers of particle were counted in these levels in each OA grade and the numerical data of the surface texture was analysed.

Smooth particle. Their surface looked like wave with small fluctuation. In this study, some spherical and all the leaf-like particles were including in this type morphology.

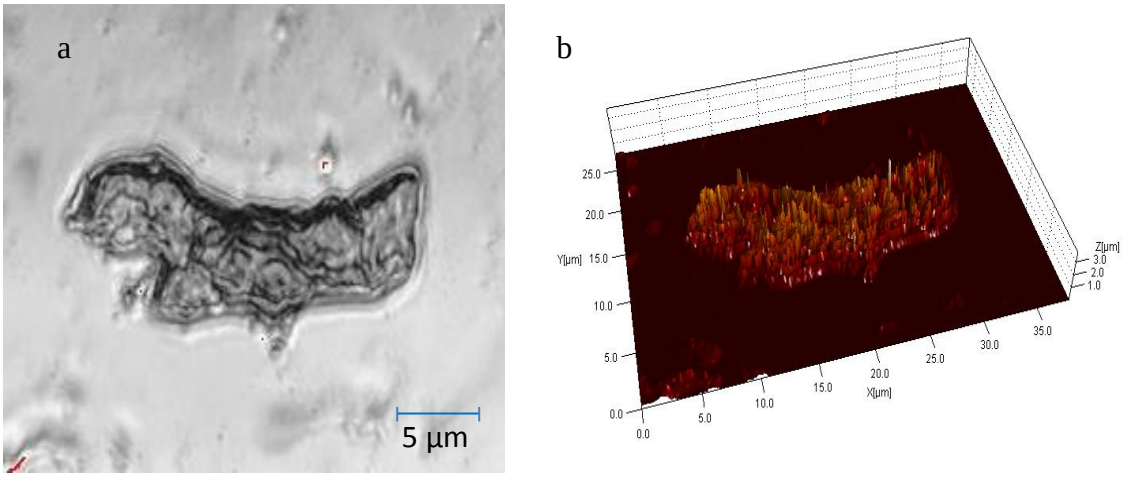

Figure 4.7 A smooth particle. (a) Larser intensity image of the particle; (b) 3D image of the particle.

Moderately rough. Two types of particles were detected in this roughness level: (a) the surface profile showed some even hills or troughs with small variation on the particle surface throughout. In my samples, some chunky particles had this surface feature (Figure 4.8). (b) The surface showed two types of features, smooth surface and small nodules or deep scratches (Figure 4.9). These particles were detected in mild and severe OA grades.

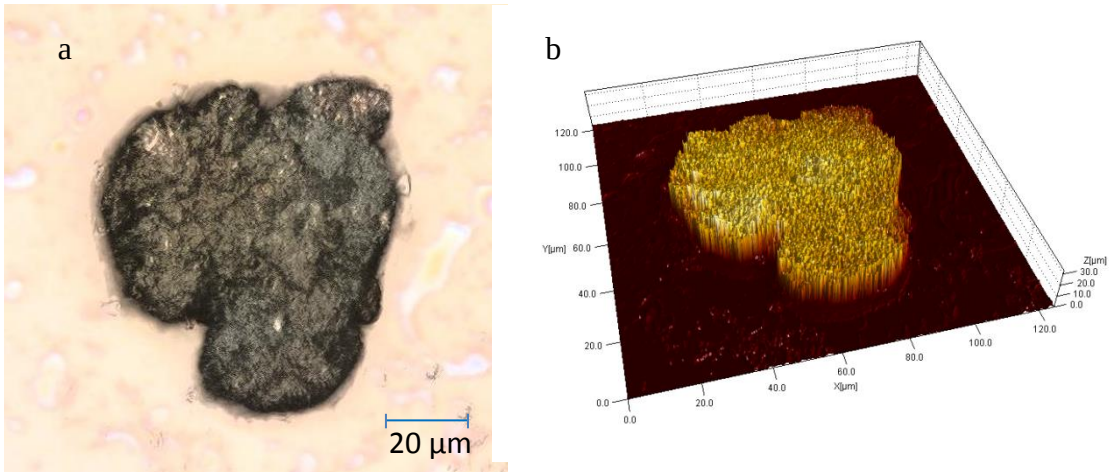

Figure 4.8 A type a moderately rough particle. (a) Colour+larser intensity image of the particle; (b) 3D image of the particle.

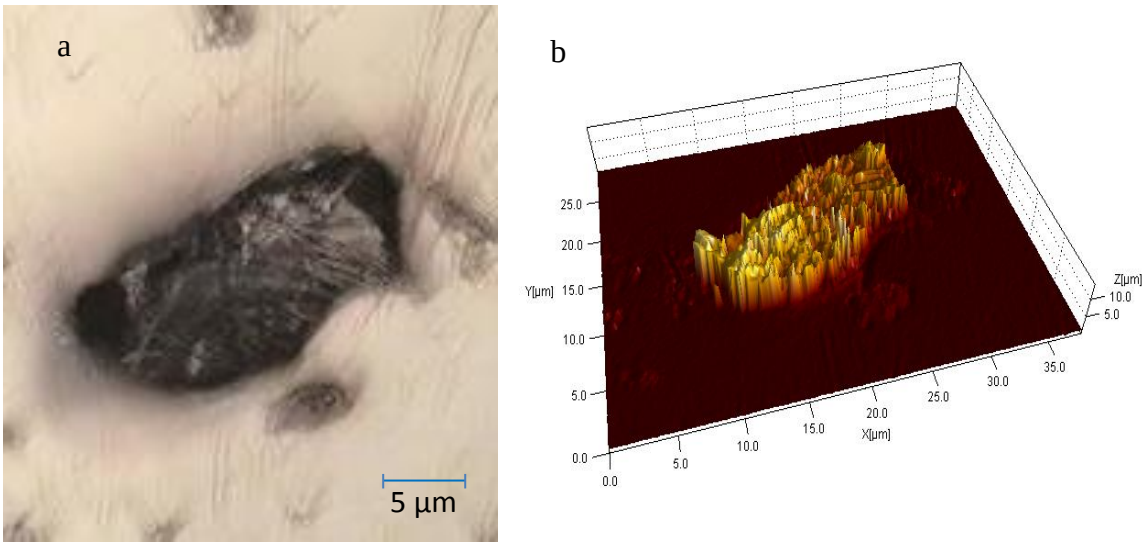

Figure 4.9 A type b moderately rough particle. (a) Colour+larser intensity image of the particle; (b) 3D image of the particle.

*Rough particles.*These particles appeared to have nodules aboundant on the surface (Figure 4.10). This type of particles were detected from some rod-shaped particles and the spherical particles with elliptical shape.

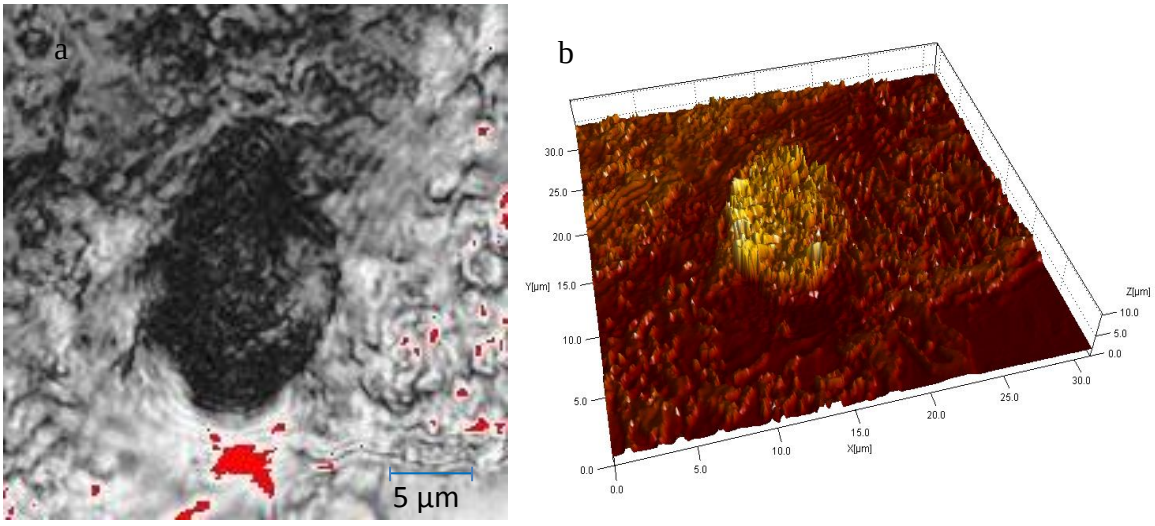

Figure 4.10 A rough particle. (a) Larser intensity image of the particle; (b) 3D image of the particle.

Very rough. They appeared with undulating surface (Figure 4.11). Deep valleys result in cleavages among the particle surfaces [82]. In this study, some irregular particles and few chunky particles had this type of surface.

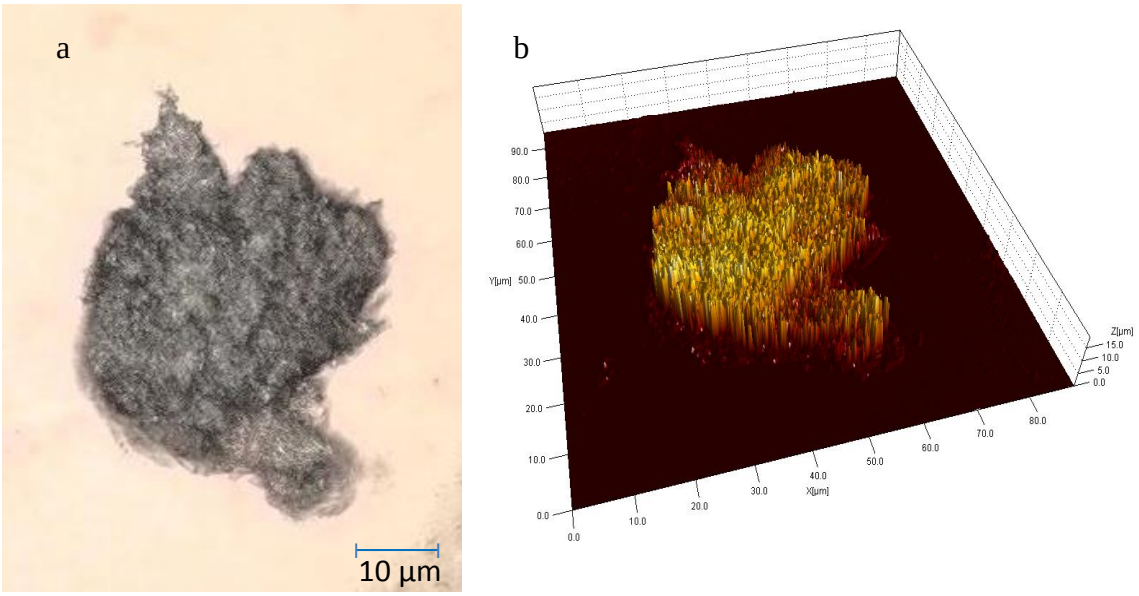

Figure 4.11 A very rough particle. (a) Colour+larser intensity image of the particle; (b) 3D image of the particle.

In Table 4.4, the number of particles with each roughness level were counted. Smooth particles were aboundant in non-OA synovial fluid which reflected minimal wear during healthy joints during normal activities. Other types of particles were also found in healthy joints. Rough and moderately rough particles accounted for approximately 29% and 27% in mild OA, respectively. The percentage of very rough particles found in mild OA approached to the maximum among all OA grades. The very rough particles may have been generated from the rough or moderately rough particles. In the severe OA, the moderately rough particles were aboundant and the percentage of rough and very rough particles decreased from mild OA. The very rough particles always irregularly shaped and they may have been transformed from other types of particles because the surfaces of them were texture mixed.

Table 4.4 The numbers of particles in each OA grade and the percentages of particles in several topographies.

OA grade (the number of particles)	**Non-OA (93)**	**Mild OA (123)**	**Severe OA (115)**	**No classification (56)**
Smooth (%)	32.3	25.2	32.2	32.1
Moderately rough (%)	23.7	26.8	40.0	30.4
Rough (%)	30.0	29.3	15.7	26.8
Very Rough (%)	14.0	18.7	12.2	10.7

The mean of magnitude parameters in each OA grade were calculated and presented in Table 4.5. The mean of the Average roughness was increased and then decreased by the severity of OA, with the mild OA having the largest mean (1267.6 nm). Compared to the non-OA, the increase of very rough particles in mild OA was contributed to the largest mean average roughness and the mean *S10z* as well. In severe OA grade, the mean of Average roughness was close to that in non-OA grade.

Even though less rough particles detected in severe OA grade, moderately rough particles mainly contributed to the mean Average roughness. Spatial parameters revealed that the mild OA had the largest mean roughness and also had the largest mean Density of summits. Texture direction showed that the main texture on the surfaces of particles was clock-wise orientated. Surface area ratio from hybrid parameter indicated the increment of the interfacial surface area relative to the area of the projected flat plane. The mild OA exhibited the largest mean roughness and also had the largest mean Surface area ratio. In the functional parameters, the mild OA grade had the largest Reduced summit height and Core roughness depth that referred to the largest mean roughness.

Table 4.5 The means of height-related parameters in each OA grade.

	Non-OA	**Mild OA**	**Severe OA**	**No classification**
	Mean ± SD	Mean ± SD	Mean ± SD	Mean ± SD
Sa (µm)	1.03 ± 0.64	1.27 ± 0.97	1.01 ± 0.58	0.94 ± 0.66
Ssq (µm)	1.28 ± 0.78	1.58 ± 1.18	1.28 ± 0.70	1.18 ± 0.76
Ssk	-0.087 ± 0.755	0.266 ± 0.776	0.168 ± 0.637	-0.169 ± 0.564
Sku	3.5 ± 1.3	3.8 ± 1.7	3.7 ± 1.3	3.5 ± 0.98
S10z (µm)	6.63 ± 3.76	8.45 ± 5.19	7.41 ± 3.98	6.46 ± 3.74
Sv (µm)	3.30 ± 1.58	3.61 ± 2.43	3.19 ± 1.63	3.10 ± 1.46
Sp (µm)	4.21 ± 2.82	5.77 ± 3.43	5.09 ± 2.84	4.04 ± 2.61
Sds ($1/\mu m^2$)	0.01 ± 0.02	0.03 ± 0.04	0.02 ± 0.04	0.01 ± 0.01
Std (˚)	90.94 ± 65.36	88.66 ± 66.66	82.21 ± 65.96	87.23 ± 63.92
Str20	0.59 ± 0.15	0.59 ± 0.16	0.59 ± 0.15	0.57 ± 0.17
Scl20 (µm)	1.85 ± 1.10	1.98 ± 1.18	1.65 ± 1.11	1.72 ± 0.99
Str37	0.69 ± 0.14	0.69 ± 0.15	0.70 ± 0.14	0.71 ± 0.16
Scl37 (µm)	1.14 ± 0.77	1.28 ± 0.88	0.97 ± 0.78	1.09 ± 0.72
Sdr (%)	2603.6 ± 2442.0	4069.1 ± 4224.1	3525.9 ± 2917.5	2146.1 ± 1566.5
Spk (µm)	1.49 ± 1.70	2.00 ± 1.82	1.60 ± 1.04	1.31 ± 0.87
Sk (µm)	2554.3 ± 1722.9	3182.6 ± 2371.5	2793.4 ± 1820.0	2454.9 ± 1780.7
Svk (µm)	1.28 ± 0.65	1.23 ± 1.81	1.10 ± 0.69	1.31 ± 0.78
Smr1 (%)	13.27 ± 8.93	15.90 ± 9.69	12.68 ± 6.21	11.42 ± 4.42
Smr2 (%)	83.23 ± 8.65	88.05 ± 8.54	87.16 ± 7.31	82.86 ± 6.55

4.4 Summary

387 particles from 25 specimens were captured using LSM. In this chapter, the size distribution was analysed and compared with the results in the literature. The visual analysis of shape and surface roughness indicated several shapes and various roughness

levels.

It was thought that the size distribution of particles was related to their OA grades. This study reports comparable size distributions of the human wear particles with previous research. The small particles are the most abundant in the joints that are not classified as having OA, which is consistent with the previous findings [9]. This study also confirmed the results reported in the previous study that the mean size of particles in healthy synovial fluid is smaller than that in OA synovial fluid. However, the percentage of different sizes in the major dimension did not change with the severity of OA.

From the visual analysis of shape features, the leaf-like and rod-shaped particles were the majority in non-OA grade, while chunky particles were abundant in both mild and severe OA grades. The visual analysis of surface roughness suggested that the mean roughness increased from non-OA to mild OA and then declined in severe OA. Therefore, the shape and surface parameters (including amplitude, spatial, hybrid and functional parameters) could be distinct parameters to differentiate the OA grades and these parameters were used in statistical analyses in chapter 5.

Chapter 5 Statistical analyses to group particles based on surface parameters

The aim of this chapter was to identify the distinct parameters that can describe the common features of particles in the same OA grade and to reveal the differences between particles collected from patients in different OA grades. Further analysis of the differences associated with the wear process based on the data values and images of surfaces was also carried out.

Some of the 29 parameters were selected as distinct parameters to distinguish different OA particles. A correlation study was the first step to identify correlated parameters from 10 shape and 19 surface parameters. The correlated parameters with a larger standard deviation were not analysed further. Secondly, a one-way ANOVA was carried out to compare the differences between patients on each parameter and some parameters were not analysed further if they showed no differences between all patients. Thirdly, discriminant analysis was used to establish linear combinations using multi-parameters based on patients' information. Finally, hierarchical clustering was used to group data by calculating the distances between particles based on the same parameters used in discriminant analysis.

5.1 Correlation study to reduce redundant parameters

A total of 29 parameters (defined in Chapter 3) were used to describe the surface and shape features of particles. For classifying features of particles from different wear

grades in a concise and simple way, the highly correlated parameters identified by Pearson correlation study were not further analysed. More specifically, if two parameters (i.e. *X* and *Y*) were highly correlated, then $Y = aX + b$ (*a* and *b* were both constant), and one of them would be redundant in the grouping method (linear combination in Chapter 5.3). Correlation analysis was conducted in Minitab 17.0.

The correlation coefficient (ρ) is defined as $\rho = \frac{Cov(X,Y)}{\sqrt{Var(X)Var(Y)}}$ [83], where *Cov(X,Y)* is the co-variance of variables *X* and Y and *Var(X)* and *Var(Y)* are the variance of *X* and *Y* respectively. ρ=1 if two parameters are positively correlated in a straight line; inversely, if two parameters are negatively related also in a straight line, then the coefficient equals -1. Normally, if the absolute value of the coefficient is greater than 0.8, two parameters are considered to be highly linearly related. The corresponding hypothesis was also carried out to test whether the correlation coefficient was reliable. The significance level was set to 0.05 and accepted $\rho = 0$ when the p-value was larger than 0.05. The correlation coefficients were calculated from 332 particles. For example, the linear correlation between Average roughness (*Sa*) and Root mean square (*Sq*) is shown in Figure 5.1. The result shows that they are closely correlated with a ρ value of 0.995 (> 0.8) and a p-value of 0. Using the same approach, pairwise correlation was carried out among all 29 parameters.

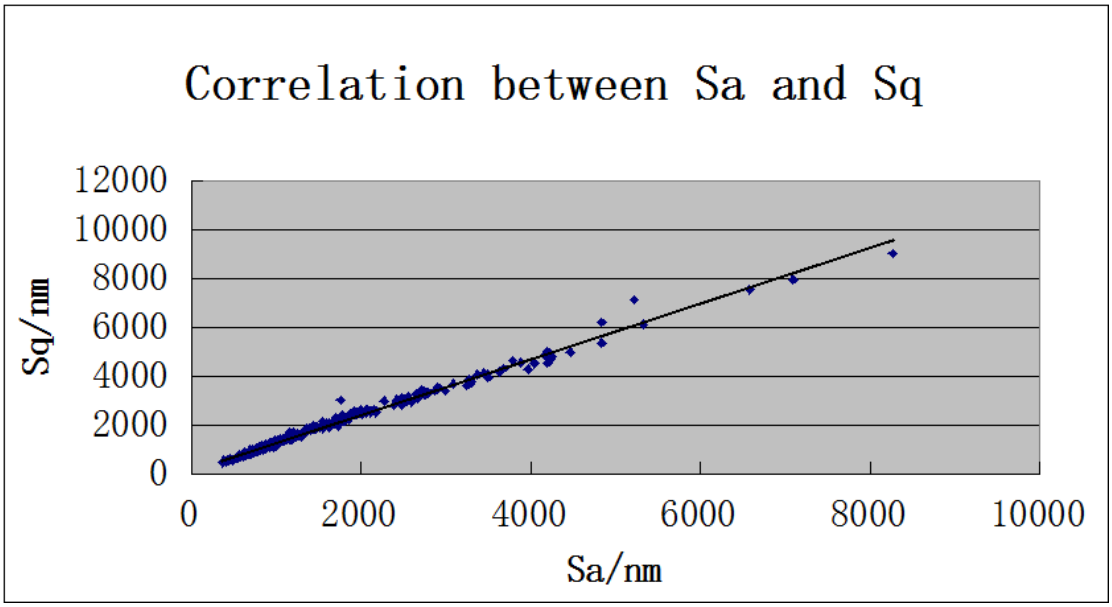

Figure 5.1 The linear correlation between parameter Sa and Sq.

There are two main parameter groups: shape parameters and surface parameters which contain height-related (amplitude) parameters, spatial parameters, hybrid parameter and functional parameters. The Correlation was firstly analysed between the parameters which were in the same group (e.g. amplitude parameters) and decided which parameter was reasonably reduced. Linear correlations between parameters mostly occurred within the same group because they described similar features of particles. Shape parameters were analysed followed by amplitude, spatial, hybrid/functional parameters. The correlation analysis of the hybrid and functional parameters was conducted in one group because Surface area ratio (*Sdr*) was the only hybrid parameter. Once the correlated parameters in each group were removed based on the comparison of their standard deviation (SD), the correlation between selected surface parameters was studied and further reduced the correlated surface parameters. Finally, the correlation between selected shape and surface parameters was conducted. The SDs of the correlated parameters was the first consideration to decide which parameter would be selected.

The parameters with a smaller SD were kept for further analysis in section 5.2, because a smaller SD indicated that the data was more stable and a smaller SD also indirectly reduced the p-value which was applied in the one-way ANOVA [84].

In Table 5.1, the correlation study was firstly applied to analyse the linear correlation within shape parameters and the coefficients greater than 0.8 were marked in red. Length (*L*) was correlated to Area *(A*) with a ρ value equalled to 0.829 and a p-value of 0 (<0.05). From definition of these two parameters, *A* would normally increase as *L* increases, thus *L* is positively correlated to *A*. Although they were not in the same magnitude (the unit of *A* was nm^2 and that of *L* was nm), it was possible to compare values over different magnitudes. The residual distribution of *A* (Figure 5.2c) was steeper than that of *L* (Figure 5.3c). In other words, the values of *A* were closer to the mean while some values of *L* were extremely small or large. Thus the SD of *A* was relatively smaller than that of *L*. Therefore, *A* was selected for further analysis while *L* was deleted. Material volume (*Mv*) was strongly correlated to Net volume (*Nv*) with the ρ = 0.999 which was acceptable because p-value = 0 (<0.05). Void volume (*Vv*) and *Mv* were the volumes of all points lower than the mean plane and higher than that plane, respectively and *Nv* = *Mv* – *Vv*. Therefore, a high correlation was expected. They were in the same magnitude but with different SD. The SD of *Nv* (5242 μm^3) was greater than that of *Mv* (5224 μm^3). Therefore material volume (*Mv*) was kept. Roundness (*R*) was reasonably correlated to Elongation (*E*) in a negative trend according to the parameter definition, i.e. The *R* of an elongated shape was small while its *E* was large. The SD of *E* (0.150538) was larger than that of *R* (0.125659). Therefore, roughness (*R*) was selected and elongation (*E*) was not analysed further. A total of 7 shape parameters were kept for further correlation analysis. Area (*A*), Roughness (*R*), Formfactor (*FF*),

Convexity (*C*) and Solidity (*S*) were selected to describe the area and circular shape of particles. Material volume (*Mv*) and Void volume (*Vv*) were kept for further correlation analysis and reflected the area, peak height and valley depth of particles.

Table 5.1 Correlation analysis within shape parameters: Data in red indicates coefficients greater than 0.8.

		Shape				
		Area (*A*)	Length (*L*)	Material volume (*Mv*)	Void volume (*Vv*)	Net volume (*Nv*)
Shape	Length (*L*)	0.829 (0)				
	Material volume (*Mv*)	0.765 (0)	0.417 (0)			
	Void volume (*Vv*)	0.314 (0)	0.413 (0)	0.032 (0.536)		
	Net volume (*Nv*)	0.751 (0)	0.398 (0)	0.999 (0)	-0.016 (0.755)	
	Roundness (*R*)	0.056 (0.273)	-0.203 (0)	0.077 (0.133)	-0.016 (0.755)	0.077 (0.129)
	Formfactor (*FF*)	-0.119 (0.019)	-0.356 (0)	0.013 (0.792)	-0.128 (0.011)	0.020 (0.701)
	Convexity (*C*)	0.156 (0.002)	0.359 (0)	0.033 (0.522)	0.153 (0.003)	0.025 (0.619)
	Elongation (*E*)	-0.039 (0.445)	0.190 (0)	-0.071 (0.163)	-0.006 (0.910)	-0.071 (0.165)
	Solidity (*S*)	0.176 (0.001)	0.113 (0.027)	0.088 (0.084)	0.094 (0.063)	0.083 (0.101)
		Roundness (*R*)	Formfactor (*FF*)	Convexity (*C*)	Elongation (*E*)	
	Formfactor (*FF*)	0.604 (0)				
	Convexity (*C*)	-0.293 (0)	-0.409 (0)			
	Elongation (*E*)	-0.828 (0)	-0.282 (0)	0.090 (0.075)		
	Solidity (*S*)	0.536 (0)	0.606 (0)	-0.322 (0)	-0.190 (0)	
The data were presented as the format of Pearson correlation coefficient and the p-value in the brackets.						

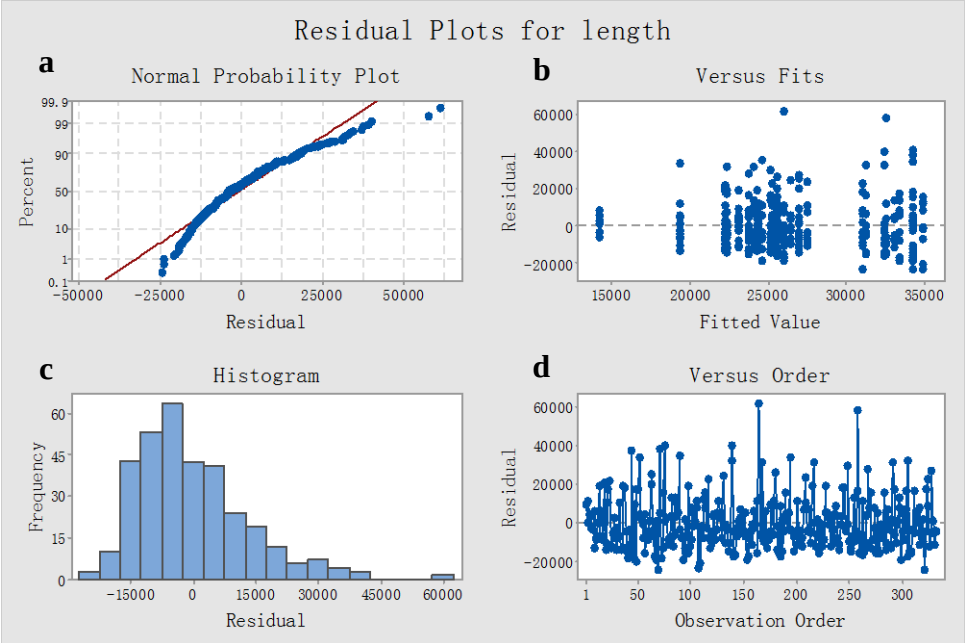

Figure 5.2 The residual plots for Length (L): (a) The normal probability plot, (b) The residual versus fits plot, (c) Histogram, and (d) The residual versus the order of the data.

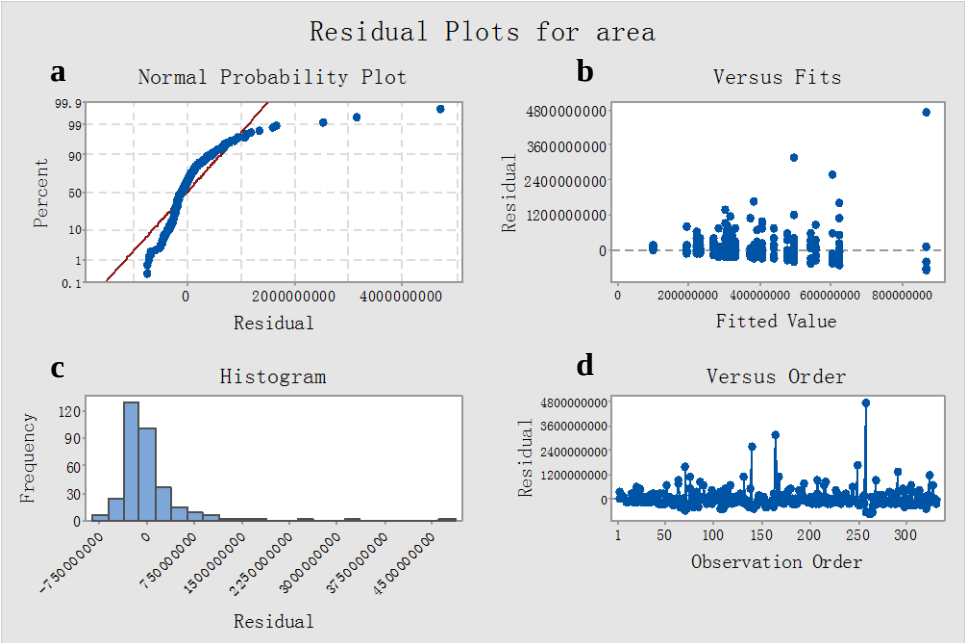

Figure 5.3 The residual plots for Area (A): (a) The normal probability plot, (b) The residual versus fits plot, (c) Histogram, and (d) The residual versus the order of the data.

Table 5.2 indicates the correlation study within amplitude parameters. Ten point height (*S10z*) was strongly linearly correlated to Average roughness (*Sa*), Root mean square (*Sq*), Max valley depth (*Sv*) and Max peak height (*Sp*); *Sa* was also considered to be linearly correlated to *Sq*, *Sv* and *Sp*; *Sq* was correlated to *Sv* and *Sp*. Actually, *S10z*, defined as the average height of 5 highest plus 5 lowest local points, contained the information of *Sp* and *Sv* and these 10 points for *S10z* calculation were the main contributors to the calculation of *Sa* and *Sq*. Therefore, *S10z* was reasonably correlated to these 4 parameters. *S10z*, *Sa*, *Sq*, *Sv* and *S*p were not in a same magnitude, the SDs of each of them therefore transformed to a ratio of the mean values (*d = SD/mean*). Ten point height (*S10z*) with the smallest *d* was selected (d_{S10z}=0.488, d_{Sa}=0.738, d_{Sq}=0.683, d_{Sv}=0.603 and d_{Sp}=0.496). Surface skewness (*Ssk*) and Surface kurtosis (*Sku*) were not correlated to other parameters because they were applied to describe asymmetry of the height distribution of surfaces and the presence of inordinately high peaks/ deep valleys, respectively. The correlation coefficient between *Ssk* and *Sku* was only 0.394. The absolute value of coefficient between *Sku* and *Sp* was smaller than that between *Sku* and *Sv* due to more deep valleys present on the surfaces of particles and more particles from severe OA were expected. To conclude, 3 amplitude parameters including Ten point height (*S10z*), Surface skewness (*Ssk*) and Surface kurtosis (*Sku*), were selected to indicate the height distribution of particle surfaces.

Table 5.2 Correlation analysis within amplitude parameters: Data in red indicates coefficients greater than 0.8.

		Amplitude		
		Average roughness (*Sa*)	Root mean square (*Sq*)	Surface skewness (*Ssk*)
Amplitude	Root mean square (*Sq*)	0.994 (0)		
	Surface skewness (*Ssk*)	0.164 (0.001)	0.184 (0)	
	Surface kurtosis (*Sku*)	-0.269 (0)	-0.218 (0)	0.394 (0)
	Ten point height (*S10z*)	0.918 (0)	0.937 (0)	0.273 (0.438)
	Max valley depth (*Sv*)	0.813 (0)	0.819 (0)	-0.179 (0)
	Max peak height (*Sp*)	0.801 (0)	0.826 (0)	0.514 (0)
		Surface kurtosis (*Sku*)	Ten point height (*S10z*)	Max vally depth (*Sv*)
	Ten point height (*S10z*)	-0.104 (0.042)		
	Max valley depth (*Sv*)	-0.261 (0)	0.827 (0)	
	Max peak height (*Sp*)	0.069 (0.176)	0.921 (0)	0.572 (0)
The data were presented as the format of Pearson correlation coefficient and the p-value in the brackets.				

Table 5.3 illustrates the correlation analysis within spatial parameters. Length at 37% (*Scl37*) was strongly correlated to correlation length at 20% (*Scl20*) with the value of ρ = 0.971. The definition of *Scl20* and *Scl37* were the auto-correlation length (ACF) in a fastest decay to 20% and 37%, respectively. From the surface inspection in section 4.3, only the isotropic surfaces without the directional texture presented on the particles. Therefore, *Scl37* was highly linearly correlated to *Scl20*. *Scl20* with a larger SD (1342.23 nm) was not used for further analysis while *Scl37* (SD=983.541 nm) was kept

for further analysis. Texture aspect ratio at 20% (*Str20*) was not highly correlated to texture aspect ratio at 37% (*Str37*) with the value of ρ = 0.628 as some particle surface appeared complex texture (i.e. nodules, scratches and troughs). Density of summits (*Sds*) and Texture direction (*Std*) also were not correlated to other members in the spatial parameters. *Std* describes the texture direction of dominant lay and *Sds* indicates the density of summits over the surface. 5 spatial parameters including Density of summits (*Sds*), Texture direction (*Std*), Correlation length at 37% (*Scl37*), Texture aspect ratio at 20% (*Str20*) and Texture aspect ratio at 37% (*Str37*) were selected as the descriptors of dominant texture of particles.

Table 5.3 Correlation analysis within spatial parameters: Data in red indicates coefficient greater than 0.8.

		Spatial		
		Density of summits (*Sds*)	Texture direction (*Std*)	Correlation length at 20% (*Scl20*)
Spatial	Texture direction (*Std*)	0.026 (0.607)		
	Correlation length at 20% (*Scl20*)	0.267 (0)	0.102 (0.044)	
	Texture aspect ratio at 20% (*Str20*)	0.081 (0.113)	-0.022 (0.660)	0.077 (0.129)
	Correlation length at 37% (*Scl37*)	0.224 (0)	0.114 (0.025)	0.971 (0)
	Texture aspect ratio at 37% (*Str37*)	0.164 (0.001)	-0.030 (0.562)	-0.060 (0.241)
		Texture aspect ratio at 20% (*Str20*)	Correlation length at 37% (*Scl37*)	
	Correlation length at 37% (*Scl37*)	0.026 (0.614)		
	Texture aspect ratio at 37% (*Str37*)	0.628 (0)	-0.073 (0.151)	
The data were presented as the format of Pearson correlation coefficient and the p-value in the brackets.				

No correlations were found between hybrid and functional parameters or within functional parameters (Table 5.4). Surface area ratio (*Sdr*) from the hybrid parameters was affected by both the texture amplitude and spacing. Reduced summit height (*Spk*), Core roughness depth (*Sk*) and Reduced valley depth (*Svk*) reflected the peak high, core roughness and valley depth, respectively. *Sk* also presented the main height over the surfaces, thus *Sdr* was roughly correlated to *Sk* with a ρ = 0.738 but still less than 0.8. Therefore, all 6 parameters in the functional and hybrid parameter were kept for the

correlation studies between groups.

Table 5.4 Correlation analysis between hybrid/functional parameters: No Data greater than 0.8.

		Hybrid	**Functional**	
		Surface area ratio (*Sdr*)	Reduced summit height (*Spk*)	Core roughness depth (*Sk*)
Functional	Reduced summit height (*Spk*)	0.762 (0)		
	Core roughness depth (*Sk*)	0.738 (0)	0.471 (0)	
	Reduced valley depth (*Svk*)	0.172 (0.001)	-0.021 (00.676)	0.367 (0)
	Peak material ratio (*Smr1*)	0.143 (0.005)	0.401 (0)	-0.087 (0.088)
	Valley material ratio (*Smr2*)	-0.035 (0.491)	-0.020 (0.695)	-0.027 (0.600)
			Reduced valley depth (*Svk*)	Peak material ratio (*Smr1*)
	Peak material ratio (*Smr1*)		-0.302 (0)	
	Valley material ratio (*Smr2*)		-0.053 (0.300)	0.051 (0.322)
The data were presented as the format of Pearson correlation coefficient and the p-value in the brackets.				

The correlation analysis between several surface parameters is presented in Table 5.5A and 5.5B. *Spk*, *Sk* and *Svk* were calculated from the area ratio curve (see Figure 2.12) and the value of *Sk* was also affected by *Spk* and *Svk*. *Sk* was highly correlated to *S10z* with the coefficient of 0.861 and a p-value of 0. *Sk* represented the core roughness of the surface and had a similar physical meaning with *S10z*, therefore the high correlations

were expected and Core roughness depth (*Sk*) was not used for further analysis because of larger *d* than *S10z* (d_{Sk}=0.684 > 0.488). *Spk* and *Svk* indicate summit height and valley depth based on the area ratio curve, and also contained the information of *Sp* and *Sv* (amplitude parameters) respectively, which were highly correlated to *S10z*. Thus *Spk* and *Svk* were slightly correlated to *S10z* with the coefficients 0.724 and 0.448 respectively. *Sdr* was highly correlated to *S10z* with the coefficient of 0.801 and a p-value of 0. *Sdr* revealed the ratio of area and the surface area and the *S10z* contributed to the surface area to some extent. Therefore the high correlation between *S10z* and *Sdr* was expected and *Sdr* with a large value of *d* (0.99>0.488) was not used for further analysis. Spatial parameters were related to spatial anisotropy, therefore the coefficients between spatial and amplitude parameters were all less than 0.8. Table 5.5 indicated that no linear correlations between Spatial and functional/hybrid parameters were observed. The calculation of functional parameters was based on the area ratio curve but the spatial parameters focused on the surface isotropy and dominant lay.

Table 5.6A and 5.6B present the correlation analysis between 7 selected shape and 12 selected surface parameters and the results indicate that no highly linear correlations between shape and surface parameters were observed. Some of them were considered to be independent of other parameters, for example there was no correlation between Surface skewness (*Ssk*) and Area (*A*). The coefficient between *A* and *Ssk* was just 0.055 and the corresponding p-value equalled to 0.279. In other words, the hypothesis test accepted $\rho = 0$ and *A* was not linearly correlated with *Ssk*. The results indicate that the changes in shape parameters would not affect the changes in surface parameters in a linear trend.

Table 5.5A Correlation analysis between remaining surface parameters: Data in red indicates coefficients greater than 0.8.

		Amplitude		
		Surface skewness (*Ssk*)	Surface kurtosis (*Sku*)	Ten point height (*S10z*)
Spatial	Density of summits (*Sds*)	0.156 (0.002)	-0.038 (0.458)	0.461 (0)
	Texture direction (*Std*)	-0.017 (0.742)	-0.003 (0.957)	0.126 (0.013)
	Texture aspect ratio at 20% (*Str20*)	0.179 (0)	0.025 (0.622)	0.102 (0.045)
	Correlation length at 37% (*Scl37*)	0.068 (0.182)	-0.204 (0)	0.727 (0)
	Texture aspect ratio at 37% (*Str37*)	0.144 (0.005)	0.085 (0.093)	0.034 (0.505)
Hybrid	Surface area ratio (*Sdr*)	0.272 (0)	-0.154 (0.002)	0.801 (0)
Functional	Reduced summit height (*Spk*)	0.537 (0)	0.101 (0.048)	0.724 (0)
	Core roughness depth (*Sk*)	0.135 (0.008)	-0.358 (0)	0.861 (0)
	Reduced valley depth (*Svk*)	-0.425 (0)	-0.140 (0.006)	0.448 (0)
	Peak material ratio (*Smr1*)	0.596 (0)	0.374 (0)	0.098 (0.054)
	Valley material ratio (*Smr2*)	0.038 (0.455)	0.030 (0.552)	-0.041 (0.425)
The data were presented as the format of Pearson correlation coefficient and the p-value in the brackets.				

Table 5.5B Correlation analysis between remaining surface parameters: Data in red indicates coefficients greater than 0.8.

		Spatial		
		Texture direction (*Std*)	Texture aspect ratio at 20% (*Str20*)	Correlation length at 37% (*Scl37*)
Hybrid	Surface area ratio (*Sdr*)	0.117 (0.021)	0.095 (0.062)	0.408 (0)
Functional	Reduced summit height (*Spk*)	0.118 (0.020)	0.125 (0.014)	0.458 (0)
	Core roughness depth (*Sk*)	0.077 (0.132)	0.039(0.445)	0.691 (0)
	Reduced valley depth (*Svk*)	0.132 (0.009)	-0.030 (0.557)	0.500 (0)
	Peak material ratio (*Smr1*)	0.003 (0.960)	0.076 (0.135)	0.074 (0.144)
	Valley material ratio (*Smr2*)	0.010 (0.846)	0.026 (0.615)	-0.036 (0.481)
		Correlation length at 37% (*Scl37*)	Texture aspect ratio at 37% (*Str37*)	
Hybrid	Surface area ratio (*Sdr*)	0.434 (0)	0.024 (0.640)	
Functional	Reduced summit height (*Spk*)	0.452 (0)	0.057 (0.265)	
	Core roughness depth (*Sk*)	0.722 (0)	-0.043 (0.401)	
	Reduced valley depth (*Svk*)	0.503 (0)	0.070 (0.172)	
	Peak material ratio (*Smr1*)	0.074 (0.144)	0.039 (0.443)	
	Valley material ratio (*Smr2*)	-0.036 (0.481)	-0.034 (0.511)	
The data were presented as the format of Pearson correlation coefficient and the p-value in the brackets.				

Table 5.6A Correlation analysis between selected shape and surface parameters: No data greater than 0.8.

		Shape			
		Roundness (R)	Formfactor (*FF*)	Convexity (*C*)	Solidity (*S*)
Amplitude	Surface skewness (*Ssk*)	0.116 (0.023)	-0.005 (0.929)	0.064 (0.210)	-0.109(0.033)
	Surface kurtosis (*Sku*)	0.120 (0.019)	0.139 (0.006)	-0.024 (0.640)	-0.091 (0.072)
	Ten point height (*S10z*)	0.062 (0.221)	-0.225 (0)	0.196 (0)	-0.029 (0.571)
Spatial	Density of summits (*Sds*)	0.023 (0.656)	0.204 (0)	0.209 (0)	0.023 (0.656)
	Texture direction (*Std*)	0.036 (0.481)	-0.043 (0.397)	0.066 (0.196)	-0.082 (0.107)
	Texture aspect ratio at 20% (*Str20*)	0.232 (0)	-0.057 (0.266)	0.121 (0.018)	-0.318 (0)
	Correlation length at 37% (*Scl37*)	0.099 (0.052)	-0.097 (0.057)	0.057 (0.266)	-0.072 (0.159)
	Texture aspect ratio at 37% (*Str37*)	0.165 (0.001)	-0.094 (0.065)	0.118 (0.021)	-0.266 (0)
Functional	Reduced summit height (*Spk*)	0.068 (0.184)	-0.133 (0.009)	0.109 (0.032)	-0.047 (0.361)
	Reduced valley depth (*Svk*)	0.054 (0.285)	-0.036 (0.048)	0.039 (0.439)	-0.050 (0.322)
	Peak material ratio (*Smr1*)	0.078 (0.128)	0.059 (0.245)	-0.075 (0.140)	-0.066 (195)
	Valley material ratio (*Smr2*)	-0.090 (0.078)	-0.091 (0.074)	0.074 (0.145)	0.034 (0.499)
The data were presented as the format of Pearson correlation coefficient and the p-value in the brackets.					

Table 5.6B Correlation analysis between selected shape and surface parameters: No data greater than 0.8.

		Shape			
		Area (*A*)	Material volume (*Mv*)	Void volume (*Vv*)	
Amplitude	Surface skewness (*Ssk*)	0.055 (0.279)	-0.094 (0.066)	0.045 (0.376)	
	Surface kurtosis (*Sku*)	-0.020 (0.695)	0 (0.998)	-0.104 (0.042)	
	Ten point height (*S10z*)	0.574 (0)	0.408 (0)	0.299 (0)	
Spatial	Density of summits (*Sds*)	0.527 (0)	0.173 (0.001)	0.298 (0)	
	Texture direction (*Std*)	0.084 (0.098)	0.087 (0.089)	0.098 (0.055)	
	Texture aspect ratio at 20% (*Str20*)	0.054 (0.294)	0.029 (0.574)	0.057 (0.264)	
	Correlation length at 37% (*Scl37*)	0.579 (0)	0.448 (0)	0.333 (0)	
	Texture aspect ratio at 37% (*Str37*)	0.072 (0.158)	0.015 (0.764)	0.030 (0.560)	
Functional	Reduced summit height (*Spk*)	0.231 (0)	0.097 (0.056)	0.128 (0.012)	
	Reduced valley depth (*Svk*)	0.573 (0)	0.774 (0)	0.151 (0.003)	
	Peak material ratio (*Smr1*)	0.003 (0.959)	-0.037 (0.474)	-0.054 (0.288)	
	Valley material ratio (*Smr2*)	-0.006 (0.905)	-0.005 (0.927)	0.001 (0.979)	
The data were presented as the format of Pearson correlation coefficient and the p-value in the brackets.					

To conclude, in Table 5.8 a total of 19 parameters were selected for further analysis in section 5.2. The parameter include *A*, *R*, *FF*, *C*, *S*, *Mv* and *Vv* from shape parameter

group, *S10z, Ssk, Sku* from amplitude parameters, *Scl37, Str20, Str37, Sds* and *Std* from spatial parameters and *Spk, Svk, Smr1, Smr2* from functional parameters.

Table 5.7 Selected parameters from shape and surface parameters.

Shape parameters	Area (*A*), Roundness (*R*), Formfactor (*FF*), Convexity (*C*), Solidity (*S*), Material volume (*Mv*), Void volume (*Vv*)
Amplitude parameters	Ten point height (*S10z*), Surface skewness (*ssk*), Surface kurtosis (*Sku*)
Spatial parameters	Density of summits (*Sds*), Texture direction (*Std*), Correlation length at 37% (*Scl37*), Area aspect ratio at 20% (*Str20*), Area aspect ratio at 37% (*Str37*)
Functional parameters	Reduced summit height (*Spk*), Reduced valley depth (*Svk*), Peak material ratio (*Smr1*), Valley material ratio (*Smr2*)

5.2 One-way ANOVA

One-way ANOVA is a statistical method used to compare the differences between patients based on the analysis of the variance. In this section, one-way ANOVA was used to compare single parameters and was carried out to further reduce common parameters which showed no differences between all patients.

The ANOVA model is based on several assumptions including that the data are from random samples and the residual should fit a normal distribution [84]. Particles were randomly captured and a data transformation on the response was required when the residual was not normally distributed. All the data requirements and ANOVA analysis was performed in Minitab 17.0.

5.2.1 Data transformation to normal distribution

The trend of some parameters presented by the residual suggested that the log-function (Log_{10}) was a suitable function to transform the data, making the residual homogeneously distributed. Figures 5.4 and 5.5 illustrate the distribution of the residuals of *S10z* parameter for original and transformed data, respectively. Four graphs are contained in both Figures 5.4 and 5.5: graph a is the normal probability plot used to assess the normal distribution of data; graph b is the residual versus fits for evaluating the quality of the residual dispersion and identifying the optimal transformation if it is required; graph c is the histogram of the residual to confirm whether the residual fits a normal distribution; graph d is the residual versus the order to evaluate the performance of data according to the treatment combination. From Figure 5.4a, the residual of the *S10z* values does not completely fit the straight line, indicating that the data does not follow a normal distribution. To obtain a homogeneous distribution, the data was transformed by the function log_{10}. Figure 5.5a shows that the transformed data mostly fits a straight line of the normal probability. The same step was carried out for all parameters except *Smr2*. 8 parameters were homogeneous distribution (an example in Figure 5.6) and the distribution of *Smr2* was distinctive. 1- *Smr2* reflected the percentage of valleys over the surface. The scratches on the surfaces of some moderately rough or very rough particles resulted in the deep valleys which resulted in small *Smr2*. Therefore, the percent of some points in the left tail of the residual plot for *Smr2* (Figure 5.7a) was higher that than the normal percentage and exponential function (e^x) would be a suitable way to transform the data into e^{Smr2}% ($e^{Smr2}\% = e^{Smr2/100}$). As depicted in Figure 5.8a, e^{Smr2}% was presented as a homogeneous distribution. To conclude, *logS10z*, *logArea*, *logMv*, *Roundness*, *logScl37*, *logConvexity*, *logSku*, *logSds*,

logSpk, *logSmr1*, *logFormfactor*, *Svk*, *Std*, *Str20*, *Str37*, *Vv*, *Solidity*, *Ssk* and e^{Smr2}% were normally distributed.

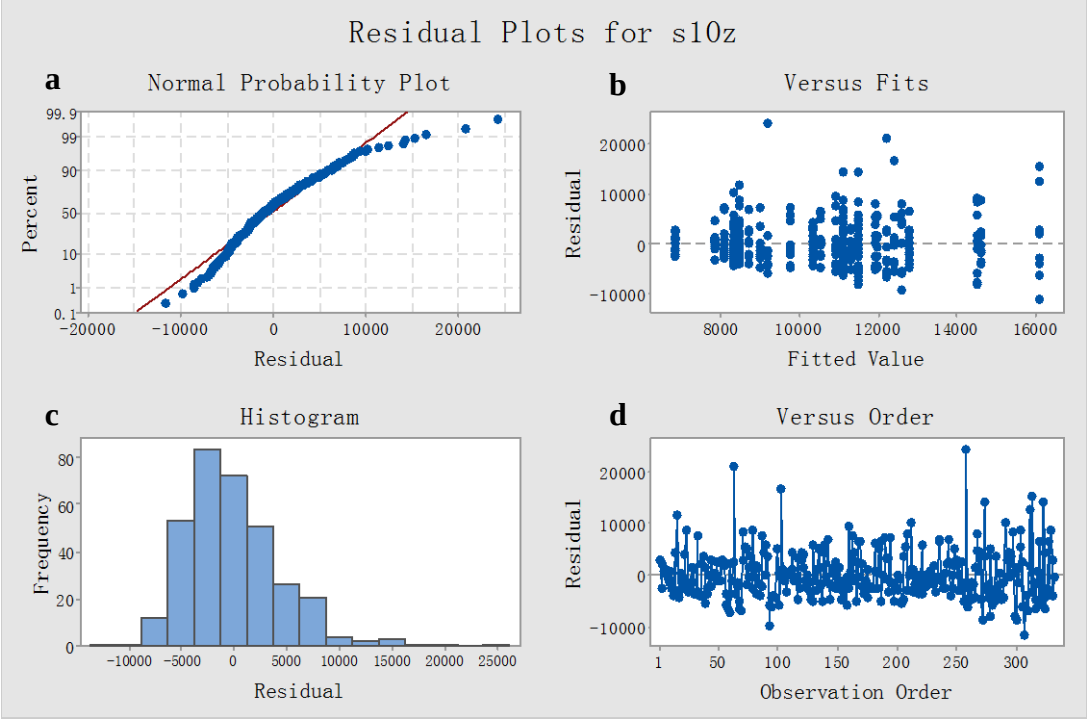

Figure 5.4 Residual plot of S10z. (a) The normal probability plot, (b) The residual versus fits plot, (c) Histogram, and (d) The residual versus the order of the data.

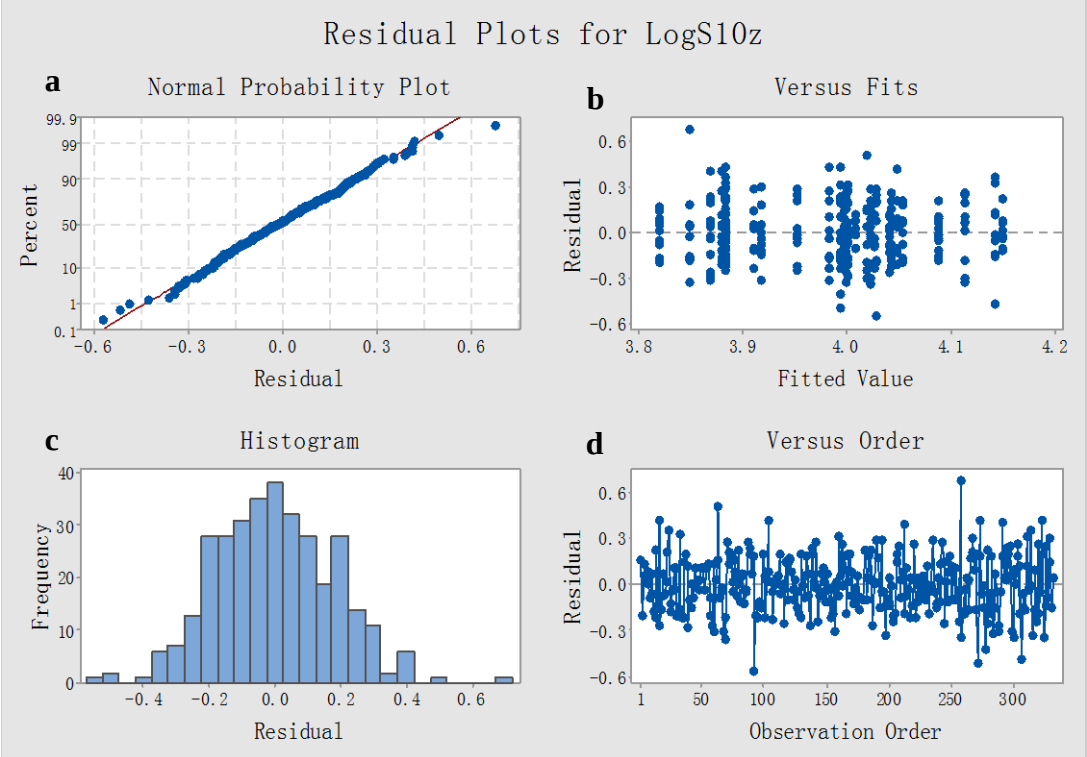

Figure 5.5 Residual plot of logS10z. (a) The normal probability plot, (b) The residual versus fits plot, (c) Histogram, and (d) The residual versus the order of the data.

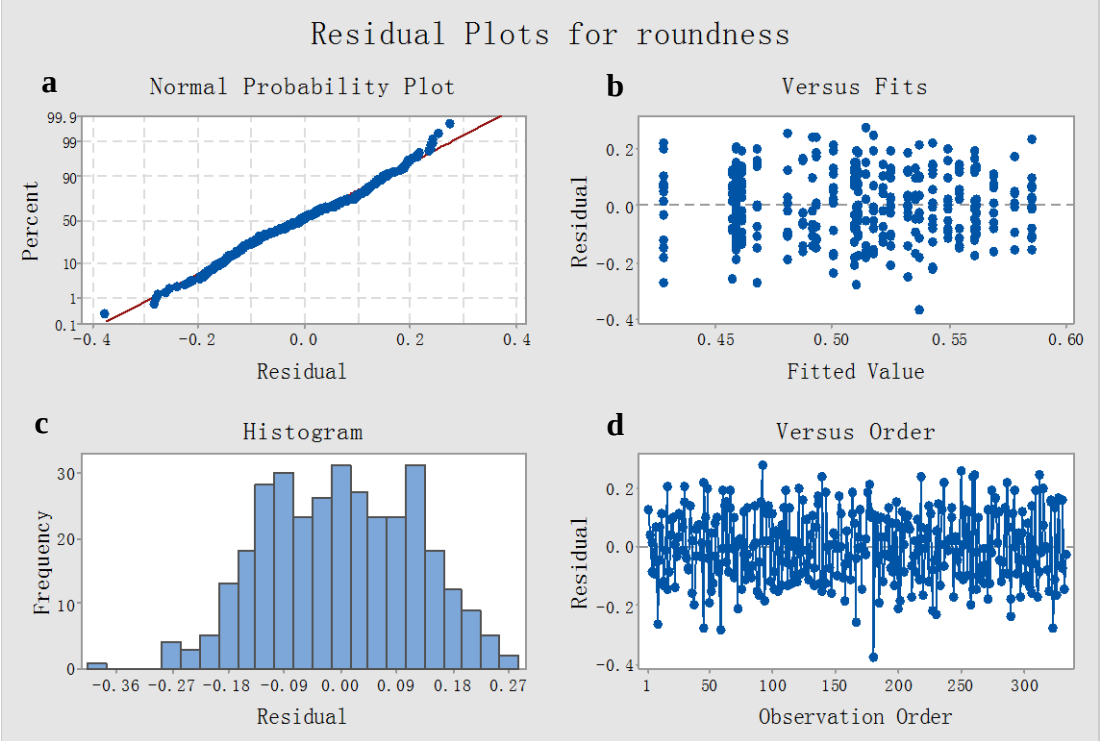

Figure 5.6 Residual plot of Roundness. (a) The normal probability plot, (b) The residual versus fits plot, (c) Histogram, and (d) The residual versus the order of the data.

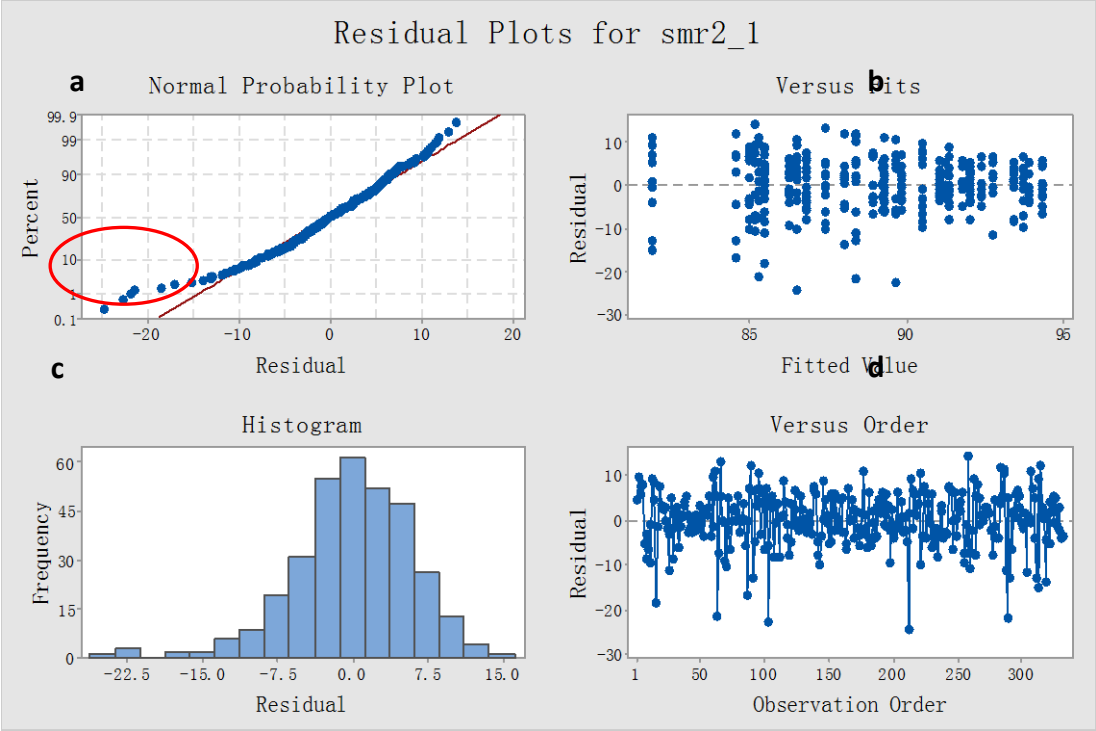

Figure 5.7 Residual plot of Smr2. (a) The normal probability plot, (b) The residual versus fits plot, (c) Histogram, and (d) The residual versus the order of the data.

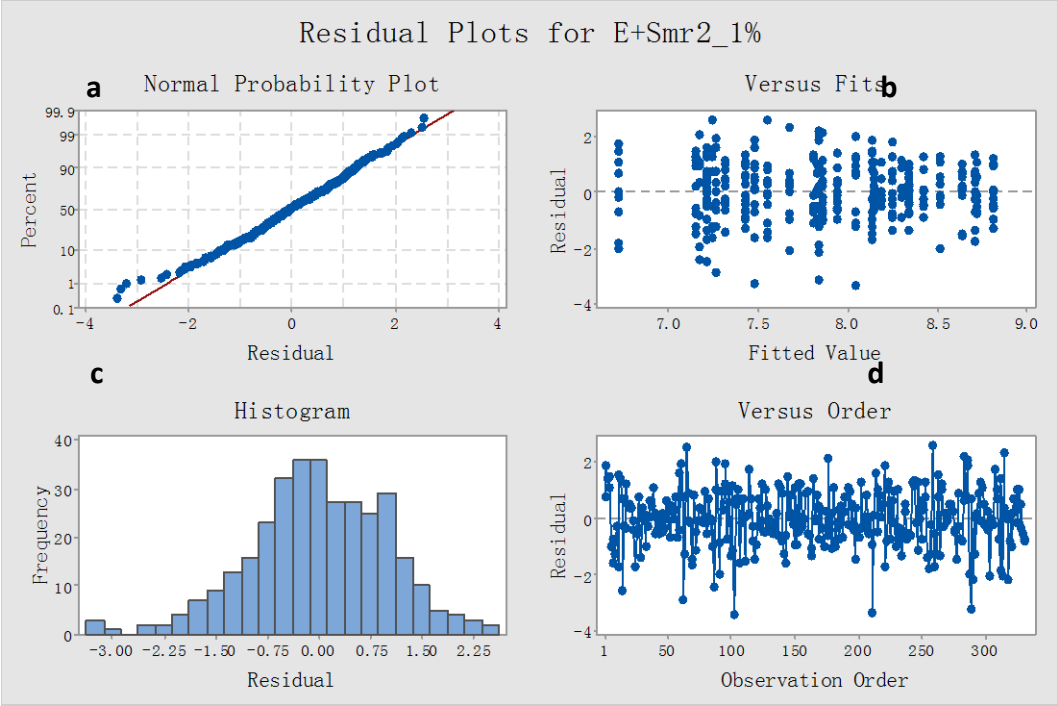

Figure 5.8 Residual plot of the transformed Smr2. (a) The normal probability plot, (b) The residual versus fits plot, (c) Histogram, and (d) The residual versus the order of the data.

5.2.2 One-way analysis to further select distinct parameters

One-way ANOVA is an extension of the two sample t-test (using the pooled estimate) to more than two groups. It is a test of equality of group means, but it is based on variances. t-value was calculated from the equation below [85]:

$$t = \frac{\overline{y_m} - \overline{y_n}}{s_w \sqrt{1/N_m + 1/N_n}} \ ,$$

where $\overline{y_m}$ and $\overline{y_n}$ were the parameter means of patients *m* and *n* respectively, N_m and N_n were the number of particles analysed correspondingly, s_w was the pooled standard deviation which was calculated from all 387 particles. From a statistical point of view, a normal distribution of y makes the *t* fit the student's t-distribution [84]. The calculation of degrees of freedom (DF) for the t distribution was similar with the DF calculation of variance. Therefore, the DF was counted based on 387 particles from 25 patients, that is, 387 - 25 = 362 [84]. The comparisons of greater or less than were both considered that the differences occurred; therefore a two-side hypothesis was applied. $t_{DF=362,\ upper\ 0.025}$ for a significance level of 5% was a threshold value to compare with calculated from the equation. The distribution of t_{362} is shown in Figure 5.9. If the calculated *t* larger than 1.96, the event with a small probability (5%) was considered happened, and thus y_m was statistically different with y_n. If the calculated *t* was smaller than 1.96, then there was statistically no difference between patients *m* and *n* based on the mean comparison. $t_{362,\ upper\ 0.025}$ was suitable for all 20 parameters because the degrees of freedom were calculated from 387 particles from 25 patients and they all equalled to 362.

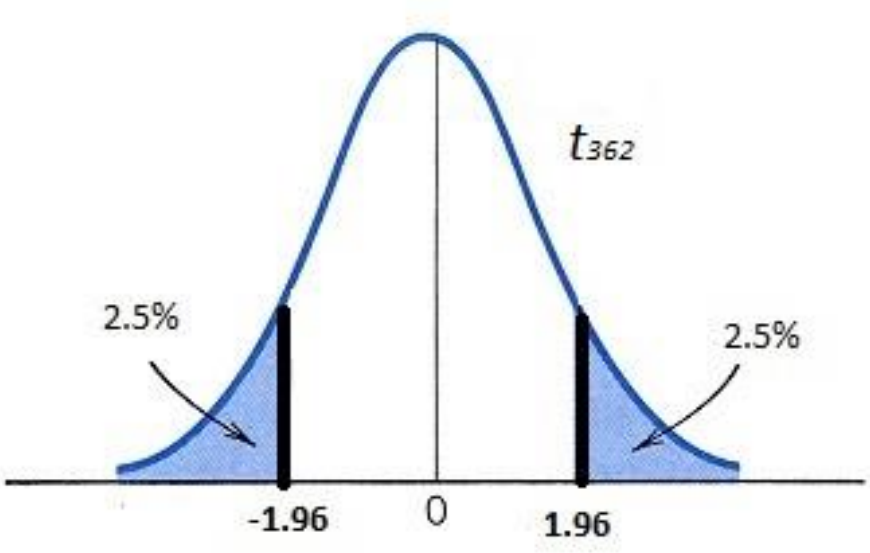

Figure 5.9 The probability density function for the t distribution at the degrees of freedom of 362.

Pairwise comparisons were conducted to compare differences between patients based on each selected parameter. Figure 5.10 indicates the details of pairwise comparisons on each parameter. Firstly, the data were sorted by the means of each parameter from largest to smallest. Secondly, the y_m (m=25), for the patient with the largest mean, was compared to other patients and assign y_{25} in group A in the same time. In the comparisons, the patients were also in group A if other patients showed no differences with y_{25} (*t* between them smaller than 1.96) otherwise they were not assigned to a group. Thirdly, y_{m-1} (y_{24}) did the comparisons to the following figures in the sorted table one by one. If y_{24} obtained the same comparison result with the patients who have done the comparisons, e.g. y_{25}, then y_{24} was only in group A, otherwise assigned y_{24} in group B. The same procedures was performed for the remaining to 23 patients and new letters (C, D, E etc.) were used to name new groups if needed.

For example, the comparison of the means of *logSds* between 25 patients is shown in

Figure 5.11 and gives the summary of *logSds* for calculating t: N is the number of particle analysed from each patient; Pooled StDev (s_w) was calculated from the function: $\sqrt{\frac{\sum\left((N_{id}-1)SD_{id}^2\right)}{\sum N_{id}-1}}$, where N_{id} was the number of analysed particles from patient id and SD_{id} was the standard deviation of patient *id* (s_w was applied because the ANOVA model assumes the same variance for all patients and also this is the main difference between sample t-test and ANOVA); 95%CI is defined as $\overline{y_{id}} \pm {S_w}/{\sqrt{N_{id}}}\, t_{362,upper\ 0.025}$, where y_{id} was the *logSds* mean of patient *id*, N_{id} was the number of particles analysed from patient ID and the degrees of freedom for the *t* statistic was related to s_w which was calculated from 387 particles of 25 patients.

Figure 5.12 shows the summary of grouping based on analysis of *logSds*. In the first column under Grouping in Figure 5.12, if the *t* between y_{25} and other patients was smaller than 1.96 ($t_{362,\ upper0.025} = 1.96$ for a significance level of 5%), then they were in the same group with y_{25} (group A), otherwise kept blank in group A column, i.e. y_2 and y_1. The comparison results of y_{24} were the same as y_{25}, therefore, this sample could be allocated to group A. During the comparisons between y_{23} and others, y_{19} and y_{18} etc. were different with y_{25} but no difference to y_{23}. In other words, the comparison result of y_{23} was different with y_{25}, thus a new group (group B) was created for y_{23}. In this round, y_{23} was performed as y_m and compared to others. The patients were in group B if their calculated t was smaller than 1.96, otherwise also keep blank in the group B column, e.g. y_1. The same procedure was applied to remaining patients. To conclude, pairwise comparisons provided the value of *t*, i.e. *t* for comparing y_{25} and y_3 equalled 3.22. The absolute value of 3.22 was greater than 1.96 (for a 5% significance level). Therefore, y_3

was not in y_{25}'s group (group A in Figure 5.12) based on the comparison of *logSds*. 25 patients were split into 7 groups (A, B, C, D, E, F and G) and some patients were in several groups using *logSds*, i.e. y_{14}, y_{13} and y_{10} show no differences with others except y_{25} and y_{24}, thus they were in the group B, C, D, E, F and G in the same time. In other words, the difference of the mean of *logSds* between patients was illustrated by using Fisher pairwise comparisons but without a clear cut-off to distinguish the groups. One-way ANOVA was also employed to the remaining 18 selected parameters.

The above procedures were applied to all 19 parameters individually. The summary of ANOVA results is presented in Table 5.8. 4 parameters, including *Str20, Str37, Std* and *Vv* showed slight differences between patients because less than 5 groups created which reflected that only a few patients were different with either large or small mean values of the parameters. Therefore, these 4 parameters would not to describe the features of different OA grade. The values of *Str20* and *Str37* depended on the length of ACF in the direction in which slowest decay occurred; thus they were related to area and elongation of particles. A light difference in the elongation of particles visually analysed in chapter 4.2, correlated with *Str20* and *Str37*. The mean of *Std* ranged from about 40 degrees to 140 degrees in the 25 patients and showed that the dominant texture of surfaces turned clockwise (if $Std < 0$, the direction of dominant texture turned anti-clockwise). The values of *Vv* would be slightly different because the reference plane made the depth of most valleys roughly the same. Figure 5.13 shows that the height of peaks ranged from 2 to 10 µm but the depth of valleys was close to each other with a maximum of 2 µm.

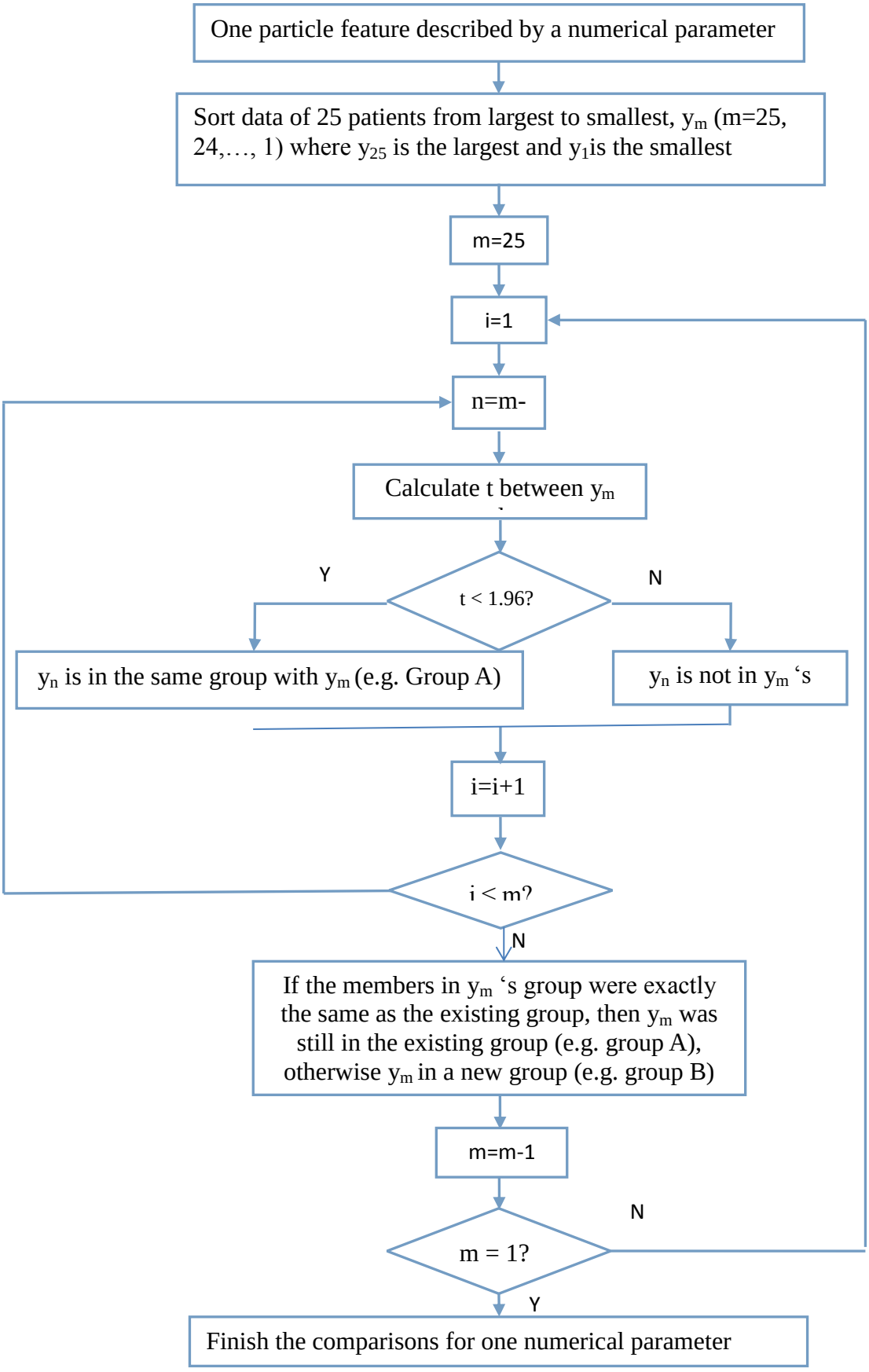
One particle feature described by a numerical parameter
Sort data of 25 patients from largest to smallest, y_m (m=25, 24,…, 1) where y_{25} is the largest and $y_1$is the smallest
m=25
i=1
n=m-
Calculate t between y_m
Y
t < 1.96?
N
y_n is in the same group with y_m (e.g. Group A)
y_n is not in y_m 's
i=i+1
i < m?
N
If the members in y_m 's group were exactly the same as the existing group, then y_m was still in the existing group (e.g. group A), otherwise y_m in a new group (e.g. group B)
m=m-1
N
m = 1?
Y
Finish the comparisons for one numerical parameter

Figure 5.10 Steps of pair comparisons on one parameter.

One-way ANOVA: logSds versus patient ID

ID	N	Mean	StDev	95% CI
11	11	-2.189	0.433	(-2.528, -1.850)
12	9	-2.369	0.516	(-2.744, -1.995)
13	8	-2.115	0.640	(-2.513, -1.718)
20	56	-2.4196	0.5355	(-2.5698, -2.2694)
21	9	-2.277	0.651	(-2.652, -1.903)
22	10	-2.013	0.502	(-2.369, -1.657)
23	18	-2.050	0.671	(-2.315, -1.785)
24	14	-2.247	0.620	(-2.548, -1.947)
25	7	-1.449	0.359	(-1.874, -1.024)
26	10	-1.903	0.561	(-2.258, -1.547)
27	16	-2.230	0.601	(-2.511, -1.949)
28	14	-1.713	0.689	(-2.013, -1.412)
29	7	-2.183	0.576	(-2.608, -1.758)
30	7	-2.134	0.539	(-2.559, -1.709)
32	14	-2.273	0.960	(-2.574, -1.973)
33	13	-2.147	0.552	(-2.459, -1.835)
34	11	-1.722	0.533	(-2.061, -1.383)
35	8	-1.748	0.637	(-2.145, -1.350)
36	12	-1.504	0.598	(-1.828, -1.179)
37	10	-2.095	0.449	(-2.451, -1.740)
38	11	-2.214	0.487	(-2.553, -1.875)
39	7	-2.129	0.499	(-2.554, -1.704)
40	12	-2.006	0.598	(-2.330, -1.681)
43	67	-2.5631	0.4579	(-2.7005, -2.4258)
57	26	-2.157	0.625	(-2.377, -1.936)

Pooled StDev = 0.571710

Figure 5.11 *Summary of logSds among 25 patients: id- Patient id; N-Sample size of patients; Mean-Mean values of each patient; StDev-Standard deviation of each patient; 95%CI-95% of confidence interval.*

Fisher Pairwise Comparisons: logSds versus ID

Grouping Information Using the Fisher LSD Method and 95% Confidence

Sort	ID	N	Mean	Grouping
y_{25}	25	7	-1.449	A
y_{24}	36	12	-1.504	A
y_{23}	28	14	-1.713	A B
y_{22}	34	11	-1.722	A B C
y_{21}	35	8	-1.748	A B C D
y_{20}	26	10	-1.903	A B C D E
y_{19}	40	12	-2.006	B C D E
y_{18}	22	10	-2.013	B C D E
y_{17}	23	18	-2.050	B C D E
y_{16}	37	10	-2.095	B C D E F
y_{15}	13	8	-2.115	B C D E F
y_{14}	39	7	-2.129	B C D E F G
y_{13}	30	7	-2.134	B C D E F G
y_{12}	33	13	-2.147	C D E F
y_{11}	57	26	-2.157	D E F
y_{10}	29	7	-2.183	B C D E F G
y_{9}	11	11	-2.189	C D E F
y_{8}	38	11	-2.214	D E F G
y_{7}	27	16	-2.230	D E F
y_{6}	24	14	-2.247	E F G
y_{5}	32	14	-2.273	E F G
y_{4}	21	9	-2.277	D E F G
y_{3}	12	9	-2.369	E F G
y_{2}	20	56	-2.4196	F G
y_{1}	43	67	-2.5631	G

Figure 5.12 Pairwise comparisons based on logSds: Numbering the sorted data by mean logSds; id-Patient id; N-Sample size of each patient; Mean-Mean values of each patient; Grouping-7 groups A, B, C, D, E, F and G.

Parameters including *Area*, *Roundness*, *logS10z*, *logScl37*, *logFormfactor*, *Svk*, *logSku*, *logConvexity*, *logSds*, *logSpk Ssk*, *logSmr1*, *Solidity*, *logMv* and e^{Smr2}% could illustrate the differences between some patients. *Area* was correlated to the *Length* which used to identify the size distribution in chapter 4.1. *Roundness* and *Convexity* revealed the circular shape of particles from each patient. Also, from the visual shape analysis in chapter 4.2, these 2 shape parameters made the main contribution to differences of the circular shape of particles from different OA grades. Thus, the mean values of the circular shape of particles would tell the differences between some patients. *Solidity* and

Formfactor were used to describe the shape features of particles, i.e. elastic property from lateral direction. *Sds* revealed the density of summits. *S10z* was sensitive to the occasional high peaks and deep valleys and made contribution to *Sdr* and also reflected the height asymmetry in *Ssk*. *Sku* indicated the presence of high peaks or deep valleys. *Mv*, *Spk* and *Smr1* referred to the core high peaks that could be generated during the wear process. For an anisotropic surface, the value of *Scl* was small; conversely, isotropic surface got large *Scl*. In the visual analysis of surface morphology in chapter 4.3, the roughness of surfaces was varied and the percentage of different types of roughness level was quite different between OA and non-OA patients. Thus, the height-related parameters could partially tell the differences among the 25 patient samples.

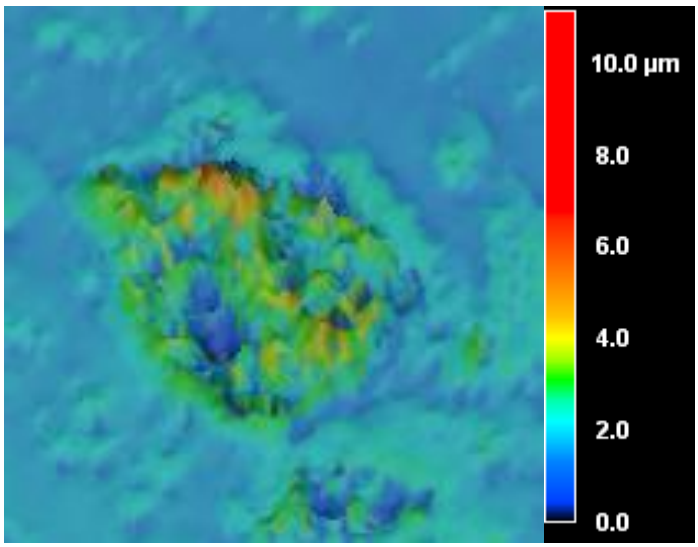

Figure 5.13 A particle surface from patient 57.

To conclude, one-way ANOVA as a single parameter analysis method could only partially tell the differences between patients. Because the properties of the groups overlapped for a range of mean values and no clear cut-offs between groups were identified. Therefore it was hard to clearly group patients into groups to differentiate the particle features from several OA grades. Even though a single parameter could not be

identified as a certain cut-off to distinguish patients' OA grades, 19 parameters (*Str20*, *Str37*, *Vv*, *Std*, *logArea*, *Roundness*, *logConvexity*, *logS10z*, *Ssk*, *Svk*, *logSmr1*, *Solidity*, *logMv*, *logSdr*, e^{smr2}%, *logScl37*, *logSds*, *logSpk* and *logFormfactor*) could potentially distinguish the particles into several OA grades and were selected into further multi-parameter analysis in section 5.3.

Table 5.8 Summary of Fisher pair comparisons.

Particle grouping using Turkey comparisons	Parameters
2 groups	*Str20*
3 groups	*Str37*, *Vv*
4 groups	*Std*
≧ 5 groups	*logArea*, *Roundness*, *logS10z*, *logScl37*, *logConvexity*, *logFormfactor*, *Svk*, *logSku*, *logSds*, *logSpk*, *Ssk*, *logMv*, *logSmr1*, e^{Smr2}%

5.3 Discriminant analysis

Discriminant analysis is a method of multi-parameter analysis and the goal of this method is to identify distinct parameters based on the known patient information and to further compare the surface features of different OA grades.

5.3.1 Background

Discriminant analysis is carried out to look for linear combinations of variables which best explain the data. The analysis is based on the known grouping information and N-1 linear functions are normally used to distinguish N groups. The samples in the

variable-space are transformed to function-space through the projection of each sample on the linear functions and also get the cut-offs between N groups in function-space. For example, the samples in three categories are in different colour in Figure 5.14. The samples in green colour tend to have larger values of the predictor on the X2 axis and larger values on the X1 axis. However, there is overlap between target categories on both axes, so an accurate classification using one of the predictors cannot be performed. Linear discriminant analysis finds a linear transformation of two predictors, X1 and X2, which yields a new set of transformed values ("best 1D subspace" in Figure 5.14), that provides a more accurate classification than either predictor alone.

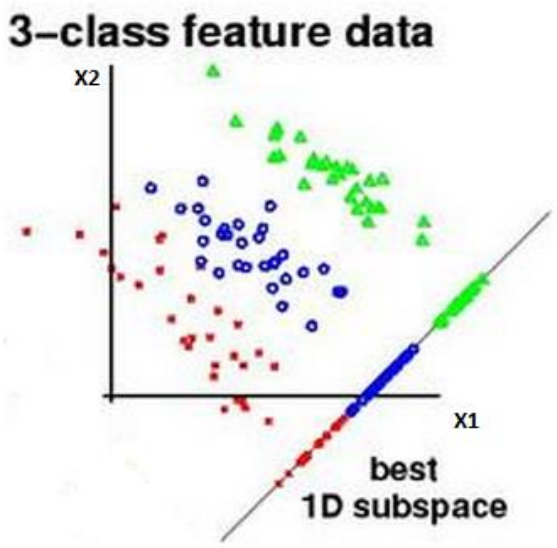

Figure 5.14 Theory of discriminant analysis [86]. The different colours (red, blue and green) indicate different groups.

A total of 331 particles from 24 patients with clinically graded OA were used to find potentially distinct parameters to describe OA grade were explored using discriminate analysis. This section also explored how these parameters might be combined into a mathematical equation to predict the most likely OA grade.

5.3.2 Step-wise method to select distinct parameters

After ANOVA study, 19 parameters were further analysed using step-wise method to find the most important discriminator. The values of 19 parameters were standardized to values ranging from 0 to 1 to avoid different magnitudes that may result in improper linear combinations. In Table 5.10, *F* was a hypothesis test to compare the difference between variances of two normal distributions and it was defined as the function: $F_{DF1,DF2} = {s_B^2}/{s_W^2}$, where s_B^2 and s_W^2 were the between-group variance and the within-group variance respectively and the *DF1* and *DF2* were the corresponding degrees of freedom [87]. $s_B^2 = \sum_{i=1}^{3} n_i(\overline{y_i} - \bar{y})^2/(k-1)$ and $s_W^2 = \sum_{i=1}^{k} S_i/(\sum_{i=1}^{k} n_1 - k)$, where $n_i$was the sample size of group y_i, $\overline{y_i}$ was the mean of group y_i and $\bar{y}$ was the mean of the population, k was the group number and S_i was the variance of group y_i. For a good grouping, a large s_B^2 and a small s_W^2 were expected. Because of 3 groups (Non-OA, Mild OA and severe OA), *DF1*=3-1=2, *DF2*=331-3=328, and thus the entered $F_{2,328}$ =2.99 for a significance level of 5% according to the table of critical value of F distribution [87]. When the values of *F* for a parameter in Table 5.10 were greater than 2.99, there were differences between group means of that parameter. Otherwise the corresponding parameter did not contribute to the grouping. Wilks' lambda is defined as the ratio of the distance between two nearest groups and the distance within these two groups and the lambda is always less than or equal to 1 [88]. The closer to 0 of Wilks' lambda, the larger of distance between two nearest groups is. From step 0 to 5 (in Table 5.10), particles were grouped using the parameters in the steps and calculated the values of *F* and Wilks' lambda based on the

corresponding parameter, i.e. in step 0, 3 groups were separated using 19 selected parameters and then the *F* and Wilks' lambda of *logS10z* were calculated using *logS10z* values. In step 0, Solidity (*S*) with the largest *F*-value and the smallest λ made the most contribution to the grouping, and therefore *S* was selected as the first distinct parameter and released from next step. Discriminant grouping was done until no *F* was greater than 2.99 (step 5 in Table 5.10) and selected the most likely descriptor for each step. Therefore, the parameters in red colour (*Solidity*, *logSds*, *logArea*, *logMv* and *logFormfactor*) were identified as the distinct parameters and selected to generate discriminant functions in the following section to better explain the features of different OA grades.

Table 5.9 Parameter selection using wise-step method.

Step		F to Enter	Wilks' Lambda (λ)	Step		F to Enter	Wilks' Lambda (λ)
0	*logS10z*	3.911	.977	1	*logS10z*	.731	.813
	Solidity	36.902	.816		*logScl37*	5.595	.789
	logScl37	6.091	.964		*logSds*	7.098	.782
	logSds	15.589	.913		*logSpk*	1.647	.808
	logSpk	5.360	.968		*logSmr1*	2.619	.803
	logSmr1	3.640	.978		*logFormfactor*	.663	.813
	logFormfactor	15.777	.912		*eSmr2%*	5.646	.789
	eSmr2%	9.934	.943		*logArea*	.310	.815
	logArea	3.352	.980		*logMv*	2.749	.803
	logMv	7.656	.955		*logConvexity*	.697	.813
	logConvexity	1.986	.988		*logSku*	1.053	.811
	logSku	1.588	.990		*Roundness*	.627	.813
	Roundness	12.411	.930		*Ssk*	2.579	.804
	Ssk	6.439	.962		*Svk*	.733	.813
	Svk	.588	.996		*Std*	.593	.813
	Std	.501	.997		*Str20*	.027	.816
	Str20	.035	1.000		*Str37*	.422	.814
	Str37	.341	.998		*Vv*	2.494	.804
	Vv	.999	.994				

Step		F to Enter	Wilks' Lambda (λ)	Step		F to Enter	Wilks' Lambda (λ)
2	*logS10z*	3.023	.768	3	*logS10z*	.324	.721
	logScl37	7.240	.749		*logScl37*	2.649	.711
	logSpk	1.133	.777		*logSpk*	1.626	.716
	logSmr1	2.660	.770		*logSmr1*	2.721	.711
	logFormfactor	8.973	.742		*logFormfactor*	5.420	.699
	eSmr2%	3.709	.765		*eSmr2%*	5.375	.700
	logArea	13.454	.723		*logMv*	5.604	.699
	logMv	2.994	.768		*logConvexity*	.582	.720
	logConvexity	.852	.778		*logSku*	1.884	.714
	logSku	1.968	.773		*Roundness*	.807	.719
	Roundness	.932	.778		*Ssk*	2.829	.710
	Ssk	1.718	.774		*Svk*	.153	.722
	Svk	1.351	.776		*Std*	.383	.721
	Std	.635	.779		*Str20*	.376	.721
	Str20	.138	.782		*Str37*	.097	.722
	Str37	.051	.782		*Vv*	4.050	.705
	Vv	4.498	.761				
Step		F to Enter	Wilks' Lambda (λ)	Step		F to Enter	Wilks' Lambda (λ)
4	*logS10z*	.600	.696	5	*logS10z*	.408	.677
	logScl37	2.334	.689		*logScl37*	2.318	.669
	logSpk	.115	.698		*logSpk*	.156	.678
	logSmr1	1.823	.691		*logSmr1*	1.775	.672
	logFormfactor	4.690	.679		*eSmr2%*	2.318	.669
	eSmr2%	2.890	.686		*logConvexity*	.579	.677
	logConvexity	.636	.696		*logSku*	1.791	.672
	logSku	2.383	.688		*Roundness*	1.044	.675
	Roundness	.457	.697		*Ssk*	1.195	.674
	Ssk	1.291	.693		*Svk*	.342	.678
	Svk	.224	.698		*Std*	.218	.678
	Std	.378	.697		*Str20*	1.492	.673
	Str20	.837	.695		*Str37*	.408	.677
	Str37	.074	.698		*Vv*	2.744	.668
	Vv	2.758	.687				

5.3.3 Description of the data using Fisher's functions

Two canonical discriminant functions [89] were applied based on parameters, *Solidity*, *logSds*, *logArea*, *logMv* and *logFormfactor,* which were identified using step-wise method employed in chapter 5.3.2. Table 5.11 indicates the new projected variables

from these five parameters:

$F1 = 7.449S + 1.912logSds + 2.633logF - 1.957logA + 0.581logMv - 7.501$;

$F2 = 14.641S - 2.497logSds - 0.824logF + 2.108logA + 0.218logMv - 37.855.$

Table 5.12 shows the central point of each group in space *F1* and *F2*. Two canonical functions were firstly identified to better explain the data in groups and each particle was projected to the functions F1 and F2 at the same time. The centroids were then calculated in space F1-F2, they were the mean value of the particles in same group. The centroid of mild OA was (-0.993, 0.029) in space *F1* and *F2* and the centroids of non-OA and severe OA were (0.441, 0.263) and (0.332, -0.305) respectively.

Table 5.10 Three parameters project to two canonical discriminant functions.

Canonical Discriminant Function

Coefficients

	Function	
	F1	F2
Solidity	7.449	14.641
logSds	1.912	-2.497
logFormfactor	2.633	-.824
logArea	-1.957	2.108
logMv	.581	.218
(Constant)	7.501	-37.855

Table 5.11 Function values at group centroids.

Functions at Group

Centroids

OA	Function	
	F1	F2
Non-OA	-.993	.029
Mild OA	.441	.263
Severe OA	.332	-.305

5.3.4 Graphing particles and grouping cut-off

331 particles and the group centroids (Table 5.12) were plotted in space *F1-F2* in Figure 5.15. One refers to the centroid of non-OA, and 2 presents to the centroid of mild OA and 3 is the centroid of severe OA. The distances between the particles and the group centroids were calculated in space F1-F2, and the particle was considered in a particular group when the distance between them was the smallest. Thus, the cut-off of groups was the perpendicular bisector between the group centres. The cut-off between severe and non-OA was $F2 = 3.97F1 + 1.174$; the boundary between mild and non-OA was $F2 = -6.13F1 - 1.544$; the cut-off between mild and severe OA was $F2 = -0.19F1 + 0.052$. Thus the area of severe OA was $\begin{cases} -0.19F1 - F2 + 0.052 < 0 \\ 3.97F1 - F2 + 1.174 > 0 \end{cases}$; the set of mild OA was $\begin{cases} -0.19F1 - F2 + 0.052 > 0 \\ -6.13F1 - F2 - 1.544 < 0 \end{cases}$; the cut off of non-OA was $\begin{cases} 3.97F1 - F2 + 1.174 < 0 \\ -6.13F1 - F2 - 1.544 > 0 \end{cases}$.

The original groups of the particles were also presented in a different colour and the

summary of classification is shown in Table 5.12. In mild OA, 62 out of 123 (50.4%) particles were in the same OA grade as the clinical classification. 63.4% (59 out of 93) particles in non-OA were correctly classified and 60.9% (70/115) of severe OA particles were correctly classified. In total 57.7% ((62+70+59)/331) of the particles were correctly classified with the clinical classification. In the non-OA group, the non-OA particles were the main contribution, being about 63.4%. The particles with the similar features to the mild OA particles and the severe OA particles both accounted for 18.3%. During mild OA, the mild particles accounted for 50.4%. Once the superficial zone has been open up, the main stress was put on the breach of the cartilages and mild OA particles were mainly produced and the particles with severe features also has been produced from unusual wear or further wear of the mild particles [15]. In mild OA, non-OA and severe particles accounted for 16.3% and 33.3%, respectively. In the severe OA, the severe OA particles rise to 60.9%. Mild OA particles decreased from 50.4 to 20.9%. The percentage of non-OA particles (18.3%) in severe joints seemed slightly increase.

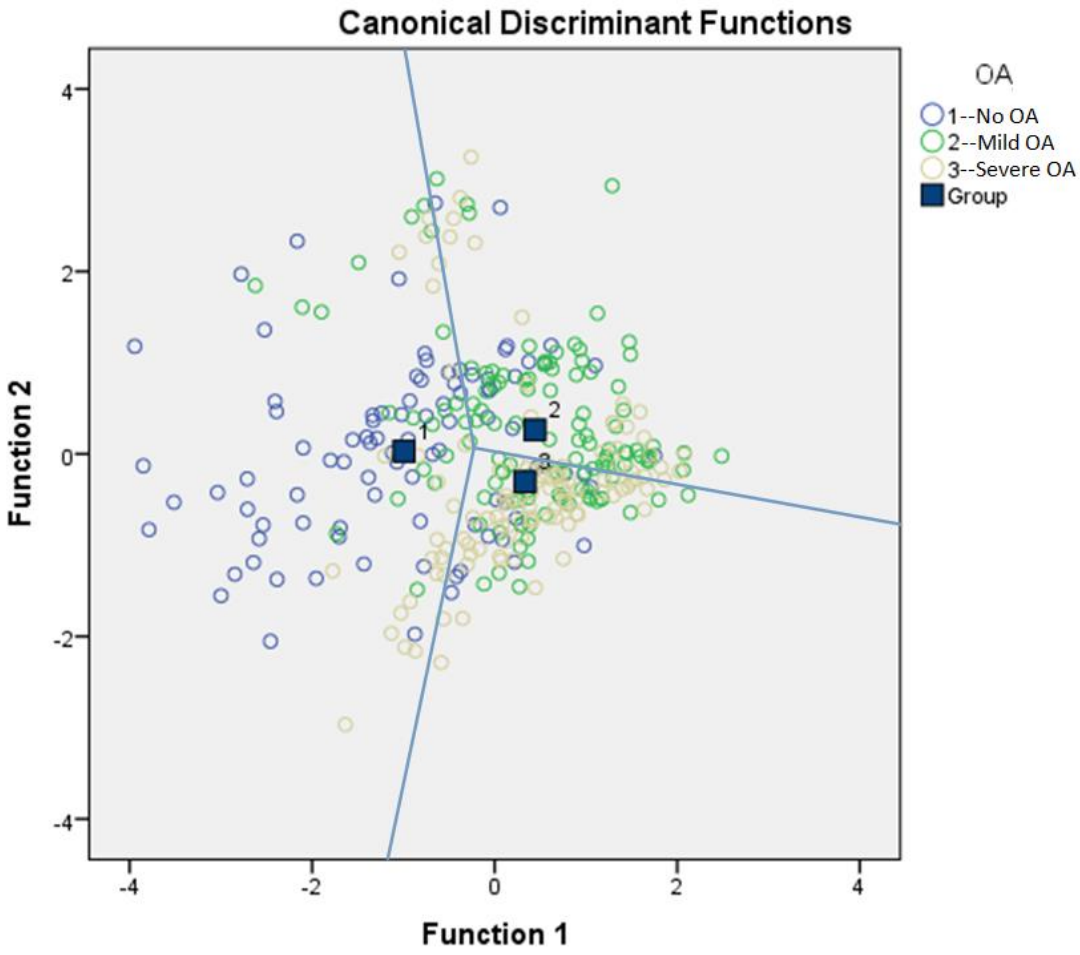

Figure 5.15 Particles transformed to space F1 and F2.

Table 5.12 Summary of classification.

			Predicted Group Membership			
		OA	No	Mild	Severe	Total
Original	Count	No	**59**	17	17	93
		Mild	20	**62**	41	123
		Severe	21	24	**70**	115
	%	No	**63.4**	18.3	18.3	100.0
		Mild	16.3	**50.4**	33.3	100.0
		Severe	18.3	20.9	**60.9**	100.0

5.3.5 Differences of distinct parameters to differentiate OA

In order to analyse the range of the distinct parameters between groups, the parameters were substituted into functions 1 and 2. From the raw data (Appendix B), the range of *Solidity* was from 0.63 to 0.98; the values of *logSds* was limited to (-3.55,-0.64); and the minimum and maximum of *logFF* were -1.15 and -0.04 respectively. The range of *logArea* was from 6.80 to 9.75 and that of *logMv* was from 6.65 to 14.03.

In the Figure 5.15, the main difference between non-OA and OA grades was that the non-OA group was mostly in the left half of the F1-F2 space while mild OA was in the right top and severe OA in the bottom right of the space F1-F2. In Table 5.13, the negative values of *logsds* and *logArea* show the main difference between OA particle groups. The value of *Sds* in non-OA group was roughly smaller than that in OA particles while *Area* of particles in non-OA was larger than those of OA particles. From the visual analysis of surface topography in Chapter 4.3, the smooth particles were most abundant in non-OA synovial fluid. Thus, the value of *Sd*s increased with the severity of OA. The *Area* was correlated to the *Length* and the size distribution showed that there were slight differences between non-OA, mild OA and severe OA based on the major dimension, with the mild OA having largest mean size. However, the circular shape of non-OA particles was changed to elongated and chunky particles with distinct edges due to increased severity of OA. The area of a circular shape was larger than that of the elongated shape particles while they were the same length. Thus, the area of non-OA particles was larger. *LogFormfactor* contributed less to the negative value of F1 compared to *logSds* and *logArea*. *Solidity* enabled differentiation of the mild OA and severe OA. Due to the increase of the number of irregular particles in severe OA, the

solidity became smaller than for mild OA. *Mv* was related to the height of the surface. The particles in the severe OA became thinner than that in the mild OA. Therefore, the average height of particles in severe OA was smaller than that in mild OA and as the value of *Mv*.

Table 5.13 The range of numerical parameters connected to the coefficients in functions 1 and 2.

	Range	Coefficients in F1	Coefficients in F2	Range*Coefficients in F1	Range*Coefficients in F2
Solidity	(0.63,0.98)	7.449	14.641	(4.69,7.3)	(9.22,14.35)
logSds	(-3.55,-0.64)	1.912	-2.497	(-6.79,-1.22)	(1.60,8.86)
logFormfactor	(-1.15,-0.04)	2.633	-0.824	(-3.03,-0.11)	(0.03,0.95)
logArea	(6.80,9.75)	-1.957	2.108	(-19.08,-13.31)	(14.33,20.55)
logMv	(6.65,14.03)	0.581	0.218	(3.86,8.15)	(1.45,3.06)
Contribution of the parameters	*LogSds* and *logArea* made main contribution to distinguish the non-OA and OA particles. *Solidity* and *logSds* were used to distinguish mild and severe particles.				

5.3.6 OA grade detection for the unsure patient

Based on the result analysis in section 5.3.4, particles from patients, whose OA grade was not detected clinically, were captured and described using distinct parameters. Further, a hypothesis test for the accuracy of the particle analysis was employed.

In Table 5.12, the OA grades of the particles from each patient were considered to follow the binomial distribution, i.e. the probability of X_1 was 60.9% (X_1 = severe particles matched their original OA grades) and other particles (X_2) including non-OA and mild OA were considered as another possibility. From this method the frequency of particles were counted separately and a test for accuracy of the analysis was needed. The binomial distribution was more similar to normal distribution by the increase of the

number of particle analysed according to central limit theorem [90]. With many particles analysed, the experiment X was considered as a normal distribution with the mean of np and a variance of $np(1-p)$ ($X \sim N(np, np(1-p)$, where n was the number of particles analysed and p was the probability of X_1 occurred). Thus, the hypothesis test for normal distribution could be applied in the binomial distribution. Figure 5.16 is the relation between binomial and normal distribution. Comparing the shape for four spreads in Figure 5.16, a and d mostly fit the normal dispersion and means that at least 20 particles should be analysed for application of the hypothesis test [90]. In Figure 5.16b, 5.16c and 5.16d show no symmetry from left to right due to the probability of 0.3 not 0.5 (symmetry in Figure5.16a). Therefore, the frequencies were revised as $k \pm 0.5$ to make up the asymmetry when $p \neq 0.5$ in the hypothesis function: $Z = \frac{k \pm 0.5 - np}{\sqrt{np(1-p)}}$ when $k < \frac{n}{2}$, $k + 0.5$ otherwise $k - 0.5$, where k was the frequencies of X_1, n was the number of particles analysed and p was the probability of X_1 occurred. If $p = 0.5$, $Z = \frac{k-np}{\sqrt{np(1-p)}}$. The $Z_{\,upper\,0.005} = 2.56$ for a significance level of 1% was as the threshold value for the hypothesis test. If $Z < 2.56$, X had the same OA grade with the analysed result in table 5.13.

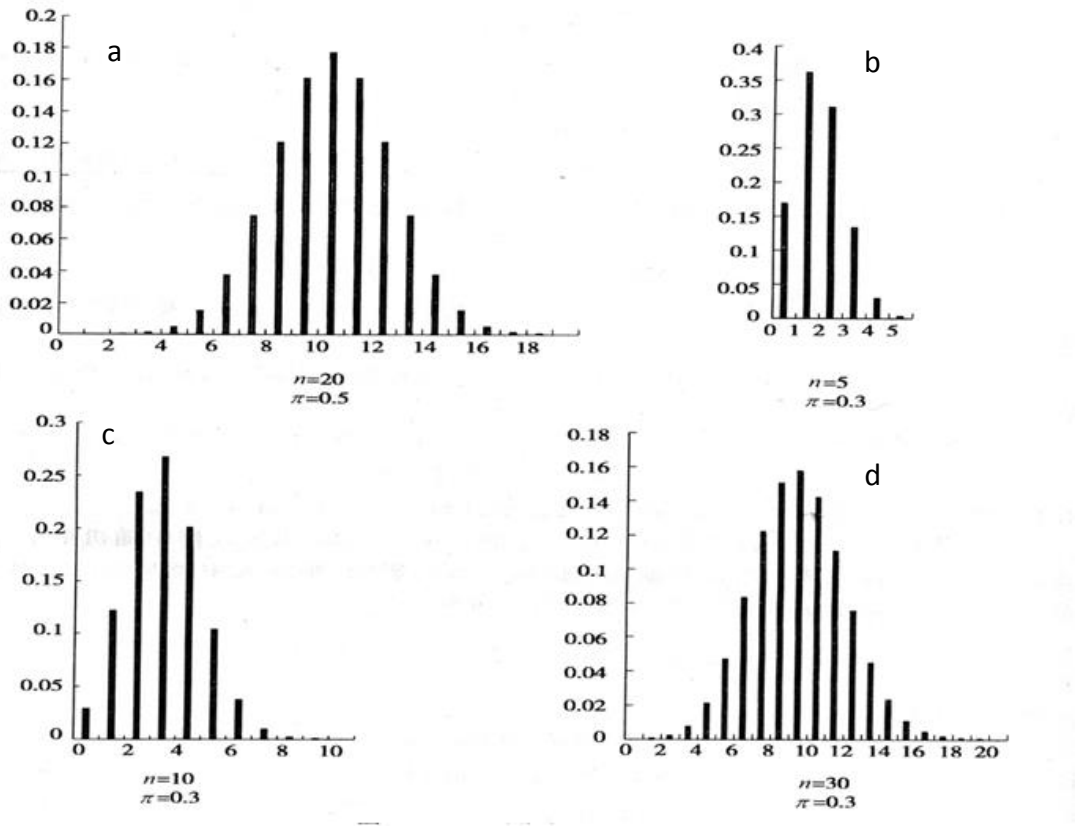

Figure 5.16 The relation between binomial and normal distribution: (a) Binomial spread for a sample size n=20 with the probability of 0.5; (b) Binomial spread for a sample size n=5 with the probability of 0.3; (c) Binomial spread for a sample size n=10 with the probability of 0.3; (d) Binomial spread for a sample size n=30 with the probability of 0.3.

To identify the OA grade of the unclassified specimen, the data of the unclassified particles were plotted in Figure 5.16. 51.8 % (29/56) of the particles were assigned to mild OA while 41.1% (23/56) and 7.1% (4/56) of particles were categorised into non-OA and severe OA, respectively. Z = 0.207 (<< 2.56), the unsure patient therefore would suffer in mild OA (p-value < 0.01).

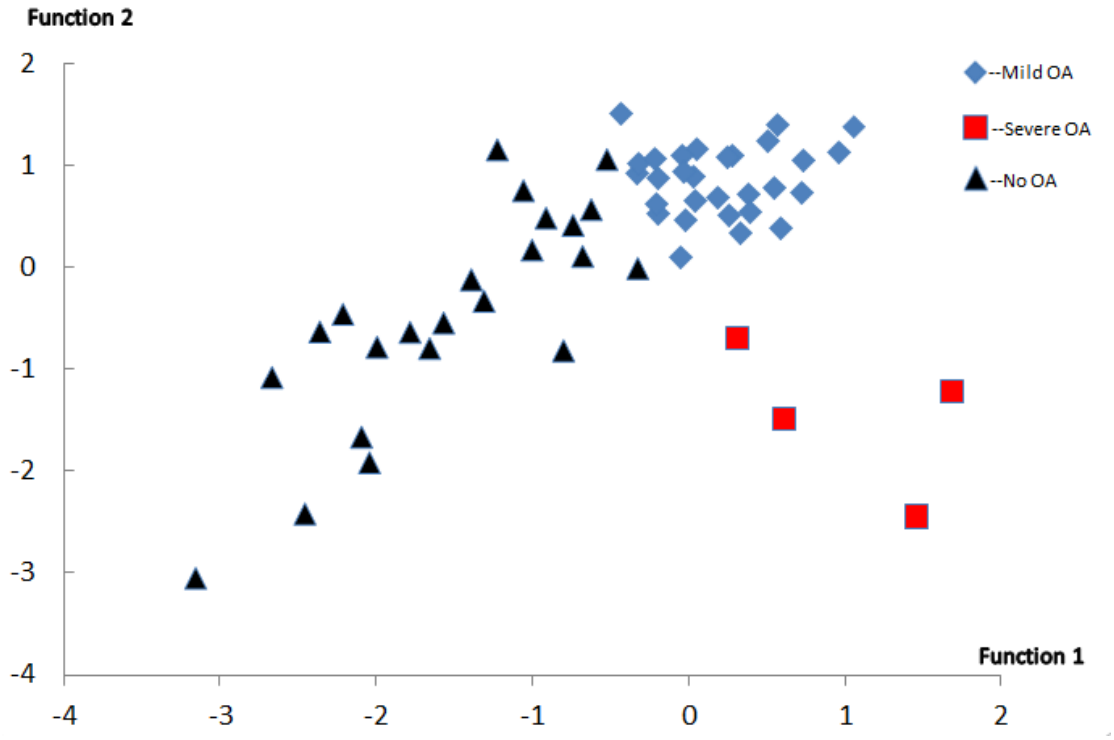

Figure 5.17 The particles from the unclassied patient.

5.4 Summary

After data acquisition in Chapter 4, correlation analyses were firstly carried out to reduce correlated parameters and 12 out of 29 parameters were selected into further statistical analyses. One-way ANOVE tried to found the distinct parameters that could differentiate the OA grades based on the comparison of the mean value of each parameter. Unfortunately, mean differences between OA grades were not significant enough. A multi-parameter analyse method, discriminant analysis was used to group particles into different OA grades and identify the distinct parameters. *S, FF, A, Mv* and *Sds* were identified as the distinct parameters and used to differentiate OA grades.

Chapter 6 Correlation study between cartilage surface and wear particle surface features

Currently, the severity of OA is assessed by the observation of the cartilage surface characteristics and joint space narrowing using X-ray or MRI [91]. Also, it has been reported that there is a linear correlation between the surface of sheep cartilage and the surface morphology of sheep wear particles [7]. However, limited studies have been conducted on the correlation between the particle surfaces and the joint surfaces of human knee samples. The objective of this chapter was to investigate correlations between particle morphology and features of the cartilage surface and identify the common surface features between cartilage and particle surfaces.

In this section, visual inspection of cartilage surfaces were conducted to identify the cartilage surface features that change during OA as well as their relation to wear particle surface features. The correlations between the cartilage parameters were then carried out using the approach applied to wear particle parameter correlations detailed in chapter 5. Finally, correlations between wear particle surface parameters and cartilage parameters were conducted to find the correlated parameters that described common trends between particle and cartilage features during OA to validate the analysis of wear particles as an OA diagnostic tool.

6.1 Visual inspection of cartilage surface and their relation to particle features

Human cartilage samples were collected from seven patients in an age range of 53 to 76 years old during their total knee replacement surgery under human ethics approval [9].

As the healthy samples from normal joints were extremely difficult to obtain, the majority of the healthy cartilage samples were collected from areas of the cartilage that looked smooth and showed similar or the same surface features as the healthy ones. The joints with OA grade 4 were not imaged as the subchondral bone was exposed and the cartilage was fully removed. More details about sample preparation are described in [9]. The LSM with a 10× objective lens and a step size of 1 µm was used to capture 36 healthy cartilage samples, 64 cartilage samples with mild OA (OA grade 1-2), and 36 cartilage samples with severe OA (OA grade 3) [68].

Representative 3D images of multiple cartilage samples at a micrometre scale are displayed in Figure 6.1. The images revealed that there were distinctive and continuous surface changes from the healthy surface (Figure 6.1a) to the surface with the OA grade 3 (Figure 6.1d). The healthy cartilage appeared to have a smooth surface and no special texture was observed. Rectangle and long textures as well as deep troughs were presented in the cartilage with OA grade 1 (Figure 6.1b). When the fissure extended to the middle zone (OA grade 2) they can be clearly observed at a micron scale. As shown in Figure 6.1c, some elongated structures were present on the boundary of the fissure. The topography with round boundary was presented on the cartilage with OA grade 2 (Figure 6.2c). The surface texture of the cartilage with OA grade 3 was much rougher. In the OA grade 3 samples, the cartilage contained fissures that reached subchondral bone. Long and sharp textures attached on the cartilage with OA grade 3 (Figure 6.2d). The long textures could be the collagen fibrils which vertically oriented to the surface in the deep zone of cartilage.

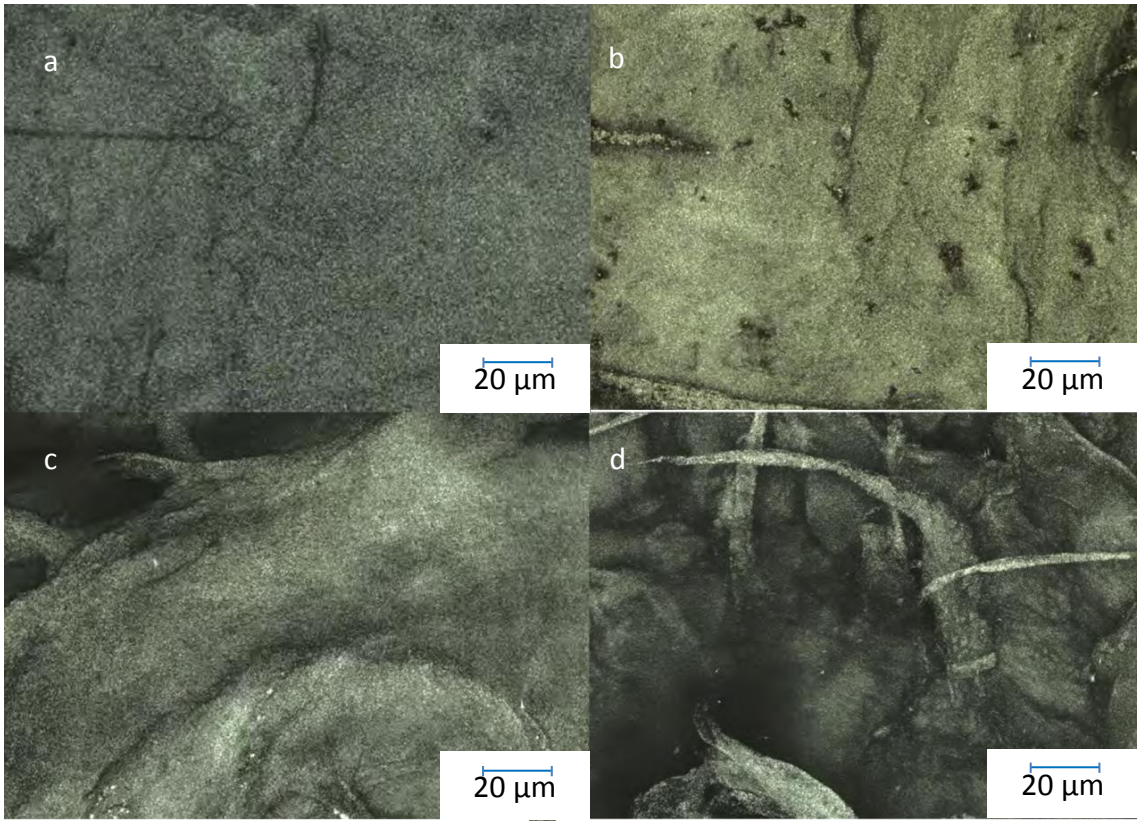

Figure 6.1 LSM images of cartilage surfaces using objective lens of 10× and a step size of 1 µm. (a) Healthy cartilage surface; (b) OA grade 1 cartilage surface; (c) OA grade 2 cartilage surface; (d) OA grade 3 cartilage surface [2].

6.2 Quantitative correlation analysis

A two-step approach was used to determine the correlated parameters between the particles and cartilage surfaces and the key steps in this approach are presented in Figure 6.2. Firstly the correlation analysis was conducted among the particle descriptors to select key surface parameters by excluding correlated ones which described the similar trend. This work was described in Chapter 5. Once the highly correlated parameters were assessed, the parameter with a small *d* was selected in the characterisation process. The correlations within the particle parameters were conducted in Section 5.1. Twelve parameters including *Ssk*, *Sku*, *S10z*, *Sds*, *Std*, *Scl37*, *Str20*, *Str37*,

Spk, Svk, Smr1 and *Smr2* were selected as key descriptors to reflect the changes of the particle surfaces. The same approach was applied to the surface parameters for the articular cartilage analysis, and the outcomes are presented in section 6.2.1. The second step analysis (Section 6.2.2) involved the correlation between particle surface and cartilage surface parameters. The highly correlated parameters revealed that the particles have common features to the cartilage surface. The Pearson coefficient was also used to conduct correlations in this section. The sign (+ or -) of the coefficients indicated the trend. The absolute value of the coefficients greater than 0.8 in a 95% confidence level was considered highly correlated.

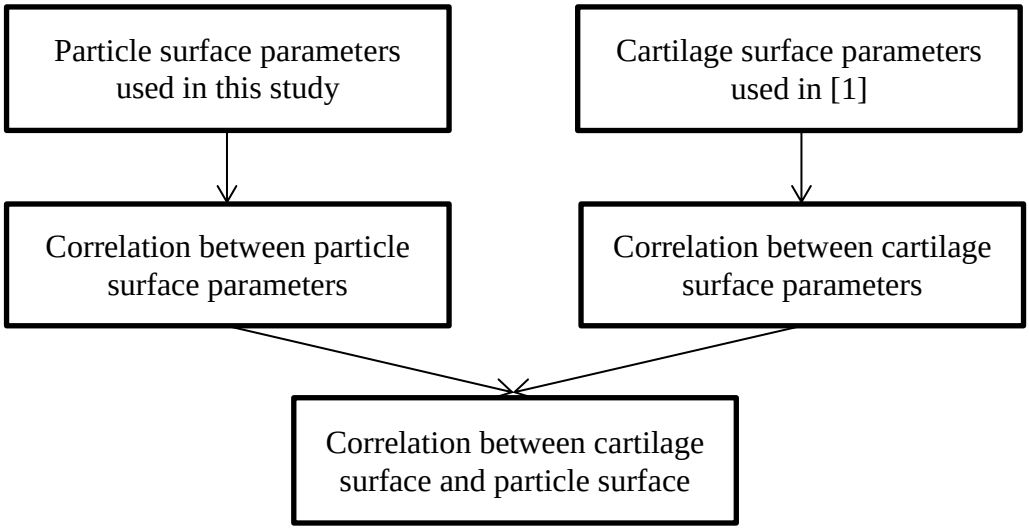

Figure 6.2 Correlation process for particle and cartilage surface.

6.2.1 Correlation between the cartilage surface parameters

The steps applied to the correlation of wear particles were adopted to study the correlation of the cartilage surfaces. The correlation analysis was firstly carried out between the parameters which were in the same group (e.g. amplitude parameters).

Amplitude parameters were analysed followed by spatial, functional parameters. The correlation within hybrid parameters was not conducted as only one hybrid parameter (mean summit curvature (*Ssc*)) was calculated from the cartilage images. Once the correlated parameters were identified, the one with the smallest nominal deviation *d* and the uncorrelated parameters were selected for further correlation analysis between the surface parameters and further reduced the correlated surface parameters.

The numerical descriptors were extracted from the 3D images of the cartilages using SPIP software. Only the uncorrelated parameters were presented in Table 6.1 as the highly linearly correlated parameters showed the same or similar texture of the cartilage surface over three OA grades. The two amplitude parameters, i.e. surface skewness (*Ssk*) and ten point height (*S10z*) differentiated healthy cartilage surface from the others. *Ssk* describes the asymmetry of the height distribution histogram. The mean *Ssk* values were 0.35 ± 0.35 μm, 0.14 ± 0.56 μm, 0.09 ± 0.65 μm for healthy cartilage, mild OA cartilage and severe OA cartilage, respectively. It is clear that with the OA progression *Ssk* decreased continuously. However, the changes in the *Ssk* were not significant enough to differentiate mild and severe OA. The hybrid parameter (mean summit curvature (*Ssc*)) revealed that the degree of summit curvature increased with the severity of OA. The increased curvature was caused by the high peaks which are presented in severe OA cartilage (Figure 6.2d). Surface bearing index (*Sbi*) indicates a bearing property of a surface, which is directly related to its anti-wear functions. The healthy cartilage surface had the largest *Sbi* (*Sbi* = 0.69 ± 0.05), indicating that the surface had a good bearing property. *Sbi* decreased to 0.60 ± 0.12 of the mild OA cartilages, and further slightly reduced to 0.58 ± 0.16 for the severe OA cartilage. The texture direction index (*Stdi*) decreased with OA severity. The healthy cartilage had a *Stdi* value of 0.79, indicating

the surface was close to isotropic. In severe OA the value was decreased to 0.60, revealing a directional surface after being subjected to a severe wear process. *Str* is defined as the ratio of the fastest decay to slowest decay and is used to identify uniformity of texture aspect. For a surface with directional lay, the parameter will tend towards 0.00, whereas a spatially isotropic texture will result in a value of 1.00. Therefore, the healthy cartilage with an isotropic surface had the largest *Str* value.

Table 6.1 The mean and SD of uncorrelated parameters for cartilage characteristics. The data presented as mean ± SD.

Cartilage parameters		Non-OA	Mild OA	Severe OA
Amplitude parameters	*Ssk*	0.35 ± 0.35	0.14 ± 0.56	0.09 ± 0.65
	Sku	3.89 ± 0.95	3.97 ± 1.79	3.88 ± 2.20
	S10z (µm)	106.86 ± 28.24	416.65 ± 233.46	454.36 ± 242.75
Hybrid parameter	*Ssc* (1/µm)	53.25 ± 4.40	70.95 ± 26.82	79.71 ± 34.24
Functional parameters	*Sbi*	0.69 ± 0.05	0.60 ± 0.12	0.58 ± 0.16
	Svi	0.14 ± 0.01	0.13 ± 0.03	0.13 ± 0.04
Spatial parameters	*Sds* (1/µm^2)	0.17 ± 0.01	0.16 ± 0.03	0.16 ± 0.03
	Std (degree)	81.41 ± 57.61	49.23 ± 51.17	53.41 ± 43.63
	Stdi	0.79 ± 0.11	0.62 ± 0.14	0.60 ± 0.16
	Str20	0.89 ± 0.23	0.49 ± 0.17	0.46 ± 0.16
	Str37	0.89 ± 0.21	0.58 ± 0.17	0.52 ± 0.14

Table 6.2 displays the correlations between the 7 amplitude parameters. *Sa, Sq, S10z, Sp Sv* were strongly correlated to each other. *S10z* with a smallest *d* was selected for further analysis (d_{Sp} = 0.88, d_{S10z} = 0.86, d_{Sv} = 0.91, d_{Sq} = 0.97 and d_{Sa} = 1.00). Therefore, *S10z*

and uncorrelated ones (surface skewness (*Ssk*) and surface kurtosis (*Sku*)) were selected for further correlation analysis.

Table 6.2 Correlation analysis between cartilage amplitude parameters: Data in red indicates coefficients greater than 0.8. The data were presented as the format of

Cartilage parameters		Amplitude parameters					
		Sa	*Sq*	*Ssk*	*Sku*	*S10z*	*Sv*
Amplitude parameters	*Sq*	0.996 (0)					
	Ssk	0.253 (0.003)	0.256 (0.003)				
	Sku	-0.180 (0.036)	-.141 (0.102)	0.056 (0.514)			
	S10z	0.931 (0)	0.950 (0)	.258 (0.002)	0.031 (0.719)		
	Sv	0.907 (0)	0.923 (0)	0.154 (0.074)	0.005 (0.958)	0.980 (0)	
	Sp	0.908 (0)	0.927 (0)	0.368 (0)	0.066 (0.446)	0.961 (0)	0.899 (0)

Pearson correlation coefficient and the p-value in the brackets.

Correlation results between the cartilage spatial parameters are presented in Table 6.3. Length at 37% (*Scl37*) was strongly correlated to correlation length at 20% (*Scl20*) with the value of ρ = 0.986. The definition of *Scl20* and *Scl37* were the auto-correlation length (ACF) in a fastest decay to 20% and 37%, respectively. From the surface inspection in Section 6.1, only the isotropic surfaces without the directional texture were present on the cartilage surface. Therefore, *Scl37* was highly linearly correlated to *Scl20*. *Scl37* with a larger *d* (d_{Scl37} = 1.13) was not used for further analysis while *Scl20* (d_{Scl20} = 1.04) was kept for further analysis. The texture aspect ratio at 20% (*Str20*) was not highly correlated to texture aspect ratio at 37% (*Str37*) with the ρ = 0.748. The *Str*-parameter was defined as the function: length of fastest decay of ACF in any direction / length of slowest decay of ACF in any direction. Even though the cartilage

with the same OA grade appeared to have a similar texture, step changes to the cartilage surfaces with OA grade 3 mainly made the *Str* parameters not highly linearly correlated. The uncorrelated parameters contained density of summit (*Sds*), texture direction (*Std*) and texture direction index (*Stdi*) which measured the summit density, the direction of dominant texture of the cartilage surface and how dominant the dominant texture was, respectively. Thus, *Scl20* and uncorrelated parameters (*Sds*, *Str37*, *Str20*, *Std* and *Stdi*) were selected for further correlations.

Table 6.3 Correlation analysis between cartilage spatial parameters: Data in red indicates the coefficient greater than 0.8. The data were presented as the format of Pearson correlation coefficient and the p-value in the brackets.

Cartilage parameters		Spatial parameters					
		Sds	*Std*	*Stdi*	*Str37*	*Scl37*	*Str20*
Spatial parameters	*Std*	0.066 (0.443)					
	Stdi	0.217 (0.011)	0.282 (0.001)				
	Str37	0.296 (0)	0.190 (0.027)	0.616 (0)			
	Scl37	-0.290 (0.001)	-0.254 (0.003)	-0.482 (0)	-0.542 (0)		
	Str20	0.279 (0.001)	0.276 (0.001)	0.688 (0)	0.748 (0)	-0.550 (0)	
	Scl20	-0.259 (0.002)	-0.266 (0.002)	-0.508 (0)	0-.535 (0)	0.986 (0)	-0.565 (0)

Correlations between functional parameters are displayed in Table 6.4. Reduced summit height (*Spk*) was highly linearly correlated to core roughness depth (*Sk*) with the coefficient of 0.807. Reduced valley depth (*Svk*), *Sk* and *Spk* were calculated from area ratio curve of the cartilage surface. For a homogenous cartilage surface, the *Sk* was increased by the increase of *Spk* to provide a good bearing property. The extremely deep

valleys that appeared in the cartilage with OA grade 3 was observed by the visual inspection on cartilage. Therefore, no correlations to *Svk* were identified from the cartilage functional parameters. Surface bearing index (*Sbi*) and valley fluid retention index (*Svi*) revealed the bearing property and lubrication property of cartilage, respectively. *Sk* with a smaller *d* (d_{Spk} = 1.07, d_{Sk} = 1.02) and uncorrelated parameters including *Svk*, *Svi* and *Sbi* were kept for further correlation study.

Table 6.4 Correlation analysis between cartilage functional parameters: Data in red indicates the coefficient greater than 0.8. The data were presented as the format of Pearson correlation coefficient and the p-value in the brackets.

Cartilage parameters		Functional parameters			
		Sbi	*Svi*	*Spk*	*Sk*
Functional parameters	*Svi*	0.556 (0)			
	Spk	-0.570 (0)	-0.343 (0)		
	Sk	-0.380 (0)	-0.497 (0)	0.807 (0)	
	Svk	-0.241 (0.005	0.093 (0.280)	0.775 (0)	0.700 (0)

Table 6.5 shows the correlations between cartilage surface parameters. The amplitude parameter, *S10z*, was strongly correlated to *Sk* and *Svk* as these two functional parameter also revealed the height distribution of the cartilage surface. *S10z* also correlated to correlation length at 20% (*Scl20*). No periodic and directional texture was observed on the cartilage surface, the value of *Scl20* therefore associated with the ten point height (*S10z*) to indicate the isotropic surface. *S10z* with a smallest d (d_{S10z} = 0.86, d_{Scl20} = 1.04, d_{Sk} = d_{Svk} = 1.02) was kept for analysis further. No other correlations were found

between the surface parameters. To conclude, a total of 11 cartilage parameters were selected for further analysis. The parameters include *S10z*, *Ssk*, *Sku* from amplitude parameters, *Ssc* from hybrid parameter, *Sbi*, *Svi* from functional parameters, *Sds*, *Std*, *Stdi*, *Str37* and *Str20* from spatial parameters.

Table 6.5 Correlation analysis between cartilage surface parameters: Data in red indicates the coefficients greater than 0.8. The data were presented as the format of Pearson correlation coefficient and the p-value in the brackets.

Cartilage parameters		Amplitude parameters			Hybrid parameter	Functional parameters			
		Ssk	*Sku*	*S10z*	*Ssc*	*Sbi*	*Svi*	*Sk*	*Svk*
Hybrid parameter	*Ssc*	0.273 (0.001)	-0.098 (0.254)	0.677 (0)					
Functional parameters	*Sbi*	-0.657 (0)	0.208 (0.015)	-0.410 (0)	-0.354 (0)				
	Svi	-0.716 (0)	0.354 (0)	-0.273 (0.001)	-0.246 (0.004)				
	Sk	0.276 (0.001)	-0.222 (0.009)	0.884 (0)	0.576 (0)				
	Svk	-0.001 (0.989)	0.013 (0.885)	0.858 (0)	0.538 (0)				
Spatial parameters	*Sds*	-0.083 (0.335)	0.014 (0.870)	-0.251 (0.003)	0.271 (0.001)	0.091 (0.292)	0.238 (0.005)	-0.35 (0)	-0.183 (0.033)
	Std	0.037 (0.672)	0.095 (0.272)	-0.229 (0.007)	-0.070 (0.416)	0.191 (0.026)	-0.008 (0.923)	-0.202 (0.019)	-0.210 (0.140)
	Stdi	-0.224 (0.009)	-0.021 (0.812)	-0.399 (0)	-0.160 (0.163)	0.379 (0)	0.079 (0.362)	-0.334 (0)	-0.411 (0)
	Str37	-0.239 (0.005)	-0.220 (0.01)	-0.512 (0)	-0.298 (0)	0.303 (0)	0.078 (0.366)	-0.411 (0)	-0.484 (0)
	Str20	-0.232 (0.006)	-0.131 (0.129)	-0.523 (0)	-0.297 (0)	0.380 (0)	0.057 (0.508)	-0.412 (0)	-0.514 (0)
	Scl20	0.250 (0.003)	-0.018 (0.831)	0.810 (0)	0.481 (0)	-0.452 (0)	-0.301 (0)	0.737 (0)	0.665 (0)

6.2.2 Correlation between the particle and cartilage surface features

Correlation between the particle surface parameters and the cartilage surface parameters will indicate whether or not the two are correlated. If the two are correlated then we can show that the particles collected from synovial fluid samples have common features to the cartilage in the same OA grade. The following sections firstly describe the uncommon features of the cartilages and their particles. Then, the correlated parameters indicate common features and statistically select parameters which can be used to differentiate particles into different OA grades. These ones may be used as key OA indicators.

Some functional properties and spatial properties were identified to be uncorrelated between particle and cartilage surface. The results (Table 6.6) show there were no correlations of two functional parameters, reduced peak height (*Spk*) and reduced valley depth (*Svk*). *Spk* may represent the nominal height of the material that may be removed during wear, while *Svk*, a measure of the valley depth below the core roughness, may be related to lubrication [71]. Cartilage *Spk* and *Svk* were highly correlated to cartilage *S10z* (Table 6.5), and together, they reveal that with OA progression the cartilage surface became rougher with more peaks and valleys (Figure 6.1). In comparison, the particles found in severe OA joints appeared to have a smoother morphology than those that were found in the mild OA joints. In the severe OA, the particles carried history information and were involved in the wear process and their surfaces were likely to be smoothened in the process. Therefore, these functional properties were found to be uncorrelated. In addition to the above two functional parameters, the spatial property

described using summit density (*Sds*) cannot reveal common features between particle and cartilage surface. *Sds* is the density of peaks of a scale limited surface. Cartilage *Sds* values were very close at a micro scale while the OA particles had larger *Sds* in comparison to that of non-OA particles. In general, cartilage *Sds* revealed the elasticity to bearing the load which in turn resulted in the surface summit density to a consistent value during OA process, even though the joint narrowing changes [92]. During the cartilage deformation the particles are generated, and *Sds* values of OA particles were increased which also has been reported previously [9].

This study has identified a number of common features of the cartilage and particle surfaces. *Ssk* of the cartilage was correlated with *Str37* of the particle. *Ssk* represents the degree of symmetry of the surface heights about the mean plane. The cartilage *Ssk* decreased by the severity of OA [1]. The decreased *Ssk* suggested that the cartilage surface was normalised in the wear process and increased the generation of particles. *Str37* is a measure of the spatial isotropy or directionality of the surface texture. The *Str37* values of particles revealed that the particle surface become a bit more anisotropic by the severity of OA. It has been observed in Section 4.4, the particle textures such as nodules and scratches (Figure 4.9 and 4.10) were not directionally or periodically distributed over the surface. *S10z* of the cartilage correlated to *Str37* of particle. The cartilage *S10z* revealed that the surface roughness increased during the OA progression. The textures on the cartilage contributed to the roughness grade and were related to their particle surface isotropy. *Std* of cartilage was correlated *Str37* of particles. *Std* was calculated from the Fourier spectrum to reveal the angle of the dominating surface texture. Cartilage *Std* showed a steep decrease from the healthy to OA cartilage surface. No specific texture was observed on the healthy cartilage (Figure 6.1a), while the

textures appeared to have topography with straight edges on cartilage with OA grade 1 (Figure 6.1b) and many sharp and long threads attached on cartilage with OA grade 3 (Figure 6.1d). Even though the particles carry history information and are involved in the complex wear process, the texture changes on the cartilage also correlated to the surface isotropy of particles. *Svi* of cartilage was correlated to *Str37* of particles. *Svi* describes large void volumes in a valley zone of a surface. Cartilage *Svi* showed the slight decreased trend with the severity of OA. The results indicated that the healthy cartilage surfaces had a large void volume [1]. It is logical to suppose that the surfaces with a large void volume would be easy to retain synovial fluid and provide a good load-bearing property. Therefore, the *Str37* of particles was positively correlated to *Svi* of cartilage. *Ssk* of cartilage was correlated to *Std* of particles. The value of particle *Std* was modified by a decreased trend under complex wear. The texture direction of particles was related to cartilage surface topography. Also, the cartilage functional property (*Svi*) revealed common features with the particle spatial property described by *Std*. Particle *Std* indicated the changes in particle texture direction during OA progression in which the cartilage degradation through fissures and changed its lubrication property.

One-way ANOVA ($p < 0.05$) was used to further select the parameters from the highly correlated parameters that could be used to differentiate OA grades or assess the grade of the cartilage. Particle *Str37* and *Std* were examined to monitor the cartilage features during OA. Cartilage *Ssk*, *S10z*, *Ssk*, *Std* and *Svi* also were examined at this stage to test that whether the differences were significant enough to differentiate OA grades. The average *Svi* values of cartilage for mild OA and severe OA were very close (~ 0.13 (Table 6.1)). The differences of *Svi* between OA grades were not significant enough to

indicate OA grade changes. The same situation was observed for particle *Str37*. The mean *Str37* of particles were approximately 0.7 in three OA grades (Table 4.5). Therefore, *Str37* of particles cannot be used to predict the cartilage parameter values. The mean of particle *Std* for non-OA, mild OA and severe OA were 90.94°, 88.66° and 82.21°, respectively. However, the difference of particle *Std* was not significant enough to differentiate non-OA and mild OA. A similar trend was observed for cartilage *Ssk* with 0.35 for non-OA, 0.14 for mild OA and 0.09 for severe OA. However, the changes in the *Ssk* were not significant enough to differentiate between mild and severe OA. *Std* may not be used to monitor cartilage were during OA.

6.3 Summary

The visual inspection of cartilage revealed that the roughness of cartilage increased from healthy to OA grade 2, and the cartilage with OA grade 3 revealed more signs of wear including areas revealing subchondral bone. The particles from severe samples were smoother than those found in the mild OA samples.

Through the investigation of the correlations between the cartilage and particle surface parameters, it is concluded that texture direction (*Std*) of particles showed the similar trend with surface skewness (*Ssk*). During the complex OA wear process, the cartilage surface appeared to normalise its height distribution, and the particles produced from the cartilage also decreased their Std. However, the differences of *Std* or *Ssk* between OA grades were not significant enough to differentiate OA grades.

The results presented in Chapter 4, 5 and 6 will be discussed in the chapter 7 to obtain a

better understanding of the wear process that related to OA.

Table 6.6 Correlation between particle and cartilage parameters. The data were presented as the format of Pearson correlation coefficient and the p-value in the brackets.

		Cartilage parameters										
		Ssk	*Sku*	*S10z*	*Ssc*	*Sds*	*Std*	*Stdi*	*Str37*	*Str20*	*Sbi*	*Svi*
Particle parameters	*Ssk*	0.42 (0.72)	0.23 (0.86)	0.33 (0.78)	0.29 (0.82)	-0.65 (0.55)	-0.39 (0.75)	-0.61 (0.58)	-0.65 (0.55)	-0.69 (0.52)	-0.63 (0.57)	-0.42 (0.72)
	Sku	0.55 (0.63)	0.36 (0.76)	0.47 (0.69)	0.42 (0.72)	-0.75 (0.46)	-0.52 (0.65)	-0.72 (0.49)	-0.75 (0.46)	-0.78 (0.43)	-0.73 (0.48)	-0.55 (0.63)
	S10z	0.10 (0.94)	-0.11 (0.93)	0.00 (1.00)	-0.05 (0.97)	-0.36 (0.77)	-0.06 (0.96)	-0.32 (0.80)	-0.36 (0.77)	-0.41 (0.73)	-0.34 (0.78)	-0.10 (0.94)
	Sds	0.54 (0.64)	0.35 (0.77)	0.46 (0.70)	0.41 (0.73)	-0.74 (0.47)	-0.51 (0.66)	-0.71 (0.50)	-0.74 (0.47)	-0.78 (0.43)	-0.72 (0.48)	-0.54 (0.64)
	Std	-1.00 (0.04)	-0.96 (0.17)	-0.98 (0.10)	-0.97 (0.13)	0.98 (0.12)	0.99 (0.06)	0.98 (0.09)	0.98 (0.12)	0.96 (0.15)	0.98 (0.11)	0.99 (0.04)
	Str20	0.06 (0.54)	0.80 (0.40)	0.72 (0.48)	0.76 (0.45)	-0.43 (0.71)	-0.68 (0.51)	-0.47 (0.68)	-0.43 (0.71)	-0.38 (0.74)	-0.45 (0.69)	-0.65 (0.54)
	Scl37	-0.78 (0.42)	-0.89 (0.29)	-0.84 (0.36)	-0.86 (0.33)	0.59 (0.59)	0.80 (0.40)	0.63 (0.56)	0.59 (0.59)	0.55 (0.62)	0.61 (0.57)	0.78 (0.42)
	Str37	1.00 (0.01)	0.98 (0.11)	0.99 (0.04)	0.99 (0.07)	-0.95 (0.18)	-1.00 (0.00)	-0.90 (0.15)	-0.95 (0.18)	-0.94 (0.21)	-0.96 (0.17)	-1.00 (0.01)
	Spk	-0.13 (0.91)	-0.33 (0.78)	-0.22 (0.85)	-0.26 (0.82)	-0.13 (0.91)	0.16 (0.89)	-0.09 (0.93)	-0.14 (0.91)	-0.19 (0.87)	-0.11 (0.92)	0.12 (0.92)
	Svk	-0.99 (0.07)	-0.95 (0.20)	-0.97 (0.13)	-0.96 (0.16)	-0.31 (0.80)	0.99 (0.09)	0.99 (0.07)	0.98 (0.10)	0.97 (0.13)	0.99 (0.08)	0.99 (0.06)
	Smr1	-0.494 (0.671	-0.66 (0.54)	-0.57 (0.61)	-0.61 (0.58)	0.98 (0.10)	0.52 (0.65)	0.28 (0.81)	0.24 (0.84)	0.19 (0.87)	-0.70 (0.50)	0.49 (0.67)
	Smr2	0.50 (0.66)	0.32 (0.79)	0.42 (0.72)	0.38 (0.75)	0.24 (0.84)	-0.47 (0.68)	-0.68 (0.51)	-0.72 (0.48)	-0.75 (0.45)	0.98 (0.11)	-0.51 (0.65)

Chapter 7 Discussion

Wear particles carry important information on knee joint grades. In the previous study [9], the surface topographies of wear particles found in human knee joints were not well studied for OA. Their feasibility in discriminating different OA grades has been investigated in this study. As found in Chapter 4, the mean comparisons of individual parameters could not appropriately cluster the particles into OA grades. In Chapter 5, the distinct parameters have been identified using discriminant analysis. The key parameters combined linear functions to group particles based on their features associated with OA grades. This study has also demonstrated the common surface features between particles and cartilage. Detailed discussions of the procedures and results are presented below.

7.1 Image acquisition techniques of biological wear particles

In the image acquisition process, the following challenges needed to be overcome: (a) the sample preparation for imaging, (b) image acquisition to obtain appropriate surface morphologies data for numerical characterisations, and (c) setting up the microscope according to the characteristics of the surface morphology of the wear particles. As the cartilage has a water content of approximately 70% [49], dehydration of wear particles during the image acquisition was an issue that needed to be controlled. During the dehydration process, the particles shrank, affecting the shape and surface properties of the particles. The shape and morphologies of the human wear particles in a hydrated grade can be potentially obtained using LSM which is discussed below.

Although the LSM is not widely used for quantitative surface characterisation, it can capture the boundary and surface topography of the wear particles at a micrometre scale. LSM has been used to capture the cartilage in a hydrated state [2]. In this study, the cartilage was immersed in PBS, pH 7.4 and only the surface of the particles exposed under the objective lens of LSM during imaging. The particles were too thin to apply this same procedure for cartilage imaging. The dehydration period was measured using sheep joint particles which have reported similar features as the human wear particles [68]. The sheep wear particles were put under the objective lens of LSM and to be found that the wear particles were in a good hydration grade between 10 to 17 minutes after the particles has been removal from the fridge. Figure 3.1 shows the continued changes in hydration of particle surface over time. Initially the particle surface was too wet to image as the PBS solution covering the surface influenced the light reflection. After 10 minutes, the particles were normally hydrated and could be imaged. After approximately 17 minutes, the particle started shrinking and wrinkles were abundant on the particle surface (see Figure 3.1b). Therefore, all particles were imaged after removal from the fridge to standardise particle hydration grades (10 minutes) for imaging that took maximum 7 minutes to complete.

Setting up LSM is another important procedure for quantitative characterisation of the particles. The main factors considered to select a suitable set up were (a) a capture time less than 7 minutes, (b) a high resolution to obtain 3D information of the particles, and (c) a uniform set up suitable for all the particles including smooth particles and chunky particles whose height more than 30 μm. The 150× magnification was not suitable for imaging wear particles due to light reflection from the particle surface. LSM with 10×, 20× and 50× objective lens were able to capture the particles within 7 minutes, while

LSM with 10× or 20× did not provide sufficient surface data of wear particles over a large range of the depth in the Z direction. It was found that rough particles and very rough particles imaged at 10× or 20× objective lens (Figure 3.2b) did not provide clear information about the surface appearance. In contrast the 50× magnification revealed clearly the surface morphology of wear particles (Figure 4.10 and Figure 4.11). Thus, LSM with 50× objective lens was used to capture the wear particles in this study.

7.2 Particle size distribution

The study of particle size was undertaken to further our understanding of the wear process. The comparative results of particle size distribution are discussed below.

In this study, particles in a wider size range (>3 µm) were analysed compared to a previous study [8] where only particles more than 8 µm in size were measured. In this study, the particles in the 3-8 µm size range accounted for 32, 21 and 30% in non-OA, mild OA and severe OA, respectively. The small particles are not as easily removed from the synovial fluid as large ones, however they may provide important information about the wear process as they have been shown to influence the lubrication of the cartilage during wear [68]. Although large particles are thought to usually be freshly produced and could obtain the newest insight into the grade of the cartilage, the particles including 3-8 µm contributed to a more presentative particle study.

This study reported comparable size distribution of human wear particles with previous studies. This study confirmed the results reported in a previous study by Athanasiou KA et al [4] that small particles (< 10 µm) are the most abundant in the joints with OA or

without OA. The mean sizes of wear particles in OA synovial fluid are larger than those in the healthy synovial fluid, which is also consistent with previous findings [8, 9]. The mean size of large wear particles is decreased in mild OA to severe OA and is believed to be caused by the change in the cartilage properties in severe OA. As the wear of the cartilage nears the subchondral bone, the wear rate is impeded due to the hardening of the cartilage [68]. Due to the change in the cartilage properties, in particular, the hardness, the size of the particles is reduced. The study of the size distribution of human wear particles suggested that the mean sizes of wear particles are related to OA grades. However, in this study the differences were not significant enough for OA diagnosis and assessment.

7.3 Statistical analysis of quantitative parameters of wear particles

This study reported that the presentative particles of non-OA displayed a smooth surface, while the majority of particles found in mild OA joints had a rough surface with high peaks. For the severe OA, it is believed that the wear rate was impeded by an increase in the hardness of the cartilage in the direction perpendicular to this top surface and its collagen fibrils [1, 9]. The structure of articular cartilage has been divided into the superficial zone, including the lamina splendens, the middle zone, the deep zone, the tide mark and the calcified zone. The uppermost layer, named as lamina splendens, appears smooth. The wear particles produced from the lamina splendens exhibit thin, smooth, leaf-like surfaces [8]. Therefore, the leaf-like particles (Figure 4.7) are commonly found in healthy joints. When the fissures extend to the superficial zone where the collagen is parallel to the cartilage surface, the wear particles exhibit a rod shape (Figure 4.5). Thus, the rod-shaped particles are commonly found in early stage of

OA (OA grade ≤ 1) [8]. In the middle zone, the collagen fibres are arranged in a series of closely packed layers or leaves without bridging fibrils [49]. The chunky particles (Figure 4.3) with distinct corners are produced during the wear to the middle zone. The rod-shaped particles can also be produced from the middle zone when the leaves are broken up along the collagen direction and become the particles. It seems that the chunky particles from the middle zone are commonly produced during mild OA process which is evidenced by the visual inspections performed in this study. The chunky particles also originate from the deep zone with the collagen fibres perpendicularly orientated to the cartilage surface and interconnected by bridging fibrils [49]. The wear particles originating from the deep zone must be torn off a solid network of collagen and are large and chunky with distinct corners [8] or complex structure (irregular particle in Figure 4.6). Therefore, the chunky particles are most abundant in mild and severe OA, and irregular particles are commonly found in severe OA. In the severe OA, the wear between subchondral bone / exposed collagen fibres and soft cartilage surface, the particles generated and appeared to be smoother than mild OA particles.

The discriminant analysis identified distinct 3D parameters and classified the majority of particles in each OA grade. In the previous studies, comparisons of mean values of parameters were commonly used to find the differences between the particles in different OA grades. However, most of the parameters could not show a significant difference between OA grades. This was also found in the present study as the comparison of particles based on the mean of a single parameter (one-way ANOVA) could not be used to identify the OA grade. This is due to the fact that various particles were produced during the very complex OA process. The mathematical expectation, defined as the probability-weighted average of all possible values, would be better to

evaluate the particle features than the average values of the parameters [93]. However, the percentage of each shape could not be counted due to similar morphologies of some particles which were hard to differentiate for human observers. In this study, the features of the major particles in different OA grades were described by the distinct parameters which were identified using discriminant analysis. The different coefficients of the parameters in Canonical functions indicated the different percentages of various particles in different OA grades. Solidity (*S*) and form factor (*FF*) revealed the shape differences between the non-OA and OA particles. The commonly found particles in the non-OA joints including leaf-like particles with a complex shape and the elongated particles, contributed to a lower *FF* which described the difference between non-OA and osteoarthritic particles. The most abundant chunky particles found in mild and severe OA joints had a larger *S* than those of non-OA. Area (*A*), Material volume (*Mv*) and density of summits (*Sds*) further distinguish the presentative particles of mild and severe OA. The *A* of severe OA particles was smaller than that of mild OA particles as the particles changed from a circular to elongated shape while the average length was similar. Inspection of particle surfaces suggested that severe OA particles were smoother than mild OA particles. *Mv* and *Sds* revealed the volume of peak section and summit density, respectively, and were used to distinguish the mild and severe OA particles in discriminant analysis. This method is able to discriminant between OA grades and non-OA joints.

The clinical grading is based on the joint narrowing and the affecting area of cartilage. The joint narrowing was related to the cartilage degeneration into different zones of cartilage. The clinical assessment was not sensitive to detect early OA (OA grades $\leqq$ 1), while the particle features associated with cartilage structures can differentiate the early OA.

7.4 Correlations between cartilage and particle surface parameters

The aim of the correlations between particle surface and cartilage surface parameters is to identify correlated parameters which describe the common features between cartilage and wear particle surface from the same OA grade. The surface texture relations are discussed based on the visual observations. Then, the common features identified by the correlation study are discussed and the parameters that were potentially key indicators to differentia OA grades are discussed.

From visual inspection between wear particles and the cartilage surface, the particle surface features were related to the cartilage surface morphologies. The leaf-like particles exhibited a smooth texture which is consistent with the healthy cartilage surface feature. The nodules on the particle surface are believed to be generated by rolling wear [68]. The morphology with round edges (Figure 6.2c) may wear the summits to nodules and formed as wear particles when one cartilage slides a distance to another. Therefore, the rough and very rough particles with many nodules were commonly found in mild OA (OA grade 1-2). During OA progression, the particles with many nodules could be modified to moderately rough particles with smooth slopes and nodules mixed and were found in the severe OA joints (OA grade 3-4). The scratches were also observed on the moderately rough particles. The smooth textures and scratches on the moderately particles are believed to be worn between the cartilage and the exposed collagen fibres attached on the cartilage with OA grade 3 [2] (Figure 6.2d). It was not easy to generate deep scratches on the subchondral bone in comparison to on a soft cartilage surface (mild OA). Therefore, the particles found in the severe OA wear appeared smoother than mild OA particles.

Some spatial parameters of particles describe common features with some cartilage amplitude, spatial and functional parameters. Spatial parameter, particle texture aspect ratio (*Str37*) was highly correlated to cartilage amplitude parameters (surface skewness (*Ssk*) and ten point height (*S10z*)), spatial parameter (texture direction (*Std*)) and functional parameter (valley fluid retention index (*Svi*)). *Ssk* indicated the predominance of peaks (*Ssk* > 0) or the valley structures (*Ssk* < 0) comprising the surface. Cartilage *Ssk* values suggested peak dominant surfaces. During the degradation process, the cartilage changed its inhomogeneous and height symmetry by the increasing formation of wear particles [1]. Also, the cartilage *S10z* revealed that the cartilage surface became rougher with the severity of OA. In particular, the cartilage with OA grade 3 was much rougher with many vertically oriented collagen fibrils on the surface (Figure 6.1d) and the subchondral bone may as be exposed. The particles with scratches found in the severe OA joints may be produced by the wear between the soft cartilage and the robust collagen fibrils which were exposed on the cartilage surface (Figure 6.1d). Cartilage *Std* illustrated dominant texture changes of cartilage surfaces. Specifically, no texture was observed on the healthy cartilage (Figure 6.1a). With the cartilage degradation through the fissures, the textures appeared to have topography with straight edges on cartilage with OA grade 1 (Figure 6.1b), the textures with round edge on the cartilage with OA grade 2 (Figure 6.1c). Cartilage *Svi* revealed that the healthy cartilage surfaces had a large void volume [1]. For mild and severe OA, that contained surfaces with signs of wear, the void volume for retaining synovial fluid reduced and functional damage occurred to the surface [68]. *Str37* is a measure of the spatial isotropy or directionality of the surface texture. Particle textures such as nodules and scratches were observed on some particles surface (Figure 4.9 and 4.10) and they were not directionally or periodically distributed over the surface. Therefore, the *Str37* values of particles were

slightly increased by the severity of OA. Wang M. et al [9] also reported the similar result of particle *Str37*. Thus, the common features were described by particle *Str37* to cartilage *Ssk*, *S10z*, *Std* and *Svi*. The correlation results also suggested that the particle spatial parameter *Std*, was highly linearly correlated to the cartilage amplitude parameter *Ssk* and the cartilage functional parameter *Svi*. The decrease of particle *Std* was related to human cartilage which has an inhomogeneous structure and non-uniform material property in the vertical direction normal to its top surface [1].

As stated in section 6.4, One-way ANOVA ($p < 0.05$) was used to further identify the parameters that can be used to differentiate OA grades from the highly correlated parameters, and *Str37*, *S10z*, *Ssk*, *Std* and *Svi* were examined at this stage. The numerical results suggested that the mean *Str37* of particles was 0.7 for all three OA grades (Table 4.5). That is, no differences between the particles with different OA grades were identified by *Str37*. Therefore, *Str37* of a particle cannot be used to predict the cartilage parameter values. The study by Ewing et al [94] showed that the average *Svi* values of cartilage for mild OA and severe OA were very close (~ 0.13 (Table 6.1)) and slightly smaller in comparison to that of the healthy cartilage (~ 0.14). Unfortunately, the differences of *Svi* between OA grades were not significant enough to indicate OA grade changes for the cartilage surface. The mean of particle *Std* for non-OA, mild OA and severe OA were 90.94°, 88.66° and 82.21°, respectively. However, the difference between particle *Std* was not significant enough to differentiate between non-OA and mild OA. Even though a similar trend shown by cartilage *Ssk* with 0.35 for non-OA, 0.14 for mild OA and 0.09 for severe OA, the changes in the *Ssk* were not significant enough to differentiate mild and severe OA. *Std* may not be used as the key indicator to monitor the cartilage grades.

The correlations between the wear particle and cartilage surface features help to further understand the wear process. The visual observations revealed the feature relation between cartilage and wear particles. Unfortunately, the statistical correlations suggested no distinct particle parameters can be used to differentiate the OA grades and to monitor the surface changes of the cartilage with corresponding OA grade.

Chapter 8 Conclusions

This project has developed an image acquisition protocol to analyse the surface morphologies of wear particles in a hydrated state. Based on 3D surface images acquired using the LSM technique, numerical characterisations were carried out on human knee wear particles involved in the wear process associated with OA. These developments allowed the identification and quantification of the main features of the particles that explain the OA wear progression. Detailed outcomes of this project are presented below.

8.1 Outcomes of the image acquisition process using LSM

The LSM was selected to capture the surface data as well as the shape features of the wear particles. Owing to its high resolution, a short time was required for image acquisition and low requirements for sample preparation. In order to obtain sufficient 3D information of the wear particle surface, the 50× objective lens was used in this project. Short capture times allowed the particles to remain in hydrated condition throughout the imaging. Compared to 10× and 20× objective lens, the high quality of particle images also has been acquired using objective lens with 50×.

8.2 Quantitative assessment of wear particles

The qualitative information obtained from the surface morphology and shape features of the studied wear particles, was essential to identify the specific characteristics of wear particles with the OA progression that would be used for hypothesis statements and

support the statistical analysis results. For the qualitative assessment, a wider range of size and more presentative particles were studied in a size range of 3 to 90 μm. The study of size distribution of wear particles reported results that were consistent with previous studies. The majority of particles (~ 82%) in all OA grades were smaller than 20 μm. The particles in mild OA had the largest mean size of all particles analysed however it was not significantly different to the other OA grades.

The quantitative assessment of wear particles was performed using 29 numerical parameters. The mean comparisons of the parameters could not show a significant difference to identify OA grades. This was also found in the present study as the comparisons of particles based on the mean of a single parameter could not be used to identify the OA grade. This is due to the fact that various particles were produced during the very complex OA process. In this study, the features of the major particles in different OA grades were described by the distinct parameters which were identified using discriminant analysis. The different coefficients of the parameters in Canonical functions indicated the different percentages of various particles in different OA grades (see Figure 5.15). Solidity, form factor and area revealed the shape differences between the non-OA and OA particles. Material volume and density of summits further distinguish the presentative particles of mild and severe OA. This method is able to discriminant between OA grades and non-OA joints.

8.3 Outcomes of correlation between particle and cartilage surface features

The surface morphology of cartilage becomes rougher and more heterogeneous with the severity of the OA grade (See Figure 6.1). The particle study in this project reported

inconsistent results about the roughness grade with cartilage that the presentative particles of non-OA displayed a smooth surface, while the majority of particles found in mild OA joints had a rough surface with high peaks. In the severe OA, particles were involved in the wear process as a third party and their surfaces are likely to be smoothened in the process. Particle *Str37* described the common feature with cartilage *Ssk, S10z Std* and *Svi*. However, the mean *Str37* of particles were all around 0.7 in three OA grades (Table 4.5). Therefore, *Str37* of particle cannot be used to predict the cartilage parameter values. Even though cartilage *Svi* revealed a common trend with particle *Std*, the average *Svi* values of cartilage for mild OA and severe OA were very close (~ 0.13 (Table 6.1)). The differences of *Svi* between OA grades were not significant enough to indicate OA grade changes. Particle *Std* was highly correlated to cartilage *Ssk.* During the complex OA process, the cartilage surface appeared to normalise its height distribution, and the particles produced from the cartilage also declined their *Std*. The difference of particle *Std* was not significant enough to differentiate non-OA and mild OA and the changes in the *Ssk* were not significant enough to differentiate mild and severe OA. *Std* may be used as the key indicator to monitor the cartilage grades.

8.4 Limitations of this study and further improvement

This project can be further extended by addressing the following issues:

(a) More wear particles from more human samples should be collected and studied to confirm the results in the project. 331 particles from 24 patients were captured and statistically analysed. This study reported consistent size distribution with previous studies [8, 9]. More wear particles should be further studied to confirm the results of

particle surface features.

(b) Examine the corresponding cartilage for each synovial fluid sample. Three cartilage groups (non-OA cartilage, mild OA cartilage and severe OA cartilage) were correlated studied with the wear particles. The correlations between cartilages and the wear particles from the corresponding synovial fluid sample may be stronger. Examine the corresponding cartilages as well to conduct the correlation to confirm the results in this study.

(c) Examine the corresponding cartilage with the same resolution as the particles. LSM with 50× magnification was used to capture wear particles while the cartilages were imaged by LSM with 10× magnification. Different magnification may describe different features. Thus, correlations between particle and cartilage based on the same resolution can be further conducted to confirm the results.

References

[1] Peng Z, Wang M. Three dimensional surface characterization of human cartilages at a micron and nanometre scale. Wear. 2013;301:210-7.
[2] Baena J, Peng Z. 3D quantitative characterization of degraded surfaces of human knee cartilages affected by osteoarthritis. Wear. 2014;319:1-11.
[3] Jordan K, Clarke AM, Symmons DP, Fleming D, Porcheret M, Kadam UT, et al. Measuring disease prevalence: a comparison of musculoskeletal disease using four general practice consultation databases. British Journal of General Practice. 2007;57:7-14.
[4] Athanasiou KA, Darling EM, Hu JC. Articular cartilage tissue engineering. Synthesis Lectures on Tissue Engineering. 2009;1:1-182.
[5] Bevill SL. Regional variations in knee joint articular cartilage mechanobiology: a consideration in the initiation of osteoarthritis: ProQuest; 2009.
[6] Martel-Pelletier J, Boileau C, Pelletier J-P, Roughley PJ. Cartilage in normal and osteoarthritis conditions. Best Practice & Research Clinical Rheumatology. 2008;22:351-84.
[7] Peng Z. Osteoarthritis diagnosis using wear particle analysis technique: investigation of correlation between particle and cartilage surface in walking process. Wear. 2007;262:630-40.
[8] Kuster M, Podsiadlo P, Stachowiak G. Shape of wear particles found in human knee joints and their relationship to osteoarthritis. Rheumatology. 1998;37:978-84.
[9] Wang M, Peng Z, Vasilev K, Ketheesan N. Investigation of Wear Particles Generated in Human Knee Joints Using Atomic Force Microscopy. Tribology Letters. 2013;51:161-70.
[10] Ronald R. Hugate Jr. RDH, James R. Counts. Handbook of Hip & Knee Joint Replacement: Through the Eyes of the Patient, Surgeon & Medical Team. 2012.
[11] Marieb EN, Hoehn K. Human anatomy & physiology: Pearson Education; 2007.
[12] Moskowitz RW. Osteoarthritis: diagnosis and medical/surgical management: Lippincott Williams & Wilkins; 2007.
[13] Buckwalter JA, Mankin HJ, Grodzinsky AJ. Articular cartilage and osteoarthritis. INSTRUCTIONAL COURSE LECTURES-AMERICAN ACADEMY OF ORTHOPAEDIC SURGEONS. 2005;54:465.
[14] Stone A, Loeser R, Vanderman K, Long D, Clark S, Ferguson C. Pro-inflammatory stimulation of meniscus cells increases production of matrix metalloproteinases and additional catabolic factors involved in osteoarthritis pathogenesis. Osteoarthritis and Cartilage. 2013.
[15] Heijink A, Gomoll AH, Madry H, Drobnič M, Filardo G, Espregueira-Mendes J, et al. Biomechanical considerations in the pathogenesis of osteoarthritis of the knee. Knee Surgery, Sports Traumatology, Arthroscopy. 2012;20:423-35.
[16] Hechtman L. Clinical Naturopathic Medicine: Elsevier Australia; 2012.
[17] McGinty JB, Burkhart SS. Operative arthroscopy: Lippincott Williams & Wilkins; 2003.
[18] Bollet AJ. An essay on the biology of osteoarthritis. Arthritis & Rheumatism. 1969;12:152-63.
[19] Maroudas A, Bullough P, Swanson S, Freeman M. The permeability of articular cartilage. Journal of Bone & Joint Surgery, British Volume. 1968;50:166-77.

[20] Buckwalter J, Mankin H. Instructional Course Lectures, The American Academy of Orthopaedic Surgeons-Articular Cartilage. Part I: Tissue Design and Chondrocyte-Matrix Interactions*†. The Journal of Bone & Joint Surgery. 1997;79:600-11.
[21] Cohen NP, Foster RJ, Mow VC. Composition and dynamics of articular cartilage: structure, function, and maintaining healthy state. Journal of Orthopaedic & Sports Physical Therapy. 1998;28:203-15.
[22] Glazebrook MA, MED DS. Practical Orthopaedic Sports Medicine & Arthroscopy 1st Edition.
[23] Newman AP. Articular cartilage repair. The American journal of sports medicine. 1998;26:309-24.
[24] Nordin M, Frankel VH. Basic biomechanics of the musculoskeletal system: Lippincott Williams & Wilkins; 2001.
[25] Bollet AJ, Nance JL. Biochemical findings in normal and osteoarthritic articular cartilage. II. Chondroitin sulfate concentration and chain length, water, and ash content. Journal of Clinical Investigation. 1966;45:1170.
[26] Maynes R. Structure and function of collagen types: Elsevier; 2012.
[27] Maroudas A. Balance between swelling pressure and collagen tension in normal and degenerate cartilage. Nature. 1976;260:808-9.
[28] Fraser J, Laurent T, Laurent U. Hyaluronan: its nature, distribution, functions and turnover. Journal of internal medicine. 1997;242:27-33.
[29] Meyer K, Smyth EM, Dawson MH. The isolation of a mucopolysaccharide from synovial fluid. Journal of Biological Chemistry. 1939;128:319-27.
[30] Bagga H, Burkhardt D, Sambrook P, March L. Longterm effects of intraarticular hyaluronan on synovial fluid in osteoarthritis of the knee. The Journal of rheumatology. 2006;33:946-50.
[31] Holmes M, Bayliss M, Muir H. Hyaluronic acid in human articular cartilage. Age-related changes in content and size. Biochem J. 1988;250:435-41.
[32] Brumback RJ, Jones AL. Interobserver agreement in the classification of open fractures of the tibia. The results of a survey of two hundred and forty-five orthopaedic surgeons. The Journal of Bone & Joint Surgery. 1994;76:1162-6.
[33] Mandelbaum BR, Browne JE, Fu F, Micheli L, Mosely JB, Erggelet C, et al. Articular cartilage lesions of the knee. The American Journal of Sports Medicine. 1998;26:853-61.
[34] Rhee DK, Marcelino J, Baker M, Gong Y, Smits P, Lefebvre V, et al. The secreted glycoprotein lubricin protects cartilage surfaces and inhibits synovial cell overgrowth. Journal of Clinical Investigation. 2005;115:622-31.
[35] Lee SY, Nakagawa T, Reddi AH. Induction of chondrogenesis and expression of superficial zone protein (SZP)/lubricin by mesenchymal progenitors in the infrapatellar fat pad of the knee joint treated with TGF-β1 and BMP-7. Biochemical and biophysical research communications. 2008;376:148-53.
[36] Athanasiou K, Rosenwasser M, Buckwalter J, Malinin T, Mow V. Interspecies comparisons of in situ intrinsic mechanical properties of distal femoral cartilage. Journal of Orthopaedic Research. 1991;9:330-40.
[37] Lai W, Mow V. Drag-induced compression of articular cartilage during a permeation experiment. Biorheology. 1980;17:111.

[38] Mow V, Kuei S, Lai W, Armstrong C. Biphasic creep and stress relaxation of articular cartilage in compression: theory and experiments. Journal of biomechanical engineering. 1980;102:73-84.
[39] Zhu W, Lai WM, Mow VC. The density and strength of proteoglycan-proteoglycan interaction sites in concentrated solutions. Journal of biomechanics. 1991;24:1007-18.
[40] Saarakkala S, Korhonen RK, Laasanen MS, Töyräs J, Rieppo J, Jurvelin JS. Mechano-acoustic determination of Young's modulus of articular cartilage. Biorheology. 2004;41:167-79.
[41] Aigner T, Rose J, Martin J, Buckwalter J. Aging theories of primary osteoarthritis: from epidemiology to molecular biology. Rejuvenation Research. 2004;7:134-45.
[42] Stachowiak G. Numerical characterization of wear particles morphology and angularity of particles and surfaces. Tribology International. 1998;31:139-57.
[43] Podsiadlo P, Stachowiak G. 3-D imaging of surface topography of wear particles found in synovial joints. Wear. 1999;230:184-93.
[44] Kuster MS, Wood GA, Stachowiak GW, Gächter A. Joint load considerations in total knee replacement. Journal of Bone & Joint Surgery, British Volume. 1997;79:109-13.
[45] Tian Y, Wang J, Peng Z, Jiang X. A new approach to numerical characterisation of wear particle surfaces in three-dimensions for wear study. Wear. 2012;282-283:59-68.
[46] Neale MJ, Britain G. Tribology handbook: Butterworths; 1973.
[47] Ratner BD, Hoffman AS, Schoen F, Lemons JE. Biomaterials science: an introduction to materials in medicine. San Diego, California. 2004:162-4.
[48] Bhushan B. Introduction to tribology: John Wiley & Sons; 2013.
[49] Jeffery A, Blunn G, Archer C, Bentley G. Three-dimensional collagen architecture in bovine articular cartilage. Journal of Bone & Joint Surgery, British Volume. 1991;73:795-801.
[50] Stachowiak GW. Wear: materials, mechanisms and practice: John Wiley & Sons; 2006.
[51] Pinchuk LS, Nikolaev V, Tsvetkova E, Goldade VA. Tribology and biophysics of artificial joints: Elsevier Science Ltd; 2005.
[52] Hills B, Monds M. Enzymatic identification of the load-bearing boundary lubricant in the joint. Rheumatology. 1998;37:137-42.
[53] Stachowiak G, Batchelor A, Griffiths L. Friction and wear changes in synovial joints. Wear. 1994;171:135-42.
[54] Ballantine GC, Stachowiak GW. The effects of lipid depletion on osteoarthritic wear. Wear. 2002;253:385-93.
[55] Topolovec M, Milošev I, Cör A, Bloebaum RD. Wear debris from hip prostheses characterized by electron imaging. Central European Journal of Medicine. 2013;8:476-84.
[56] Roylance B. Ferrography—then and now. Tribology International. 2005;38:857-62.
[57] Mears D, Hanley E, Rutkowski R, Westcott V. Ferrographic analysis of wear particles in arthroplastic joints. Journal of biomedical materials research. 1978;12:867-75.
[58] Evans C, Mears D, Stanitski C. Ferrographic analysis of wear in human joints. Evaluation by comparison with arthroscopic examination of symptomatic knees. Journal of Bone & Joint Surgery, British Volume. 1982;64:572-8.

[59] Meyer DM, Tillinghast A, Hanumara NC, Franco A. Bio-ferrography to capture and separate polyethylene wear debris from hip simulator fluid and compared with conventional filter method. Journal of tribology. 2006;128:436-41.
[60] Elsner JJ, Mezape Y, Hakshur K, Shemesh M, Linder-Ganz E, Shterling A, et al. Wear rate evaluation of a novel polycarbonate-urethane cushion form bearing for artificial hip joints. Acta biomaterialia. 2010;6:4698-707.
[61] Danilatos G. Foundations of environmental scanning electron microscopy. Advances in electronics and electron physics. 1988;71.
[62] Cappella B, Dietler G. Force-distance curves by atomic force microscopy. Surface science reports. 1999;34:1-104.
[63] Hildebrand M, Doktycz MJ, Allison DP. Application of AFM in understanding biomineral formation in diatoms. Pflügers Archiv-European Journal of Physiology. 2008;456:127-37.
[64] Masajada J, Popiołek-Masajada A, Augustyniak I, Sokolenko B. Towards superresolution imaging with optical vortex scanning microscope. SPIE Optical Metrology 2013: International Society for Optics and Photonics; 2013. p. 87882V-V-10.
[65] Paddock SW. Principles and practices of laser scanning confocal microscopy. Molecular biotechnology. 2000;16:127-49.
[66] Wang W, Ferguson DJ, Quinn JM, Simpson AHR, Athanasou NA. Biomaterial particle phagocytosis by bone-resorbing osteoclasts. Journal of Bone & Joint Surgery, British Volume. 1997;79:849-56.
[67] Lucas L, Gilbert N, Ploton D, Bonnet N. Visualization of volume data in confocal microscopy: comparison and improvements of volume rendering methods. Journal of microscopy. 1996;181:238-52.
[68] Lipshitz H, Etheredge 3rd R, Glimcher MJ. In vitro wear of articular cartilage. The Journal of Bone & Joint Surgery. 1975;57:527-34.
[69] Podsiadlo P, Kuster M, Stachowiak G. Numerical analysis of wear particles from non-arthritic and osteoarthritic human knee joints. Wear. 1997;210:318-25.
[70] Swanson P, Vetter A. The measurement of abrasive particle shape and its effect on wear. ASLE transactions. 1985;28:225-30.
[71] Dong W, Sullivan P, Stout K. Comprehensive study of parameters for characterising three-dimensional surface topography: III: Parameters for characterising amplitude and some functional properties. Wear. 1994;178:29-43.
[72] Jiang X, Scott PJ, Whitehouse D, Blunt L. Paradigm shifts in surface metrology. Part II. The current shift. Proceedings of the Royal Society A: Mathematical, Physical and Engineering Science. 2007;463:2071-99.
[73] Stachowiak G, Podsiadlo P. Characterization and classification of wear particles and surfaces. Wear. 2001;249:194-200.
[74] Vasilev K, Michelmore A, Martinek P, Chan J, Sah V, Griesser HJ, et al. Early stages of growth of plasma polymer coatings deposited from nitrogen-and oxygen-containing monomers. Plasma Processes and Polymers. 2010;7:824-35.
[75] Vasilev K, Michelmore A, Griesser HJ, Short RD. Substrate influence on the initial growth phase of plasma-deposited polymer films. Chem Commun. 2009:3600-2.
[76] Iyengar GV, Subramanian KS, Woittiez JR. Element Analysis of Biological Samples: Principles and Practices: CRC Press; 1997.
[77] Bozzola JJ, Russell LD. Electron microscopy: principles and techniques for biologists: Jones & Bartlett Learning; 1999.

[78] Larsen KS, Jonasson S, Michelsen A. Repeated freeze–thaw cycles and their effects on biological processes in two arctic ecosystem types. Applied Soil Ecology. 2002;21:187-95.
[79] Stout KJ. Development of methods for the characterisation of roughness in three dimensions2000.
[80] Dong W, Sullivan P, Stout K. Comprehensive study of parameters for characterizing three-dimensional surface topography II: Statistical properties of parameter variation. Wear. 1993;167:9-21.
[81] Jones C, Stoffel K, Ozturk H, Stachowiak G. The effect of surface active phospholipids on the lubrication of osteoarthritic sheep knee joints: Wear. Tribology Letters. 2004;16:291-6.
[82] Tiainen V-M. Amorphous carbon as a bio-mechanical coating—mechanical properties and biological applications. Diamond and Related Materials. 2001;10:153-60.
[83] Benesty J, Chen J, Huang Y, Cohen I. Pearson correlation coefficient. Noise reduction in speech processing: Springer; 2009. p. 1-4.
[84] Montgomery DC, Runger GC, Hubele NF. Engineering statistics: John Wiley & Sons; 2009.
[85] Heiberger RM, Neuwirth E. One-way anova. R Through Excel: Springer; 2009. p. 165-91.
[86] Scholkopft B, Mullert K-R. Fisher discriminant analysis with kernels. Neural networks for signal processing IX. 1999;1:1.
[87] Jekel JF, Katz DL, Elmore JG, Wild D. Epidemiology, biostatistics and preventive medicine: Elsevier Health Sciences; 2007.
[88] Kuo R, Ho L, Hu CM. Integration of self-organizing feature map and K-means algorithm for market segmentation. Computers & Operations Research. 2002;29:1475-93.
[89] Rencher AC. Interpretation of canonical discriminant functions, canonical variates, and principal components. The American Statistician. 1992;46:217-25.
[90] Agresti A, Kateri M. Categorical data analysis: Springer; 2011.
[91] Fidelix T, Macedo CR, Maxwell LJ, Fernandes Moça Trevisani V. Diacerein for osteoarthritis. Cochrane Database Syst Rev. 2014;2.
[92] Mologhianu G. Osteoarthritis pathogenesis.
[93] Gnedenko BV, Belyayev YK, Solovyev AD. Mathematical methods of reliability theory: Academic Press; 2014.
[94] Ewing JW. Articular cartilage and knee joint function: basic science and arthroscopy: Raven Pr; 1990.

Appendixes

Appendix A Presentative 3D images of wear particle surface using LSM.

A.1 LSM images of wear particles found in healthy joints.

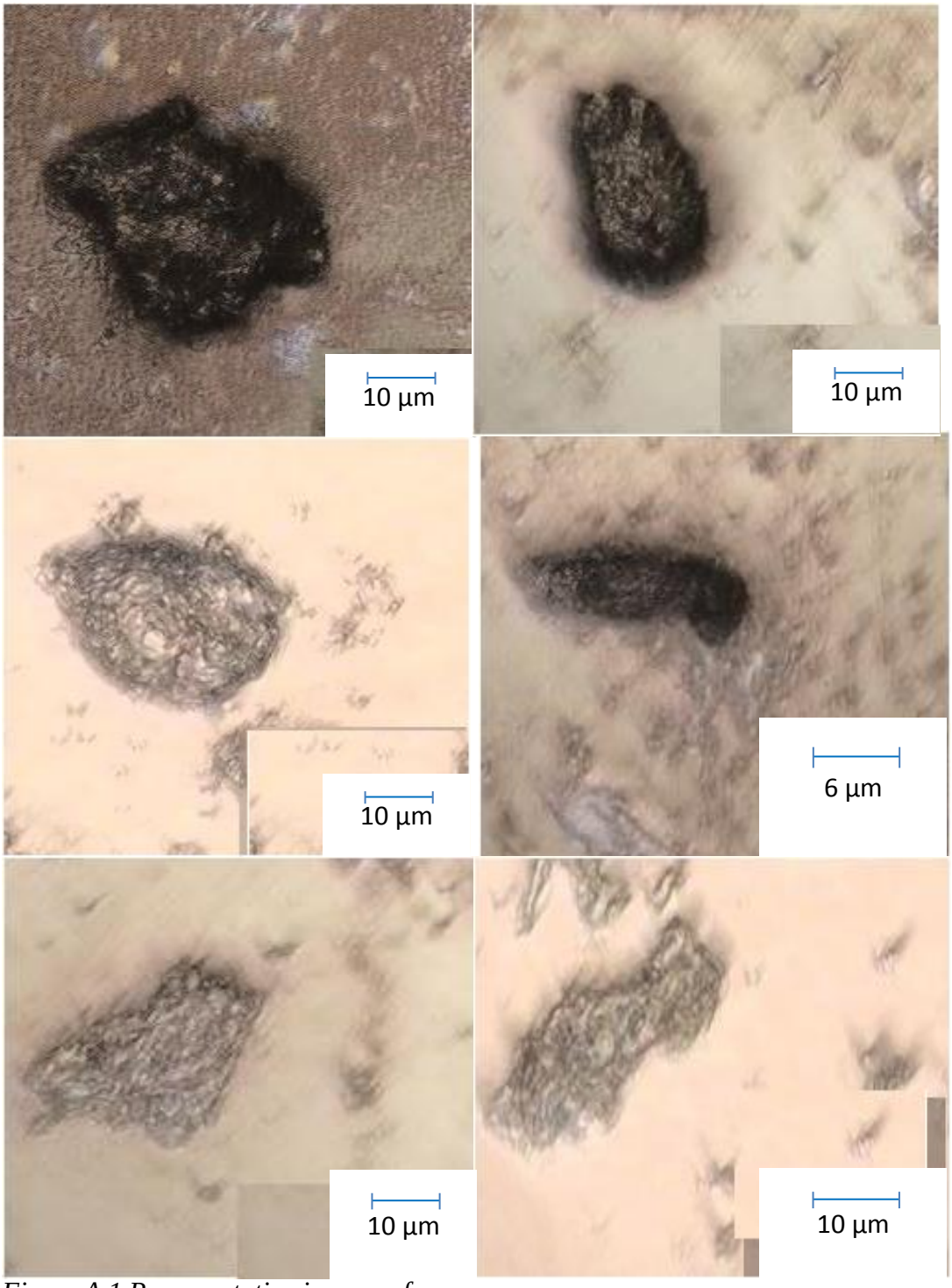

Figure A.1 Representative images of wear particles found in healthy joints.

A.2 LSM images of wear particles found in mild OA joints.

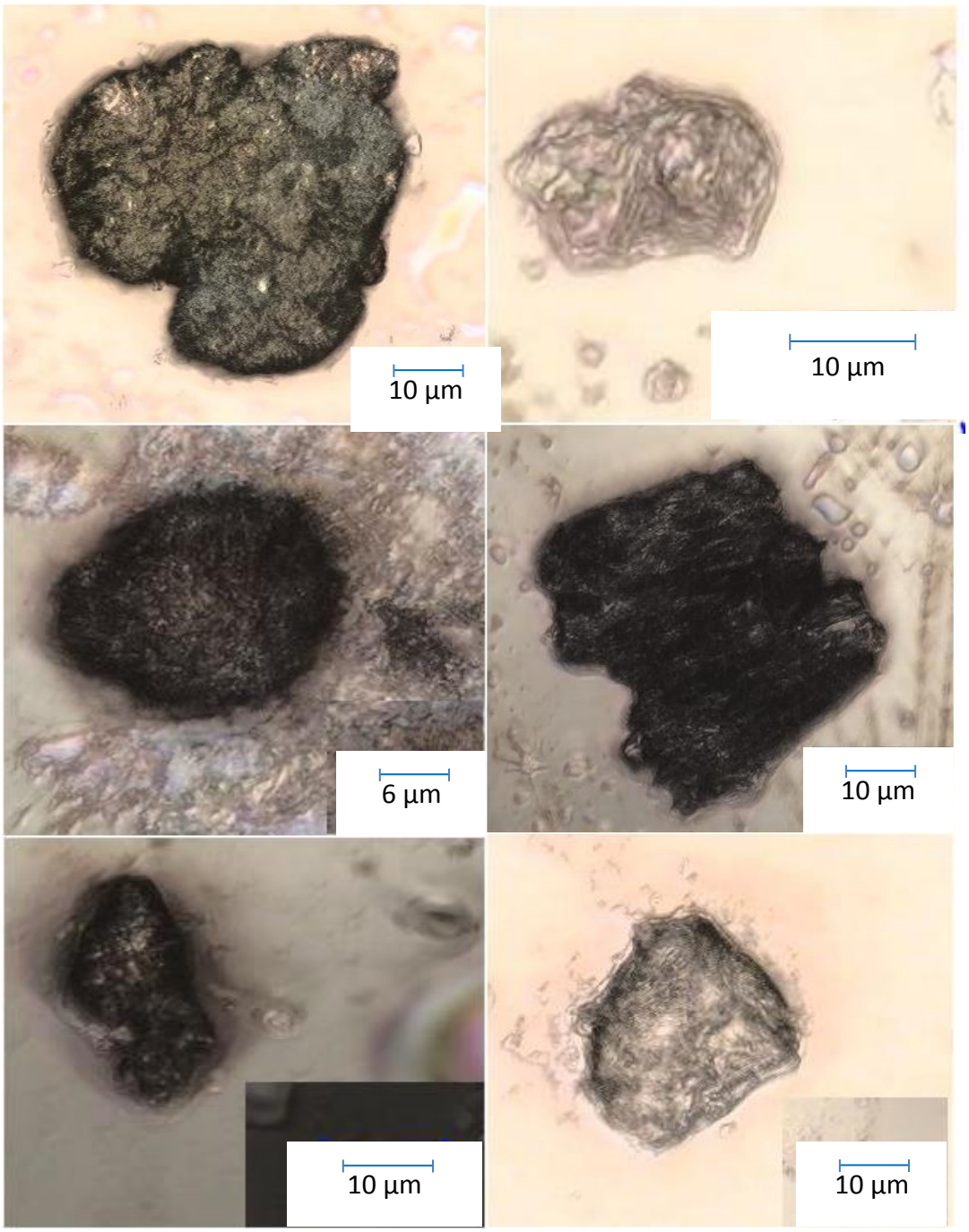

Figure A.2.1 Representative images of wear particles found in mild OA joints.

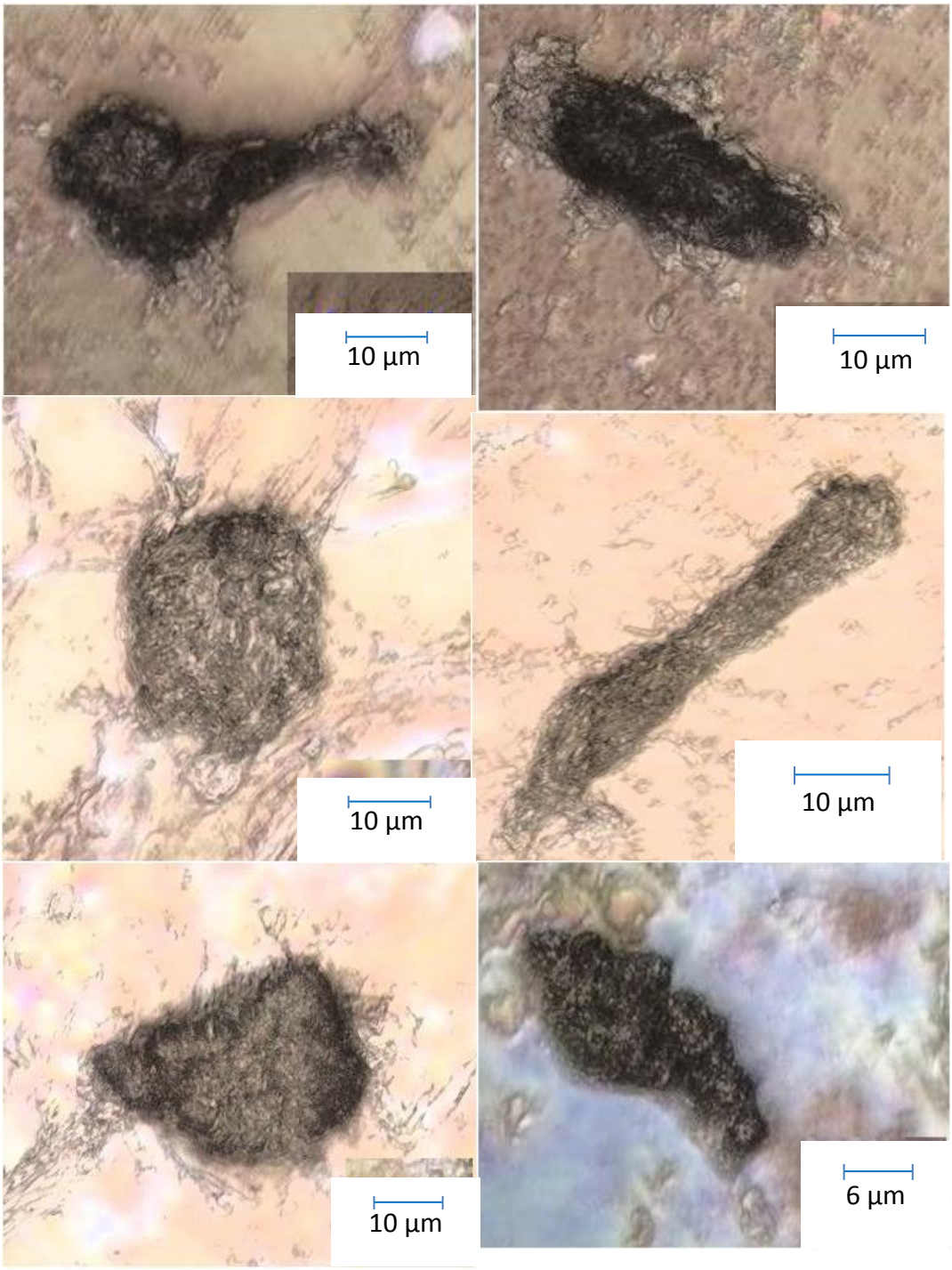

Figure A.2.2 Representative images of wear particles found in mild OA joints.

A.3 LSM images of wear particles found in severe OA joints.

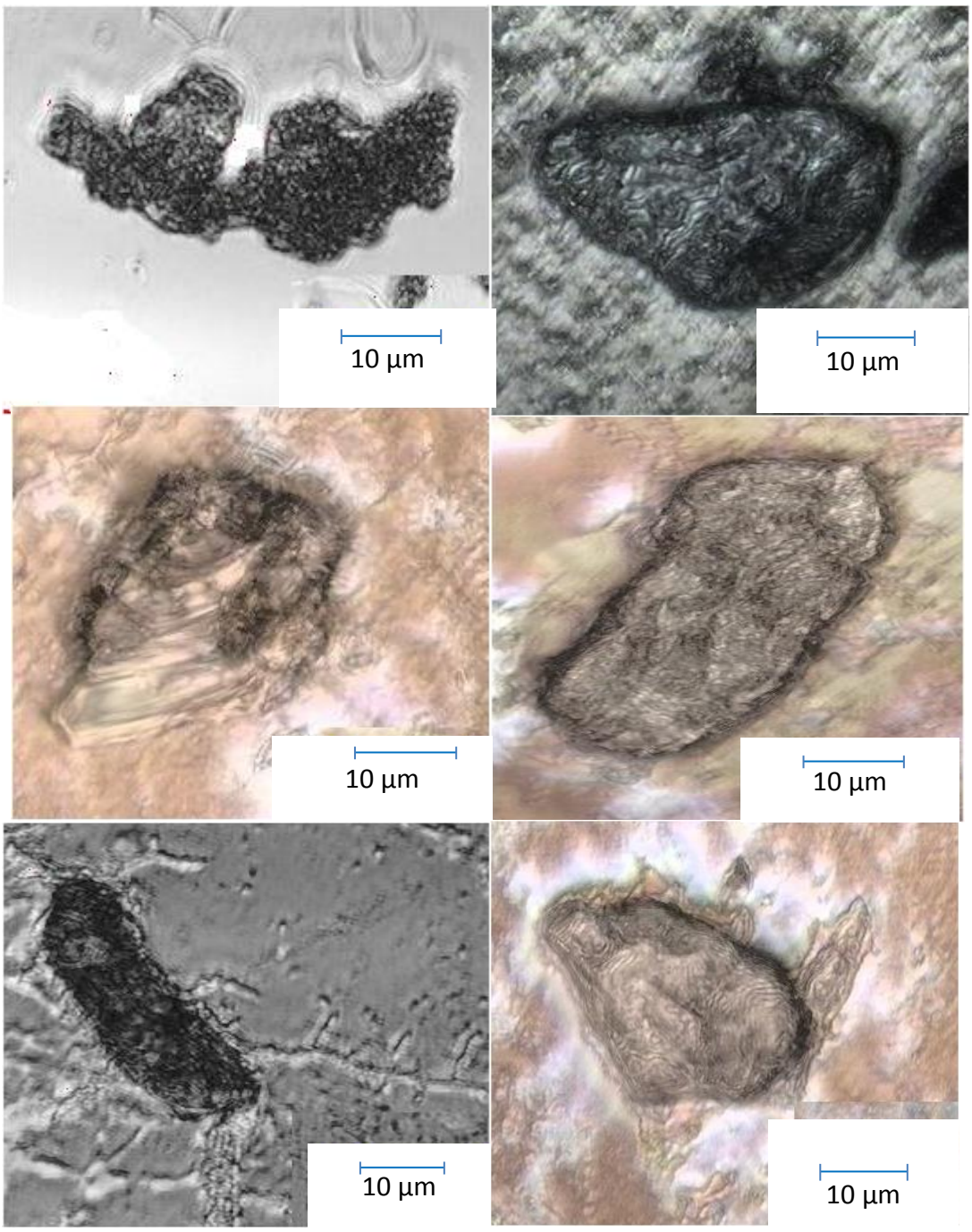

Figure A.3.1 Representative images of wear particles found in severe OA joints.

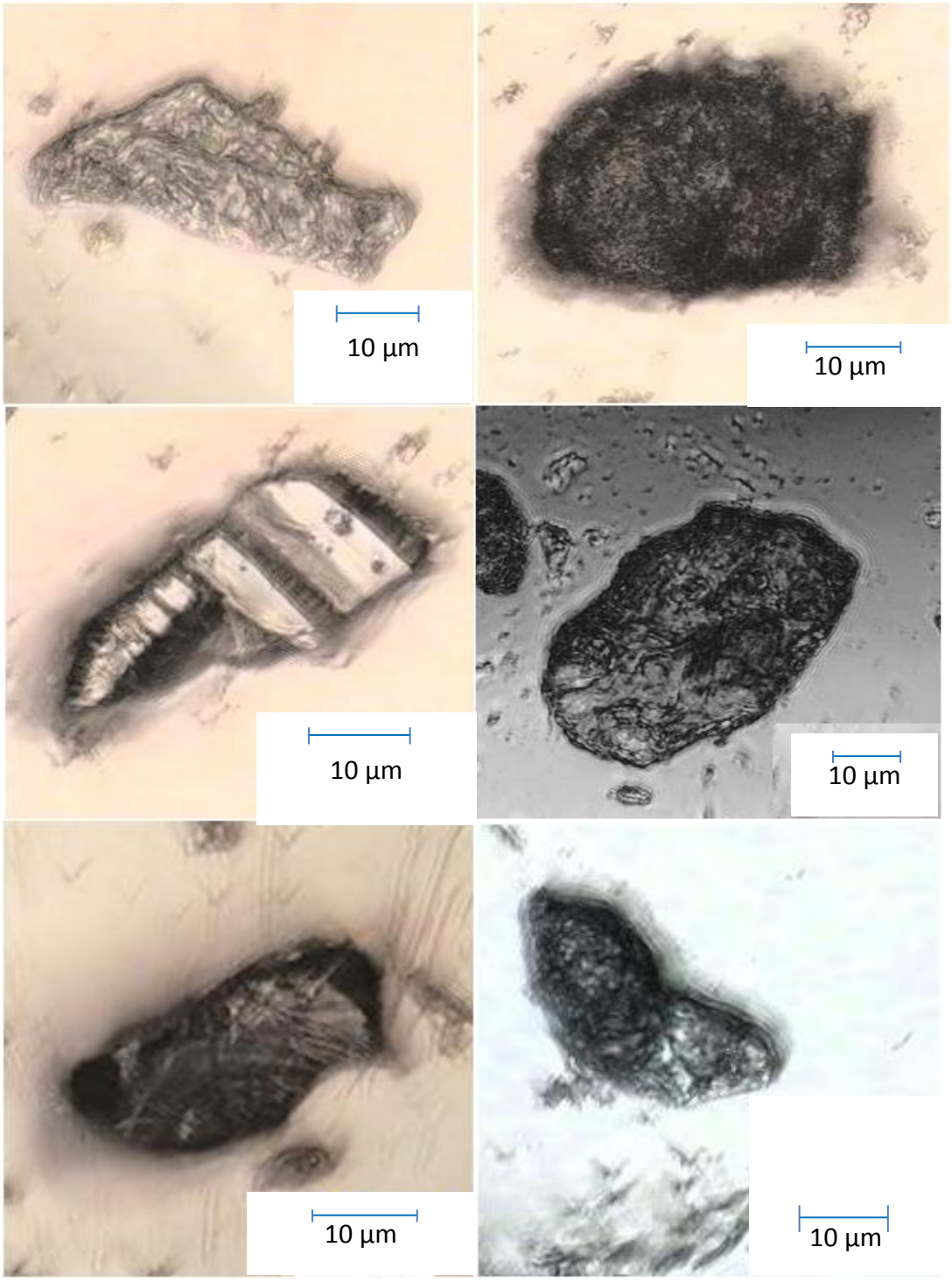

Figure A.3.2 Representative images of wear particles found in severe OA joints.

Appendix B Numerical values of wear particles.

Table B.1 Numerical values of non-OA wear particles.

Shape parameters				
Area (μm^2)	**Length (μm)**	**Material Volume (μm^3)**	**Void Volume (μm^3)**	**Net Volume (μm^3)**
6.38E+02	42.10	2.36E+03	3.72E+01	2.33E+03
1.81E+02	20.07	1.02E+03	5.14E+00	1.02E+03
1.53E+02	15.94	5.18E+02	9.89E+01	4.19E+02
1.74E+02	19.06	4.82E+02	6.32E+01	4.18E+02
2.26E+02	18.88	5.33E+02	5.21E+01	4.80E+02
7.78E+01	11.83	1.45E+02	3.95E+01	1.05E+02
3.15E+03	71.96	5.74E+03	1.63E+03	4.10E+03
4.54E+01	8.55	1.81E+02	3.41E-03	1.81E+02
1.11E+03	51.89	1.59E+03	5.86E+02	1.00E+03
4.23E+02	27.57	1.04E+03	4.34E+01	1.00E+03
4.01E+01	8.47	4.39E+01	2.63E+01	1.76E+01
1.11E+03	64.57	1.12E+03	6.19E+02	5.05E+02
1.01E+02	19.90	3.00E+01	2.11E+02	-1.80E+02
2.09E+02	19.97	6.41E+02	3.17E+00	6.37E+02
6.54E+01	16.96	6.22E+01	3.18E+01	3.05E+01
2.54E+01	7.70	6.60E+01	2.81E-01	6.57E+01
4.60E+01	8.28	1.91E+01	3.67E+01	-1.80E+01
2.88E+02	30.43	6.19E+02	8.36E+00	6.10E+02
1.34E+01	5.41	2.42E+00	1.16E+01	-9.20E+00
1.66E+01	5.97	9.57E+00	8.66E+00	9.11E-01
6.45E+01	14.56	1.68E+01	5.39E+01	-3.70E+01
5.95E+01	12.79	5.51E+00	8.55E+01	-8.00E+01
1.74E+02	17.84	1.87E+01	2.18E+02	-2.00E+02
1.68E+01	6.17	6.76E+00	1.00E+01	-3.30E+00
1.39E+02	20.21	3.47E+01	1.08E+02	-7.30E+01
3.39E+01	7.78	4.35E+01	1.13E+00	4.23E+01
2.39E+02	28.20	1.92E+02	6.35E+01	1.28E+02
6.97E+01	15.47	2.80E+01	4.55E+01	-1.70E+01
8.20E+01	11.55	2.68E+01	5.35E+01	-2.70E+01
3.54E+02	31.47	2.16E+02	1.39E+02	7.64E+01
3.90E+01	11.63	2.46E+00	3.58E+01	-3.30E+01
1.53E+02	18.71	2.51E+02	6.69E+00	2.44E+02
1.33E+01	6.08	4.70E+00	7.80E+00	-3.10E+00
1.99E+01	7.16	8.05E+00	1.02E+01	-2.10E+00

2.86E+01	8.54	3.00E+01	4.49E+00	2.55E+01
3.13E+01	7.50	4.92E+01	1.12E+00	4.81E+01
2.00E+01	7.97	4.55E+00	1.36E+01	-9.10E+00
1.23E+01	6.06	1.45E+00	8.86E+00	-7.40E+00
4.89E+01	12.73	4.29E+00	5.60E+01	-5.20E+01
3.48E+01	11.25	1.20E+01	2.06E+01	-8.60E+00
4.68E+01	13.00	2.20E+01	2.05E+01	1.51E+00
4.73E+01	11.71	1.98E+01	2.25E+01	-2.70E+00
1.32E+01	4.74	1.19E+00	9.78E+00	-8.60E+00
3.17E+01	8.02	1.16E+01	1.65E+01	-4.90E+00
4.42E+02	33.47	1.37E+02	2.55E+02	-1.20E+02
1.64E+02	20.27	2.81E+02	2.10E+00	2.78E+02
3.40E+01	10.39	7.17E+01	2.22E-01	7.14E+01
3.09E+01	8.51	4.30E+01	1.57E+00	4.14E+01
5.17E+01	14.69	4.16E+00	5.98E+01	-5.60E+01
2.44E+01	8.31	8.18E+00	1.22E+01	-4.00E+00
2.45E+01	6.56	1.74E+00	2.27E+01	-2.10E+01
7.00E+01	11.51	1.18E+02	2.42E-02	1.18E+02
7.03E+01	19.64	9.56E+00	5.55E+01	-4.60E+01
1.74E+01	5.80	2.71E+00	1.25E+01	-9.80E+00
8.70E+00	5.00	2.74E+00	4.42E+00	-1.70E+00
1.08E+01	5.01	2.33E+00	5.38E+00	-3.00E+00
3.54E+01	13.76	4.34E+00	2.28E+01	-1.80E+01
3.90E+01	11.85	4.43E+01	2.75E+00	4.16E+01
1.85E+01	6.29	7.21E-01	1.76E+01	-1.70E+01
1.95E+01	7.85	1.36E+00	1.35E+01	-1.20E+01
6.13E+01	11.39	8.94E+01	3.05E-01	8.91E+01
3.84E+01	11.82	3.72E+01	1.60E-02	3.72E+01
2.46E+01	7.25	3.79E+00	1.43E+01	-1.10E+01
7.44E+01	17.42	1.06E+02	1.77E+00	1.04E+02
2.08E+02	22.96	1.73E+00	2.57E+02	-2.60E+02
4.64E+01	11.58	4.86E+00	3.26E+01	-2.80E+01
1.74E+01	6.44	7.60E+00	5.05E+00	2.55E+00
1.69E+01	6.32	8.94E+00	3.93E+00	5.01E+00
3.52E+02	30.07	7.96E+01	1.58E+02	-7.80E+01
3.40E+01	11.85	6.40E+00	1.68E+01	-1.00E+01
3.48E+01	9.11	1.12E+01	1.24E+01	-1.20E+00
6.90E+01	15.45	5.06E+01	1.29E+01	3.78E+01
1.31E+01	6.02	3.15E+00	5.10E+00	-1.90E+00
7.65E+01	18.85	1.78E+01	3.09E+01	-1.30E+01
5.89E+01	16.16	2.07E+01	1.78E+01	2.86E+00
1.35E+01	7.60	3.42E+01	1.67E-01	3.40E+01
2.91E+01	9.83	1.54E+00	1.85E+01	-1.70E+01
1.68E+01	5.39	5.67E+00	5.10E+00	5.67E-01

1.42E+02	22.03	2.62E+01	6.36E+01	-3.70E+01
2.68E+01	9.32	4.59E+00	1.09E+01	-6.30E+00
1.64E+01	5.46	2.94E+00	7.29E+00	-4.30E+00
3.32E+01	10.00	6.68E+00	1.39E+01	-7.30E+00
3.64E+01	10.29	1.37E+01	7.22E+00	6.50E+00
1.60E+01	6.38	1.11E+00	8.13E+00	-7.00E+00
4.97E+01	11.61	9.68E+01	1.45E-01	9.67E+01
2.10E+01	5.70	1.55E+01	9.92E-02	1.54E+01
3.65E+01	10.22	3.11E+01	1.38E+00	2.97E+01
2.93E+01	7.24	1.86E+01	2.85E-02	1.86E+01
2.49E+01	7.73	1.89E+01	1.18E+00	1.77E+01
1.71E+01	6.40	4.15E+00	4.41E+00	-2.60E-01
4.09E+01	14.06	4.07E-02	2.99E+01	-3.00E+01
2.10E+01	5.56	4.28E+00	5.98E-01	3.68E+00
3.99E+01	9.30	3.16E+00	8.27E+00	-5.10E+00

Shape parameters				
Roundness	**Form Factor**	**Convexity**	**Elongation**	**Solidity**
0.45	0.20	2.46	0.37	0.95
0.56	0.32	1.86	0.33	0.92
0.68	0.50	1.33	0.12	0.96
0.61	0.61	1.16	0.35	0.96
0.72	0.46	1.43	0.07	0.94
0.69	0.46	1.89	0.18	0.95
0.73	0.40	1.43	0.17	0.97
0.68	0.30	1.18	0.11	0.91
0.46	0.09	3.12	0.23	0.87
0.65	0.37	1.55	0.16	0.95
0.65	0.66	1.19	0.16	0.97
0.34	0.32	1.24	0.65	0.91
0.32	0.37	0.92	0.62	0.89
0.63	0.16	1.77	0.00	0.86
0.29	0.38	1.66	0.59	0.89
0.54	0.33	2.55	0.21	0.83
0.69	0.39	1.39	0.03	0.91
0.39	0.28	3.49	0.37	0.82
0.55	0.45	1.50	0.26	0.89
0.58	0.34	1.42	0.18	0.85
0.37	0.17	1.62	0.35	0.83
0.40	0.15	1.64	0.34	0.82
0.66	0.56	1.11	0.20	0.96
0.54	0.41	0.80	0.22	0.81
0.42	0.31	1.28	0.50	0.87

0.70	0.58	1.46	0.15	0.91
0.37	0.33	8.06	0.45	0.95
0.37	0.27	2.71	0.43	0.86
0.65	0.39	1.20	0.22	0.93
0.45	0.21	5.27	0.39	0.90
0.36	0.28	1.08	0.48	0.80
0.53	0.28	1.49	0.24	0.93
0.45	0.43	0.98	0.46	0.87
0.49	0.41	0.95	0.33	0.88
0.45	0.33	1.16	0.27	0.88
0.62	0.53	1.21	0.21	0.92
0.40	0.37	1.44	0.47	0.91
0.42	0.24	1.50	0.34	0.82
0.38	0.18	2.78	0.49	0.78
0.35	0.28	1.20	0.39	0.88
0.33	0.17	2.35	0.30	0.77
0.43	0.28	0.83	0.42	0.81
0.73	0.61	1.08	0.12	0.92
0.56	0.46	2.16	0.12	0.88
0.50	0.42	2.10	0.44	0.92
0.49	0.32	1.62	0.37	0.92
0.38	0.33	1.21	0.36	0.90
0.54	0.36	2.84	0.24	0.85
0.30	0.24	1.75	0.56	0.81
0.45	0.44	1.34	0.39	0.84
0.69	0.69	1.15	0.17	0.95
0.60	0.31	1.27	0.17	0.87
0.23	0.14	1.03	0.69	0.88
0.64	0.74	1.42	0.25	0.95
0.43	0.30	1.03	0.31	0.73
0.48	0.44	1.40	0.33	0.82
0.23	0.24	1.94	0.69	0.86
0.34	0.30	2.18	0.46	0.68
0.56	0.43	1.02	0.12	0.88
0.40	0.47	1.37	0.53	0.96
0.58	0.38	1.18	0.32	0.89
0.35	0.53	1.19	0.60	0.92
0.59	0.51	1.20	0.19	0.92
0.30	0.20	1.94	0.38	0.72
0.50	0.53	1.50	0.38	0.97
0.43	0.19	3.19	0.24	0.82
0.52	0.47	1.56	0.25	0.89
0.53	0.37	1.46	0.21	0.89
0.49	0.28	1.95	0.43	0.95

0.31	0.16	1.40	0.46	0.80
0.53	0.32	1.65	0.22	0.89
0.36	0.22	3.76	0.44	0.75
0.45	0.53	1.33	0.43	0.92
0.27	0.16	1.45	0.57	0.87
0.28	0.24	2.20	0.57	0.80
0.29	0.27	1.65	0.57	0.83
0.37	0.35	1.08	0.56	0.88
0.65	0.45	1.25	0.19	0.91
0.37	0.32	1.49	0.53	0.96
0.39	0.44	1.17	0.53	0.94
0.70	0.49	1.06	0.19	0.90
0.38	0.21	2.58	0.33	0.84
0.43	0.42	1.61	0.40	0.91
0.47	0.47	1.22	0.41	0.86
0.45	0.23	1.15	0.23	0.84
0.68	0.57	0.99	0.10	0.92
0.44	0.25	3.10	0.33	0.72
0.65	0.45	1.44	0.10	0.89
0.50	0.19	1.58	0.19	0.78
0.51	0.44	1.70	0.21	0.86
0.26	0.23	1.96	0.54	0.84
0.78	0.80	1.28	0.07	0.97
0.58	0.47	1.13	0.28	0.88

Amplitude parameters							**Hybrid parameter**
Sa (µm)	**Sq (µm)**	**Ssk**	**Sku**	**S10z (µm)**	**Sv (µm)**	**Sp (µm)**	**Sdr (%)**
3.89	5393.70	1.77	4.80	22.23	4.12	19.93	19293.00
3.76	4158.40	0.29	1.82	18.67	8.79	10.18	7614.60
3.30	3770.90	-0.17	1.87	16.78	9.10	8.03	11793.00
2.52	2942.30	-0.08	2.14	14.20	7.55	7.32	5536.80
2.21	2663.10	0.53	2.74	14.92	6.72	9.54	4309.50
2.17	2585.50	0.21	2.28	11.84	4.83	7.51	5942.80
2.12	2587.80	0.19	2.38	14.12	6.89	7.49	3593.40
1.99	2335.60	0.33	2.07	9.28	4.05	5.54	4344.80
1.87	2342.80	0.26	2.73	14.86	6.12	10.81	2249.20
1.81	2176.50	0.32	2.59	11.24	4.44	8.38	2316.70
1.76	2178.40	0.20	2.72	11.22	6.26	6.03	5616.40
1.72	2252.50	0.85	4.46	15.46	5.80	10.01	3203.10

1.61	2066.70	0.58	2.92	9.31	3.65	5.68	6717.80
1.53	1982.30	0.64	3.66	11.63	3.52	8.28	6285.20
1.46	2001.10	1.17	4.55	9.94	3.64	8.68	2294.10
1.20	1385.20	-0.74	2.31	4.22	3.92	2.26	1339.70
1.17	1579.30	0.32	4.01	9.62	4.10	6.92	4019.00
1.15	1464.30	0.49	3.43	8.93	3.30	5.73	3009.60
1.13	1430.20	-1.18	3.87	5.54	5.99	2.71	2842.40
1.10	1364.10	0.30	2.73	6.28	3.06	4.08	4710.90
1.07	1294.00	0.00	3.01	7.32	2.55	7.14	3404.70
1.06	1301.10	-0.01	2.39	5.97	2.34	5.01	3236.80
1.03	1249.50	0.06	2.63	7.52	2.50	5.38	3169.10
0.99	1288.00	0.14	3.07	5.77	2.44	4.04	2811.00
0.99	1246.40	-0.44	3.15	8.45	4.77	4.93	2913.40
0.98	1253.50	0.19	3.45	6.69	2.75	4.27	2739.10
0.97	1246.00	0.10	3.60	9.39	4.40	5.37	3403.00
0.96	1282.50	0.35	3.92	8.57	3.67	5.54	4565.50
0.96	1264.50	0.13	5.04	9.85	4.30	6.81	3222.00
0.95	1181.70	0.04	3.16	8.56	4.17	4.95	2167.80
0.94	1150.60	-0.94	2.84	5.12	3.33	2.14	1946.50
0.94	1172.80	0.08	3.09	7.21	2.07	6.83	1874.60
0.94	1254.30	-0.05	3.84	6.39	4.87	3.57	2675.50
0.94	1150.10	-0.86	2.78	4.47	2.69	2.14	1493.20
0.93	1126.70	-0.06	3.09	6.22	3.25	4.77	2299.20
0.93	1340.30	1.25	5.36	6.93	2.36	4.89	2684.30
0.93	1129.20	-0.67	2.83	5.14	3.40	2.29	2046.80
0.93	1127.70	-1.06	2.98	4.20	3.20	1.65	1987.60
0.93	1145.20	-0.11	2.68	5.70	2.26	3.64	2889.90
0.91	1134.20	0.45	3.00	5.42	1.84	4.09	2382.80
0.91	1145.60	-0.03	3.38	7.19	4.03	4.45	2681.30
0.89	1100.40	-0.16	3.07	6.56	3.17	4.28	2844.90
0.88	1051.90	-0.85	2.80	4.47	3.12	3.16	1979.60
0.88	1107.60	0.02	3.37	6.96	3.74	4.45	2613.80
0.86	1050.90	0.26	3.11	7.53	2.70	5.09	2784.00
0.86	1050.70	0.08	2.56	5.39	2.01	3.93	1980.80
0.85	1024.80	-0.53	2.54	4.57	2.39	2.76	1434.70
0.85	1124.90	0.40	3.74	6.25	3.26	4.22	2179.20
0.85	1030.20	0.18	2.63	4.99	2.93	3.14	973.22
0.84	1002.20	-0.11	2.75	5.32	3.56	3.37	2023.10
0.81	1035.90	-0.81	3.70	5.13	3.84	2.37	1573.30
0.80	1118.10	1.08	5.55	6.31	1.70	5.96	2265.30
0.80	980.13	-0.22	2.72	5.70	3.17	3.89	1690.00
0.80	1082.40	-0.13	4.33	6.11	3.43	3.83	2406.60
0.78	1051.90	0.36	3.49	4.26	2.72	2.69	3027.50
0.77	961.57	-1.08	4.01	4.25	3.66	2.05	2038.40

0.77	898.99	-0.55	2.26	3.75	2.65	1.66	1428.10
0.76	955.17	-0.13	2.93	4.87	2.63	2.61	1295.60
0.76	941.22	-0.65	2.64	4.22	2.76	2.05	1987.40
0.76	942.75	-0.99	3.08	3.94	3.47	1.49	1159.80
0.76	920.64	0.22	3.02	4.85	1.58	4.97	1328.90
0.75	892.33	0.81	3.48	4.48	0.98	4.17	1568.90
0.75	909.42	-0.36	2.49	4.24	2.18	2.21	1936.70
0.73	911.97	-0.07	2.98	5.14	2.97	2.70	828.74
0.72	870.38	-0.35	2.42	5.11	3.99	2.25	1213.20
0.71	838.29	-0.14	2.40	4.56	2.33	2.98	1379.10
0.70	917.59	-0.78	3.90	5.35	3.41	2.97	2006.60
0.69	891.53	-0.80	4.12	5.34	3.53	3.62	2242.90
0.69	828.13	-0.44	2.44	5.21	2.47	3.55	1393.00
0.68	804.69	-0.33	2.26	3.66	2.28	1.94	1385.40
0.67	1091.00	1.24	7.91	6.81	2.48	5.77	1852.50
0.67	808.96	-0.97	2.57	3.72	2.34	1.59	854.08
0.67	933.78	-1.23	4.74	4.62	3.46	2.68	1618.50
0.65	782.59	-0.46	2.37	3.58	2.04	1.74	787.48
0.64	855.41	-0.87	3.78	4.77	3.74	1.69	1445.60
0.64	952.94	-1.82	7.51	4.12	4.74	1.82	1446.80
0.64	850.41	-1.41	4.81	4.01	2.60	1.55	1179.30
0.64	790.90	-0.72	3.37	3.90	3.21	1.55	1114.40
0.63	821.29	-0.62	3.25	4.85	2.54	2.85	1563.20
0.61	781.69	-0.89	3.15	3.52	2.58	1.43	932.00
0.61	780.03	-0.64	3.09	3.69	2.52	1.80	1457.80
0.60	756.30	-0.03	2.67	3.66	2.02	1.75	1674.40
0.59	708.23	0.33	2.57	3.52	1.95	2.19	887.86
0.59	828.58	-1.71	6.69	4.38	3.44	1.93	1129.70
0.58	767.16	-1.03	3.60	3.74	2.67	1.39	1055.20
0.57	712.88	1.17	4.44	3.26	0.78	3.07	1285.20
0.56	703.22	0.35	3.16	3.52	1.15	2.64	1053.80
0.55	682.12	1.27	4.47	3.14	0.66	2.72	711.34
0.55	669.84	0.02	2.28	2.97	1.63	1.97	864.72
0.50	713.60	-0.86	4.02	3.47	2.49	1.52	1387.60
0.34	518.50	-1.65	5.59	2.66	1.85	1.12	530.64
0.30	423.87	2.49	9.92	2.23	0.33	2.21	428.63
0.28	349.64	1.17	4.91	1.89	0.39	1.58	293.31

Functional parameters				
Spk (µm)	**Sk (µm)**	**Svk (µm)**	**Smr1 (%)**	**Smr2 (%)**
14.98	4.37	0.00	26.58	100.00
5.64	7.17	1.55	40.35	95.85
1.77	9.18	2.54	5.93	77.05
1.91	7.59	2.09	7.32	86.18
3.61	5.37	1.07	23.72	91.41
2.15	7.89	0.76	7.89	95.90
2.54	6.29	1.79	17.20	91.60
2.27	5.93	0.69	18.25	95.67
2.74	5.31	1.96	17.09	90.34
2.27	6.50	0.70	8.33	96.24
2.37	5.06	1.92	16.11	91.80
3.78	5.22	1.23	12.85	92.32
3.14	4.31	1.25	17.88	88.38
2.98	4.45	1.20	14.34	88.31
4.11	3.24	1.07	19.91	86.80
0.49	1.67	2.95	6.61	64.06
2.68	2.63	1.73	15.86	81.40
2.05	3.24	1.20	15.90	91.20
0.83	1.77	3.40	6.92	73.72
1.53	3.58	0.80	11.30	91.62
1.53	2.84	1.26	7.98	78.37
1.27	3.07	1.01	10.51	82.59
1.39	3.31	0.85	6.97	86.61
1.43	2.43	1.60	16.83	82.55
1.18	2.31	1.81	10.46	77.72
1.91	2.94	1.39	9.87	89.18
1.60	3.09	1.28	9.88	90.60
2.11	2.34	1.36	12.73	80.24
1.52	2.57	1.41	11.61	83.03
1.35	3.05	1.08	8.61	90.37
0.56	1.29	2.64	10.55	68.88
1.51	2.52	1.23	9.97	79.91
1.73	2.18	1.53	14.27	79.96
0.44	1.84	2.21	7.49	73.87
1.51	2.48	1.23	5.47	79.75
3.83	2.18	1.04	11.52	83.87
0.79	2.02	1.77	7.35	74.30
0.35	1.21	2.85	11.27	71.14

1.25	2.69	1.13	7.11	81.37
1.53	2.85	0.48	11.01	88.82
1.37	2.49	1.13	9.92	82.59
1.08	2.83	1.10	7.59	88.06
0.55	1.11	2.15	7.79	62.02
1.17	2.62	1.07	11.96	89.81
1.39	2.98	0.73	6.72	93.60
1.03	2.81	0.72	8.98	88.49
0.55	2.01	1.47	7.99	75.42
1.72	2.42	1.22	14.29	90.17
1.19	2.95	0.64	7.36	94.10
0.80	2.44	0.87	8.04	84.72
0.66	2.08	1.45	8.71	79.28
2.21	1.75	0.99	16.05	79.62
0.83	2.28	0.94	9.01	81.75
1.79	1.76	1.69	9.86	79.16
1.76	1.96	1.29	16.37	88.88
0.47	1.34	1.56	11.08	67.55
0.50	1.60	1.33	6.48	68.75
0.97	2.49	1.03	7.83	90.00
0.38	2.26	1.21	3.18	80.67
0.51	1.03	2.15	7.80	68.03
1.16	2.24	0.63	8.64	83.66
1.63	1.16	0.00	43.09	100.00
0.87	1.18	1.51	14.80	66.31
0.95	2.14	1.01	10.77	86.72
0.47	2.21	0.81	4.90	83.69
0.76	2.09	0.67	5.12	81.56
0.53	1.95	1.38	9.11	83.82
0.91	1.51	1.53	6.62	77.68
0.66	1.66	1.08	7.55	74.79
0.41	1.85	0.84	7.01	78.25
2.45	1.18	1.64	16.42	84.02
0.40	0.96	2.10	5.14	72.48
0.69	0.93	2.13	21.44	76.21
0.31	1.92	0.84	5.48	81.76
0.59	1.45	1.46	14.16	79.21
0.58	1.06	2.35	18.13	81.21
0.49	0.94	1.46	11.73	65.49
0.50	1.53	1.21	7.74	78.41
0.73	1.67	1.29	8.82	81.70
0.41	1.19	1.61	11.99	75.73
0.53	1.69	1.23	8.06	84.17
0.84	1.66	0.69	12.97	83.93

0.85	1.44	0.58	26.08	93.77
0.61	0.85	1.89	9.65	74.80
0.43	1.26	1.53	10.83	78.89
1.23	1.11	0.00	31.79	100.00
0.81	1.72	0.43	11.30	85.65
1.46	0.58	0.00	45.42	100.00
0.46	1.57	0.46	16.70	86.10
0.89	0.82	1.53	17.18	78.18
0.45	0.42	1.67	18.38	83.01
1.10	0.03	0.18	36.49	73.54
0.54	0.41	0.00	52.23	100.00

Spatial parameters					
Sds ($1/\mu m^2$)	**Std (^{o})**	**Scl20 (nm)**	**Str20**	**Scl37 (nm)**	**Str37**
0.0468	143.96	4.26	0.59	2.97	0.62
0.0121	162.81	3.71	0.71	2.97	0.73
0.0314	168.69	3.20	0.79	2.36	0.85
0.0129	5.76	2.97	0.42	2.22	0.50
0.0141	177.31	3.52	0.73	2.41	0.72
0.0055	177.12	2.97	0.80	2.22	0.80
0.0519	129.35	5.56	0.53	3.06	0.69
0.0026	135.73	2.60	0.74	1.85	0.71
0.0166	17.61	6.95	0.54	4.73	0.59
0.0063	2.02	5.00	0.72	3.61	0.81
0.0027	0.00	2.22	0.71	1.67	0.75
0.0185	23.15	4.17	0.65	2.50	0.69
0.0076	87.24	1.67	0.41	1.11	0.50
0.0154	172.10	2.97	0.73	1.48	0.73
0.0006	146.37	2.50	0.41	1.67	0.46
0.0003	140.08	3.06	0.48	1.39	0.33
0.0096	3.72	1.95	0.64	1.39	0.67
0.0195	178.12	2.22	0.67	1.11	0.67
0.0007	58.54	1.85	0.38	1.30	0.41
0.0011	91.45	1.67	0.60	0.74	0.57
0.0043	43.42	2.22	0.71	0.93	0.71
0.0040	108.10	2.22	0.52	1.30	0.58
0.0354	34.44	1.25	0.69	0.70	0.83
0.0010	90.54	2.22	0.55	1.30	0.64
0.0108	9.00	1.67	0.35	0.93	0.45

0.0027	148.68	2.78	0.79	1.85	0.83
0.0515	173.01	1.25	0.69	0.70	1.00
0.0138	167.89	1.25	0.53	0.70	0.83
0.0057	24.90	1.30	0.64	0.56	0.75
0.0250	5.49	1.30	0.78	0.56	0.75
0.0020	175.36	1.85	0.83	1.11	0.86
0.0105	116.44	2.22	0.52	1.30	0.64
0.0007	33.77	2.04	0.52	1.30	0.64
0.0010	39.43	1.67	0.45	1.30	0.47
0.0019	137.92	1.85	0.56	0.93	0.83
0.0018	33.36	1.85	0.71	0.93	0.62
0.0014	100.41	2.22	0.41	1.48	0.50
0.0015	82.46	2.09	0.54	1.67	0.63
0.0033	16.74	0.93	0.56	0.56	1.00
0.0023	96.81	1.48	0.44	0.93	0.63
0.0030	169.19	0.74	0.67	0.56	1.00
0.0033	13.33	0.56	0.60	0.37	1.00
0.0026	91.91	1.67	0.60	1.25	0.75
0.0067	1.48	1.81	0.68	0.97	0.64
0.1026	14.73	0.97	0.87	0.42	1.00
0.0116	37.69	1.48	0.67	0.56	0.75
0.0023	13.46	2.78	0.65	2.04	0.79
0.0018	103.38	0.74	0.80	0.37	0.67
0.0005	153.68	2.50	0.32	1.67	0.37
0.0014	41.74	0.93	0.56	0.56	0.60
0.0014	47.01	2.04	0.61	1.30	0.70
0.0050	174.25	2.78	0.83	1.48	0.73
0.0038	71.42	0.74	0.40	0.37	0.50
0.0031	53.63	1.39	0.42	0.83	0.67
0.0004	0.86	1.48	0.80	0.93	0.83
0.0019	39.58	1.39	0.77	0.83	0.75
0.0019	164.95	1.67	0.56	0.74	0.67
0.0005	123.19	1.67	0.67	0.83	0.60
0.0044	177.37	1.53	0.85	0.83	0.75
0.0013	142.67	1.48	0.38	0.93	0.71
0.0038	52.40	1.67	0.35	0.93	0.71
0.0024	0.00	0.93	0.62	0.56	0.75
0.0038	177.60	0.70	0.56	0.42	0.75
0.0009	86.48	2.22	0.40	1.39	0.50
0.0141	98.58	0.74	0.67	0.37	0.67
0.0022	177.22	0.93	0.42	0.56	0.75
0.0033	174.81	1.53	0.79	0.97	0.78
0.0030	39.27	1.39	0.67	0.83	0.86
0.0688	152.10	0.70	0.71	0.42	0.75

0.0016	172.60	0.93	0.42	0.37	0.50
0.0019	175.22	2.22	0.67	1.30	0.70
0.0037	163.46	2.04	0.79	0.93	0.83
0.0007	127.79	1.48	0.47	0.74	0.80
0.0032	67.64	1.11	0.38	0.74	0.57
0.0034	57.05	0.74	0.44	0.56	0.75
0.0007	148.77	1.85	0.33	1.11	0.55
0.0053	90.66	1.11	0.50	0.70	0.50
0.0030	176.55	1.67	0.71	1.25	0.82
0.0287	0.00	0.56	0.80	0.28	0.67
0.0014	146.07	0.93	0.33	0.56	0.50
0.0030	0.56	1.53	0.44	0.97	0.58
0.0049	3.90	0.42	0.60	0.28	0.67
0.0018	18.90	1.30	0.64	0.56	0.60
0.0007	32.42	1.67	0.36	0.93	0.50
0.0025	177.38	0.74	0.57	0.37	0.67
0.0016	0.00	2.22	0.75	1.48	0.80
0.0024	0.00	1.67	0.60	0.93	0.71
0.0013	177.04	2.22	0.60	1.67	0.90
0.0013	160.49	0.74	0.67	0.56	0.75
0.0031	9.30	0.42	0.75	0.28	1.00
0.0020	170.78	0.56	0.50	0.37	0.67
0.0012	37.85	0.56	0.43	0.37	0.50
0.0020	89.22	1.67	0.43	0.93	0.63

Table B.2 Numerical values of mild OA wear particles.

Shape parameters				
Area (μm^2)	**Length（μm）**	**Material Volume (μm^3)**	**Void Volume (μm^3)**	**Net Volume (μm^3)**
7.71E+02	47.51	5.19E+03	2.15E+02	4.98E+03
5.59E+03	90.38	1.07E+05	6.01E-02	1.07E+05
3.03E+02	22.26	1.65E+03	8.80E+00	1.64E+03
1.12E+03	63.16	8.27E+03	1.47E-02	8.27E+03
7.94E+02	39.99	5.36E+03	1.62E+00	5.35E+03
4.21E+02	25.82	2.87E+03	8.07E+00	2.86E+03
1.17E+02	13.90	5.46E+02	1.26E-02	5.46E+02
2.20E+02	24.66	1.02E+03	1.15E-02	1.02E+03
2.43E+02	19.94	9.23E+02	3.15E+00	9.20E+02
1.41E+02	18.75	4.86E+02	3.43E+01	4.52E+02
1.18E+03	51.85	4.70E+03	6.63E+00	4.70E+03
1.35E+02	16.69	4.09E+02	3.91E+02	1.87E+01
4.57E+02	33.81	1.32E+03	9.56E+01	1.22E+03
4.75E+01	9.41	1.51E+02	1.34E-02	1.51E+02
3.89E+02	29.70	1.05E+03	6.64E+00	1.05E+03
2.97E+02	24.37	1.50E+03	1.88E-02	1.50E+03
2.24E+02	26.54	5.82E+02	2.63E+00	5.80E+02
3.18E+02	34.14	3.94E+02	2.33E+02	1.61E+02
8.15E+01	14.31	2.88E+02	3.99E+00	2.84E+02
2.03E+03	54.40	6.08E+03	1.42E+00	6.08E+03
1.08E+02	14.84	4.84E+02	1.07E+00	4.83E+02
1.40E+02	17.54	3.69E+02	3.60E+02	9.09E+00
1.66E+02	17.93	2.29E+02	6.92E+01	1.59E+02
9.60E+01	15.22	1.69E+02	2.35E+01	1.46E+02
1.11E+02	17.28	6.70E+01	1.38E+02	-7.10E+01
8.76E+01	14.43	1.13E+02	1.76E+01	9.53E+01
3.85E+01	9.80	8.82E+01	1.00E+00	8.72E+01
1.06E+02	14.72	2.47E+02	4.71E-02	2.47E+02
5.87E+02	43.54	5.45E+02	2.92E+02	2.53E+02
1.76E+02	18.87	2.32E+02	4.19E+01	1.90E+02
6.72E+01	11.73	2.06E+01	9.33E+01	-7.30E+01
1.03E+02	14.31	6.27E+01	8.00E+01	-1.70E+01
4.01E+01	8.37	6.80E+01	3.56E-01	6.76E+01
1.20E+02	14.51	7.13E+01	7.95E+01	-8.20E+00
1.03E+02	12.77	7.22E+01	5.62E+01	1.60E+01

5.12E+01	12.80	8.19E+01	8.04E-02	8.18E+01
5.33E+01	9.94	1.80E+01	5.87E+01	-4.10E+01
3.76E+01	8.24	1.13E+02	7.67E-01	1.12E+02
9.25E+00	5.14	7.36E+00	3.30E+00	4.06E+00
2.05E+02	27.53	5.02E+02	2.58E+00	5.00E+02
4.68E+02	26.90	7.33E+02	1.33E-01	7.33E+02
2.37E+01	8.40	4.17E+01	5.99E-03	4.17E+01
8.47E+01	13.46	2.66E+01	7.83E+01	-5.20E+01
1.48E+02	18.31	2.69E+02	1.31E-01	2.69E+02
1.47E+02	15.57	3.47E+02	8.68E-01	3.46E+02
6.18E+01	9.63	9.15E+01	4.60E+00	8.69E+01
3.96E+01	8.63	3.86E+01	8.62E+00	2.99E+01
2.97E+01	8.84	4.80E+01	4.94E-04	4.80E+01
1.24E+02	16.20	1.67E+02	1.83E+01	1.49E+02
1.57E+01	5.09	2.08E+01	1.02E+00	1.98E+01
5.11E+01	9.94	8.39E+01	5.44E+00	7.85E+01
5.98E+01	10.31	1.62E+01	5.64E+01	-4.00E+01
3.86E+01	9.25	7.03E+00	3.77E+01	-3.10E+01
4.76E+02	29.04	9.62E+01	6.56E+02	-5.60E+02
1.02E+02	16.55	2.31E+02	3.84E-01	2.31E+02
7.52E+01	10.97	1.04E+00	2.01E+02	-2.00E+02
2.49E+01	6.67	9.91E+00	1.53E+01	-5.40E+00
1.79E+01	6.87	2.16E+01	4.09E-01	2.11E+01
6.40E+01	10.99	3.53E+01	2.90E+01	6.24E+00
7.58E+02	41.04	6.57E+02	1.62E+02	4.96E+02
1.05E+02	18.03	9.89E+01	8.78E+01	1.11E+01
3.86E+01	10.70	5.07E+01	1.81E-02	5.07E+01
3.75E+01	9.90	9.20E+00	2.60E+01	-1.70E+01
9.19E+00	4.15	5.66E+00	3.13E+00	2.53E+00
1.91E+01	6.14	5.97E+01	2.60E-02	5.97E+01
1.15E+02	15.38	4.60E+01	6.17E+01	-1.60E+01
1.98E+02	19.94	1.40E+02	5.88E+01	8.11E+01
3.34E+01	7.72	5.54E+01	4.93E-01	5.49E+01
2.47E+01	7.00	3.26E+01	7.72E-03	3.26E+01
3.43E+02	51.87	7.57E+01	2.57E+02	-1.80E+02
5.59E+01	9.77	3.38E+01	1.95E+01	1.43E+01
2.15E+01	6.83	1.94E+01	3.13E+00	1.62E+01
7.82E+02	36.67	1.69E+02	6.04E+02	-4.40E+02
4.16E+01	9.45	2.77E+01	1.07E+01	1.71E+01
4.94E+01	9.88	1.54E+01	2.99E+01	-1.40E+01
3.16E+01	8.44	5.29E+00	2.03E+01	-1.50E+01
3.41E+01	9.94	4.19E+00	2.83E+01	-2.40E+01
3.67E+01	9.91	5.91E+00	2.37E+01	-1.80E+01
7.82E+01	11.52	1.36E+01	5.61E+01	-4.20E+01

6.35E+01	9.96	5.66E+00	6.67E+01	-6.10E+01
9.15E+01	16.11	1.06E+02	4.92E-02	1.06E+02
2.55E+01	6.59	5.31E+01	3.47E-01	5.28E+01
1.04E+02	16.00	2.19E+02	9.46E-01	2.18E+02
5.58E+01	14.45	1.08E+02	6.70E-01	1.07E+02
2.04E+01	5.78	1.20E+01	5.62E+00	6.39E+00
1.25E+02	19.02	6.59E+01	3.61E+01	2.98E+01
1.19E+02	17.95	1.04E+02	8.28E+01	2.09E+01
3.86E+02	25.48	4.38E+02	4.38E-01	4.37E+02
9.29E+02	43.67	1.75E+03	1.36E+00	1.75E+03
8.67E+01	15.92	2.63E+01	4.04E+01	-1.40E+01
1.02E+01	4.25	4.40E+00	3.43E+00	9.68E-01
4.23E+01	7.97	2.30E+01	9.84E+00	1.32E+01
2.15E+01	6.61	7.57E+01	6.29E-02	7.56E+01
1.09E+03	53.56	4.20E+02	3.89E+01	3.81E+02
1.73E+02	17.15	3.13E+01	9.22E+01	-6.10E+01
1.38E+01	5.10	1.67E+00	7.32E+00	-5.70E+00
5.44E+01	9.91	1.11E+02	1.11E+02	1.19E-03
4.37E+01	9.75	2.34E+01	8.92E+00	1.44E+01
7.59E+02	34.52	4.97E+02	3.42E+01	4.63E+02
5.06E+01	9.76	1.43E+01	2.05E+01	-6.20E+00
6.36E+00	3.79	6.18E-01	4.02E+00	-3.40E+00
8.21E+01	11.78	3.61E+01	1.31E+01	2.30E+01
9.60E+02	41.44	3.50E+02	6.14E+01	2.88E+02
3.57E+01	8.13	2.32E+01	4.78E+00	1.84E+01
3.01E+01	6.72	4.47E+00	1.27E+01	-8.20E+00
2.68E+01	7.24	2.08E+01	1.72E+01	3.57E+00
3.09E+01	8.73	6.34E+00	1.13E+01	-4.90E+00
1.72E+01	6.20	2.50E+00	6.97E+00	-4.50E+00
2.45E+01	9.58	3.07E+00	1.05E+01	-7.40E+00
2.01E+01	5.84	1.29E+01	3.15E-01	1.25E+01
1.57E+01	6.41	3.21E+00	5.10E+00	-1.90E+00
4.78E+01	10.19	1.95E+01	3.85E+00	1.57E+01
2.22E+01	6.58	9.52E+00	3.38E+00	6.14E+00
8.06E+01	15.35	6.85E+01	7.19E-01	6.78E+01
3.19E+01	8.41	1.16E+01	5.29E+00	6.31E+00
3.34E+01	8.93	1.81E+01	7.59E-03	1.81E+01
3.33E+01	9.45	1.81E+00	1.30E+01	-1.10E+01
1.23E+01	5.34	5.86E+00	6.34E-01	5.23E+00
8.89E+00	4.54	3.54E+00	5.80E-01	2.96E+00
1.27E+02	16.41	2.55E+01	2.31E+01	2.39E+00
1.25E+01	5.56	9.52E-01	4.02E+00	-3.10E+00
4.21E+01	9.14	1.38E+01	1.26E-01	1.37E+01
1.46E+01	4.94	1.10E+00	3.01E-02	1.07E+00

Shape parameters				
Roundness	**Form Factor**	**Convexity**	**Elongation**	**Solidity**
0.43	0.14	2.13	0.52	0.96
0.73	0.60	1.69	0.08	0.98
0.74	0.35	1.63	0.12	0.95
0.36	0.32	1.24	0.58	0.95
0.59	0.36	2.26	0.26	0.95
0.76	0.41	2.32	0.07	0.96
0.67	0.48	1.44	0.16	0.95
0.46	0.48	1.86	0.45	0.94
0.68	0.33	3.54	0.00	0.93
0.51	0.19	1.49	0.42	0.91
0.56	0.48	1.38	0.41	0.97
0.61	0.74	1.19	0.37	0.98
0.50	0.46	1.13	0.46	0.95
0.68	0.83	1.13	0.30	0.98
0.56	0.63	1.58	0.39	0.98
0.61	0.66	1.95	0.26	0.91
0.40	0.46	1.07	0.55	0.92
0.35	0.22	3.68	0.54	0.89
0.50	0.43	1.13	0.40	0.93
0.74	0.43	1.14	0.09	0.95
0.62	0.49	0.99	0.29	0.93
0.57	0.38	1.65	0.26	0.95
0.64	0.34	1.59	0.08	0.93
0.53	0.33	1.18	0.40	0.93
0.47	0.47	1.25	0.47	0.96
0.53	0.75	1.17	0.43	0.96
0.51	0.50	2.27	0.37	0.93
0.56	0.35	1.43	0.24	0.95
0.39	0.19	4.28	0.39	0.87
0.63	0.36	1.58	0.25	0.93
0.62	0.57	1.06	0.29	0.92
0.62	0.44	1.73	0.19	0.91
0.69	0.60	1.72	0.20	0.95
0.62	0.40	1.70	0.22	0.90
0.66	0.73	1.08	0.11	0.95
0.40	0.60	1.04	0.52	0.93
0.62	0.57	1.80	0.26	0.94
0.68	0.80	1.23	0.14	0.95
0.44	0.65	1.09	0.51	0.96
0.34	0.23	1.15	0.55	0.91
0.66	0.39	1.78	0.01	0.96

0.41	0.43	1.10	0.42	0.86
0.59	0.46	1.31	0.26	0.94
0.51	0.30	1.94	0.30	0.87
0.71	0.42	1.22	0.18	0.92
0.61	0.53	1.22	0.15	0.97
0.64	0.44	1.32	0.22	0.92
0.49	0.67	1.00	0.46	0.95
0.60	0.60	1.22	0.32	0.96
0.76	0.63	1.20	0.11	0.93
0.55	0.49	1.06	0.39	0.95
0.65	0.37	2.21	0.14	0.92
0.56	0.47	1.30	0.34	0.92
0.68	0.33	1.59	0.12	0.95
0.46	0.23	2.37	0.42	0.90
0.69	0.60	1.62	0.07	0.94
0.67	0.51	1.18	0.21	0.91
0.48	0.45	1.12	0.26	0.89
0.65	0.50	1.37	0.25	0.95
0.57	0.59	1.80	0.35	0.96
0.40	0.34	1.86	0.50	0.90
0.43	0.32	1.19	0.36	0.92
0.40	0.57	1.14	0.51	0.97
0.62	0.21	1.52	0.16	0.83
0.58	0.40	2.38	0.21	0.86
0.60	0.67	1.02	0.29	0.96
0.63	0.42	1.71	0.18	0.93
0.67	0.66	1.01	0.15	0.95
0.62	0.36	1.23	0.14	0.85
0.16	0.09	5.99	0.74	0.91
0.63	0.51	1.18	0.12	0.92
0.58	0.78	1.11	0.35	0.97
0.63	0.33	3.99	0.14	0.97
0.59	0.41	1.18	0.27	0.91
0.63	0.40	1.50	0.15	0.92
0.53	0.42	1.30	0.22	0.90
0.44	0.40	1.11	0.50	0.92
0.46	0.26	1.24	0.43	0.91
0.70	0.49	1.91	0.18	0.96
0.72	0.60	1.08	0.16	0.94
0.43	0.50	1.03	0.45	0.89
0.74	0.73	1.31	0.11	0.97
0.51	0.37	2.93	0.35	0.89
0.34	0.38	2.01	0.54	0.86
0.76	0.69	1.11	0.20	0.96

0.44	0.49	1.26	0.47	0.97
0.47	0.43	2.33	0.42	0.93
0.56	0.36	1.46	0.19	0.95
0.59	0.46	1.36	0.35	0.95
0.42	0.29	1.30	0.53	0.94
0.69	0.81	1.33	0.21	0.97
0.78	0.71	1.01	0.09	0.97
0.62	0.75	1.00	0.33	0.95
0.47	0.43	1.58	0.47	0.98
0.73	0.64	1.17	0.19	0.97
0.65	0.76	1.06	0.19	0.95
0.65	0.69	1.41	0.18	0.95
0.57	0.56	1.24	0.33	0.95
0.75	0.62	1.29	0.05	0.97
0.67	0.80	1.01	0.31	0.95
0.56	0.80	1.24	0.36	0.97
0.61	0.39	1.49	0.08	0.87
0.68	0.49	2.04	0.26	0.98
0.65	0.38	1.83	0.22	0.93
0.82	0.63	1.01	0.10	0.95
0.65	0.51	1.26	0.32	0.92
0.51	0.41	0.91	0.30	0.89
0.49	0.36	1.46	0.19	0.85
0.34	0.44	0.98	0.53	0.88
0.66	0.65	0.97	0.22	0.94
0.47	0.57	0.95	0.51	0.93
0.55	0.67	1.13	0.31	0.97
0.63	0.51	1.25	0.33	0.94
0.43	0.47	1.46	0.48	0.91
0.57	0.47	1.31	0.26	0.91
0.52	0.60	1.01	0.35	0.94
0.39	0.58	1.70	0.56	0.97
0.53	0.42	1.32	0.37	0.90
0.54	0.77	1.19	0.38	0.97
0.51	0.40	1.11	0.01	0.88
0.51	0.66	1.03	0.40	0.93
0.58	0.55	1.28	0.22	0.92
0.43	0.14	2.13	0.52	0.96

Amplitude parameters							Hybrid parameter
Sa (µm)	**Sq (µm)**	**Ssk**	**Sku**	**S10z (µm)**	**Sv (µm)**	**Sp (µm)**	**Sdr (%)**
5.32	6131.50	-0.07	1.90	28.61	11.96	17.21	24115.00
5.22	7138.30	-1.50	4.37	33.42	20.94	13.03	4992.00
4.89	6385.30	1.41	3.81	24.99	5.88	19.14	24463.00
4.83	5374.80	-0.07	1.62	18.54	9.20	9.73	9072.60
4.07	4768.80	0.53	2.31	21.86	6.90	15.61	10444.00
3.63	4189.50	-0.55	1.94	18.07	9.29	10.75	11136.00
3.45	4130.80	0.87	2.55	17.61	5.80	12.14	24820.00
3.25	3633.60	0.16	1.68	12.77	5.04	7.94	6906.10
2.75	3387.80	1.15	3.47	16.45	5.31	12.24	11077.00
2.73	3221.50	-0.06	2.27	15.12	7.86	7.35	11045.00
2.56	3161.50	-0.02	2.80	19.63	7.75	12.68	9382.20
2.47	2813.20	0.14	1.93	13.96	6.85	7.61	13086.00
2.47	2887.10	0.07	1.97	14.00	7.41	7.36	6622.90
2.13	2507.80	0.67	3.09	12.61	3.19	10.69	6056.50
2.09	2753.70	1.53	5.34	14.61	2.94	12.82	5805.70
2.06	2544.80	-0.40	2.40	11.72	5.06	7.32	5974.30
2.00	2571.80	1.40	4.37	13.37	3.30	10.68	9930.40
1.94	2451.40	0.32	2.89	15.45	6.86	9.59	9741.70
1.86	2262.00	0.08	2.50	11.15	4.96	6.71	7533.00
1.78	2415.50	1.49	6.11	16.27	3.83	12.65	7900.50
1.75	2159.90	0.22	2.65	10.30	5.97	5.56	3746.80
1.73	1981.70	0.12	2.04	9.55	4.58	5.31	3748.10
1.66	2056.20	0.31	2.60	11.20	5.51	7.78	5209.10
1.56	1896.90	-0.23	2.72	11.31	6.16	6.36	6590.70
1.55	2151.00	0.83	4.26	12.60	4.43	8.29	8726.40
1.51	2014.40	1.45	4.89	10.34	2.61	8.03	3473.70
1.51	1929.80	1.02	3.65	9.32	2.89	6.66	6159.50
1.47	1837.60	0.93	3.94	10.48	3.57	7.87	6569.30
1.41	1777.20	0.11	2.92	11.63	5.77	6.72	4522.30
1.41	1786.40	0.61	3.39	11.45	3.65	8.36	7077.70
1.38	1714.70	0.55	3.16	9.69	3.16	8.34	5460.10
1.37	1740.40	0.08	2.94	9.24	3.63	6.49	2100.70
1.26	1646.60	1.31	4.65	8.68	2.83	6.96	5095.40
1.25	1615.50	0.29	3.36	10.21	4.82	6.45	5097.30
1.25	1565.20	0.51	3.35	9.43	3.80	6.39	2986.00
1.24	1597.60	1.52	6.41	7.59	1.64	9.20	3049.60
1.22	1630.50	0.94	5.11	9.87	3.14	7.80	6407.50

1.22	1592.40	-0.17	2.91	7.25	3.64	4.53	3047.90
1.21	1476.60	0.78	3.13	6.30	3.82	4.00	2580.00
1.21	1588.20	0.72	3.81	9.42	3.26	7.73	4601.20
1.20	1498.60	1.06	3.35	7.60	1.59	6.71	2893.70
1.18	1422.90	0.69	2.93	6.51	1.95	5.55	5528.50
1.17	1471.20	-0.06	3.16	8.47	3.62	5.39	3599.60
1.14	1471.70	0.97	4.36	9.14	2.41	7.72	3696.60
1.12	1416.30	0.62	4.73	11.99	3.44	9.83	4078.10
1.12	1384.70	0.47	2.89	7.25	2.60	4.87	4027.30
1.12	1487.60	0.94	5.20	10.70	4.04	8.26	5427.70
1.11	1395.20	1.13	3.52	5.58	1.62	5.18	1411.70
1.08	1362.30	0.32	3.27	8.31	3.87	5.48	3268.10
1.08	1328.60	0.82	3.87	5.80	1.64	5.61	5386.80
1.07	1448.80	0.61	6.83	11.52	4.85	8.77	5423.50
1.07	1343.20	0.61	3.75	8.50	3.21	6.31	4213.90
1.06	1355.50	-0.70	3.55	7.54	4.33	3.86	3521.00
1.04	1361.60	0.15	3.79	9.59	4.47	5.57	2063.20
1.04	1320.00	0.63	4.62	9.70	2.56	9.33	5095.10
1.01	1290.70	0.18	3.14	6.75	4.10	4.20	2217.00
1.01	1298.70	-0.11	2.93	6.75	3.75	3.41	2278.70
1.01	1307.30	1.45	5.36	5.96	1.39	6.03	4486.40
1.00	1230.70	0.17	2.46	5.72	2.27	3.78	3611.00
0.96	1193.50	0.16	3.24	9.96	4.70	6.28	3711.10
0.96	1179.90	0.67	3.11	7.45	3.33	4.61	1646.90
0.95	1122.90	0.69	3.31	5.95	1.33	6.18	3092.00
0.94	1073.30	-0.32	2.05	4.69	2.61	2.33	2050.10
0.93	1204.60	-0.06	3.22	4.78	3.32	3.75	3986.20
0.93	1138.70	-0.70	2.92	5.71	4.02	3.06	2512.70
0.93	1266.60	0.31	4.54	8.71	3.59	5.60	1614.80
0.92	1200.70	-0.43	3.62	8.16	4.54	4.36	3066.70
0.92	1127.20	0.46	3.66	6.09	2.12	5.31	2793.20
0.91	1156.00	1.19	4.96	6.10	1.44	5.78	2407.70
0.91	1128.90	-0.22	2.95	7.90	3.75	4.55	2982.50
0.90	1141.00	-0.52	3.60	8.01	4.90	4.95	2573.00
0.90	1178.40	0.58	4.37	5.76	2.76	4.09	1429.10
0.89	1111.70	-0.11	2.93	8.04	3.81	5.11	2182.30
0.89	1148.10	0.34	3.21	6.33	3.44	4.11	2427.00
0.89	1145.30	-0.05	3.30	6.57	3.40	3.77	3319.20
0.88	1037.90	-0.79	2.52	4.75	2.73	2.85	2001.90
0.87	1065.70	-0.52	2.75	5.20	2.98	2.74	2977.20
0.86	1043.60	-0.85	2.59	4.49	2.87	2.25	1877.70
0.86	1077.70	-0.39	3.06	6.57	3.02	4.33	2355.80
0.86	1103.00	-0.44	3.83	7.04	3.80	4.02	1560.00
0.85	1087.10	1.40	6.02	6.88	1.18	8.64	2358.40

0.83	1025.10	-0.41	3.03	5.01	3.28	2.91	1785.10
0.83	1076.00	0.39	3.45	6.33	2.85	3.97	1400.00
0.82	1094.90	0.24	4.34	6.72	3.61	4.81	1412.00
0.81	1031.10	-0.34	3.57	5.91	3.37	3.55	3503.80
0.79	1083.50	0.48	5.27	8.60	3.96	6.04	1474.70
0.79	1009.20	-0.31	3.99	8.30	3.51	5.06	3308.80
0.78	980.09	1.14	5.69	8.48	1.17	9.17	2489.40
0.77	946.16	0.49	3.25	7.75	2.55	5.78	887.11
0.76	913.85	-0.12	2.59	5.56	3.06	3.27	2171.70
0.76	986.74	-0.07	3.01	5.00	3.25	2.24	3238.10
0.75	1043.20	1.97	12.97	7.81	1.41	8.59	3240.10
0.75	1047.60	-1.03	5.29	5.93	4.14	3.47	1993.30
0.72	893.49	-0.33	2.94	6.91	3.86	3.46	1767.40
0.71	841.22	-0.32	2.29	4.64	2.50	2.46	1376.40
0.70	851.41	-0.90	2.68	2.56	2.01	1.48	688.45
0.68	822.50	-0.06	2.47	4.59	2.15	3.20	1397.80
0.68	834.11	-0.38	2.70	4.31	2.72	2.36	1740.60
0.68	873.33	1.73	8.06	8.22	0.81	8.38	1707.30
0.66	950.75	1.17	6.39	5.65	1.92	4.38	728.73
0.66	767.17	-0.25	2.03	3.02	1.86	1.79	1657.50
0.66	814.04	-0.10	2.82	4.94	2.49	2.99	1774.90
0.64	794.05	0.25	3.01	6.42	3.46	3.48	1177.20
0.62	791.92	-0.52	3.54	4.50	3.01	2.35	1902.60
0.61	769.88	-1.28	4.15	3.62	2.49	1.35	1184.10
0.60	819.86	-0.87	4.14	4.60	3.08	2.22	2343.60
0.58	742.60	-0.38	3.05	3.85	2.81	2.08	882.62
0.56	690.49	-0.39	2.95	3.58	2.21	2.33	1616.70
0.55	723.21	-0.63	5.20	3.23	2.21	3.32	594.17
0.54	627.75	0.64	2.23	2.28	0.80	1.97	357.22
0.52	701.95	-0.62	3.49	3.35	2.35	1.39	1068.60
0.51	656.37	1.13	4.37	3.87	2.29	3.11	518.45
0.51	678.13	-0.19	4.16	3.60	2.52	2.46	1140.90
0.48	586.05	0.30	2.57	3.01	1.21	2.08	438.75
0.45	639.65	-1.28	5.88	3.73	2.67	2.36	777.51
0.45	527.20	0.69	2.34	1.88	0.54	1.44	293.31
0.44	533.61	-0.93	3.53	2.67	2.21	1.32	355.70
0.42	550.09	1.06	5.21	2.37	0.70	2.55	650.18
0.40	446.70	-0.33	2.19	1.91	1.36	1.31	593.13
0.38	563.18	-0.56	5.64	4.56	2.86	2.23	302.35
0.38	532.44	-1.02	5.21	3.09	2.23	1.39	487.66
0.35	485.76	2.26	9.19	2.80	0.34	3.10	498.18
0.10	164.83	3.04	11.84	0.81	0.10	0.81	69.03

Functional parameters				
Spk (μm)	**Sk (μm)**	**Svk（μm）**	**Smr1 (%)**	**Smr2 (%)**
3.92	15.22	3.84	7.05	77.91
2.80	8.65	18.43	8.05	77.82
14.94	6.07	0.00	32.92	100.00
0.70	14.32	2.97	2.75	82.62
5.78	10.58	0.32	25.06	97.70
1.91	6.84	7.70	5.29	68.91
8.62	6.31	0.85	29.02	95.38
5.25	6.00	0.00	45.64	100.00
7.33	4.44	0.78	30.68	96.49
2.15	9.05	2.49	9.63	93.20
2.94	8.43	2.97	9.25	90.80
2.35	7.05	1.11	19.78	96.99
2.13	7.02	2.09	22.38	93.38
3.21	5.12	0.00	29.06	100.00
5.38	4.25	0.00	25.69	100.00
1.80	6.27	2.85	5.56	81.60
5.85	2.93	0.59	30.38	94.25
3.11	5.11	1.96	18.97	88.54
2.14	5.37	1.96	15.22	89.87
4.82	4.62	0.65	17.47	93.98
2.68	4.49	1.81	20.93	90.40
1.56	5.39	0.86	13.17	95.72
2.43	4.57	1.60	19.72	91.17
1.45	5.44	1.84	5.93	92.19
4.50	3.37	1.98	16.67	82.95
4.57	2.95	0.54	23.26	93.30
3.57	3.55	0.85	21.76	93.48
2.95	3.69	0.73	20.77	94.34
2.07	4.05	1.56	14.93	88.66
2.73	3.40	1.40	21.15	89.52
2.31	4.47	0.79	12.91	94.28
1.75	4.05	1.57	12.67	84.92
3.44	2.69	0.49	22.55	93.53
2.24	3.56	1.45	14.37	89.09
2.12	4.09	0.94	11.35	93.95
3.00	2.19	0.00	32.70	100.00
2.90	3.44	1.03	13.00	87.52

1.77	3.17	2.05	13.98	82.20
2.24	2.66	0.50	26.44	93.05
2.71	3.31	0.99	14.92	86.91
3.05	2.25	0.00	29.36	100.00
1.75	3.38	0.00	19.96	100.00
1.59	3.60	1.64	9.01	88.13
2.64	3.24	0.55	14.65	92.08
2.03	3.72	0.81	9.52	92.67
1.67	3.49	0.55	12.67	91.09
2.63	3.16	1.03	15.12	91.25
2.79	2.21	0.10	25.72	93.61
1.79	3.48	1.11	10.95	92.18
1.73	2.95	0.00	21.56	100.00
2.63	2.48	1.79	9.71	78.82
2.20	3.57	0.84	9.26	94.95
1.02	2.87	1.92	7.75	82.14
1.83	3.17	1.51	11.16	89.84
2.17	3.29	0.77	9.42	89.03
1.63	3.08	1.21	13.49	91.72
1.53	2.71	1.55	10.85	82.16
2.66	2.03	0.00	25.45	100.00
1.17	3.23	0.71	10.87	89.04
1.41	3.25	1.04	9.42	93.51
1.90	2.04	0.69	26.60	90.24
1.62	1.96	0.00	35.60	100.00
0.65	2.34	1.11	3.58	73.12
1.37	2.57	1.38	15.10	87.65
0.81	2.36	1.67	3.85	77.78
1.85	2.30	1.72	15.60	86.34
1.11	2.63	1.71	12.37	87.40
1.41	2.96	0.58	8.85	88.86
1.92	2.05	0.00	27.14	100.00
1.19	2.56	1.24	8.50	83.08
1.12	2.66	1.36	6.45	83.52
2.22	2.60	1.15	10.96	91.58
1.11	2.94	1.10	8.79	90.43
1.54	2.47	1.06	17.01	90.23
1.37	2.69	1.29	10.87	88.78
0.49	1.38	2.12	7.25	67.62
0.76	2.27	1.47	6.87	79.95
0.39	1.50	1.97	9.62	69.31
1.17	2.09	1.47	7.79	76.73
1.04	2.66	1.47	8.57	89.57
2.00	1.76	0.00	28.03	100.00

0.96	2.41	1.25	6.53	86.04
1.61	2.26	1.01	14.54	87.76
1.61	2.27	1.21	12.26	87.06
1.15	2.26	1.36	7.34	82.91
1.70	2.00	1.28	17.26	88.12
1.10	2.21	1.28	7.66	82.71
1.56	2.00	0.00	22.71	100.00
1.21	2.45	0.48	13.27	94.38
0.91	2.38	0.79	5.99	87.63
1.05	1.83	0.99	19.38	81.11
2.64	2.26	0.30	8.67	87.59
0.97	1.85	2.10	12.11	85.68
0.76	2.08	1.01	9.28	84.44
0.51	1.75	0.94	8.67	74.49
0.48	0.95	2.03	7.86	69.19
0.71	2.25	0.63	6.76	89.61
0.49	2.35	0.96	4.69	90.67
1.88	0.60	0.00	48.95	100.00
1.86	1.61	0.95	16.04	87.52
0.29	1.79	0.61	7.13	73.91
0.82	2.09	0.77	7.52	87.97
0.88	2.00	0.60	13.60	92.84
0.72	1.59	1.08	10.19	81.56
0.26	0.99	1.34	6.81	66.10
0.82	1.11	1.48	15.42	76.35
0.68	1.23	0.98	17.40	75.13
0.57	1.12	0.94	15.22	71.66
0.74	1.27	1.18	7.62	79.21
1.06	1.10	0.01	30.41	96.04
0.60	1.30	1.18	16.51	83.67
1.35	0.91	0.34	28.07	93.61
0.84	1.39	0.88	9.94	83.08
0.61	1.71	0.21	9.21	94.59
0.39	1.04	1.27	15.57	84.01
1.10	0.51	0.00	49.11	100.00
0.26	0.84	0.90	7.17	69.89
0.89	1.12	0.10	15.26	80.94
0.27	0.79	0.55	5.40	61.30
0.74	0.67	1.07	21.03	81.38
0.65	0.79	1.38	9.57	85.20
1.10	0.12	0.00	49.78	100.00
0.43	0.04	0.02	29.57	93.44

Spatial parameters					
Sds ($1/\mu m^2$)	**Std (^{o})**	**Scl20 (µm)**	**Str20**	**Scl37 (µm)**	**Str37**
0.1869	144.61	4.31	0.33	3.34	0.44
0.0878	168.19	9.73	0.66	6.40	0.74
0.0217	161.95	4.08	0.85	2.97	0.94
0.0174	78.23	5.01	0.37	3.89	0.42
0.0527	172.74	5.75	0.57	4.26	0.70
0.0958	172.85	4.03	0.81	3.06	0.85
0.0247	167.19	2.36	0.85	1.67	1.00
0.0161	13.17	3.15	0.41	2.41	0.52
0.0176	177.17	2.97	0.52	1.85	0.62
0.0237	42.02	2.64	0.45	1.95	0.50
0.0903	72.44	4.26	0.51	2.97	0.64
0.0339	88.95	2.50	0.56	1.95	0.74
0.0356	37.89	2.78	0.47	2.04	0.58
0.0027	5.20	2.22	0.50	1.48	0.50
0.0285	151.93	3.34	0.75	2.41	0.93
0.0475	8.80	2.50	0.72	1.81	0.81
0.0498	28.46	2.22	0.40	1.53	0.69
0.0724	18.89	2.36	0.14	1.53	0.33
0.0061	23.70	2.22	0.37	1.67	0.53
0.1658	124.55	2.41	0.68	1.11	0.75
0.0016	178.14	3.89	0.87	2.22	0.73
0.0267	159.91	2.64	0.59	1.95	0.64
0.0120	24.57	2.60	0.64	1.67	0.69
0.0075	0.83	2.41	0.72	1.67	0.82
0.0226	123.74	1.95	0.56	1.25	0.60
0.0014	0.72	2.22	0.36	1.11	0.67
0.0085	175.42	1.53	0.46	1.11	0.57
0.0196	166.65	1.81	0.68	0.97	0.70
0.0469	1.46	2.78	0.62	1.30	0.70
0.0370	28.87	2.50	0.56	1.53	0.73
0.0050	9.95	2.22	0.71	1.48	0.80
0.0015	175.31	3.89	0.70	3.06	0.85
0.0029	175.29	1.85	0.48	1.30	0.64
0.0089	29.65	2.22	0.60	0.93	0.83
0.0058	38.04	2.97	0.76	2.04	0.85
0.0033	78.49	1.85	0.33	1.30	0.33
0.0107	3.30	0.97	0.64	0.56	0.80

0.0022	168.00	2.41	0.68	1.67	0.69
0.0011	134.81	1.53	0.61	0.97	0.54
0.0463	42.80	2.64	0.49	1.67	0.57
0.0864	154.34	3.20	0.77	1.67	0.86
0.0051	30.91	1.25	0.82	0.70	0.83
0.0061	4.93	2.04	0.69	0.74	0.67
0.0302	6.82	2.09	0.58	1.53	0.79
0.0284	136.97	1.39	0.63	0.83	0.75
0.0105	84.57	1.53	0.38	0.97	0.58
0.0079	132.03	1.39	0.67	0.70	0.71
0.0004	1.97	3.06	0.65	1.95	0.70
0.0246	159.88	1.81	0.45	1.25	0.56
0.0036	152.54	1.25	0.82	0.56	0.80
0.0102	74.89	1.11	0.53	0.56	0.50
0.0130	6.77	1.67	0.55	0.83	0.55
0.0066	49.02	2.09	0.50	1.39	0.67
0.0329	152.93	3.34	0.60	2.22	0.80
0.0232	167.88	1.11	0.73	0.56	0.80
0.0050	174.72	2.04	0.52	1.30	0.64
0.0031	45.55	1.95	0.74	1.39	0.71
0.0037	154.41	1.53	0.73	0.83	0.75
0.0125	7.41	1.39	0.67	0.70	0.83
0.1818	167.13	1.11	0.73	0.42	0.75
0.0200	7.13	2.36	0.57	1.81	0.62
0.0078	52.65	1.25	0.64	0.70	0.62
0.0067	123.84	1.11	0.23	0.70	0.42
0.0011	52.50	1.11	0.33	0.70	0.71
0.0030	54.27	1.67	0.40	1.25	0.47
0.0076	89.52	2.60	0.56	1.67	0.69
0.0415	170.36	2.22	0.67	1.53	0.85
0.0024	3.21	1.48	0.62	0.74	0.57
0.0049	5.44	1.81	0.72	1.39	0.83
0.0707	149.72	1.53	0.46	0.70	0.62
0.0109	106.84	2.09	0.58	1.53	0.69
0.0003	128.27	1.67	0.43	1.11	0.44
0.1694	2.92	2.09	0.68	1.11	0.89
0.0028	3.22	1.67	0.69	0.74	0.67
0.0090	164.98	0.97	0.78	0.56	0.80
0.0054	2.04	1.81	0.81	1.11	0.80
0.0058	110.57	1.11	0.24	0.70	0.50
0.0057	90.37	1.53	0.24	1.11	0.35
0.0151	157.37	1.11	0.47	0.70	0.71
0.0047	38.87	2.78	0.71	2.22	0.86
0.0071	3.37	1.30	0.58	0.74	0.67

0.0036	168.89	1.11	0.42	0.83	0.46
0.0065	1.26	1.85	0.56	1.30	0.70
0.0008	11.25	2.50	0.75	1.11	0.67
0.0045	161.98	1.11	0.73	0.56	0.67
0.0084	156.42	2.22	0.63	1.11	0.60
0.0251	173.71	0.56	0.67	0.28	0.67
0.0775	2.03	0.83	0.75	0.42	1.00
0.0605	27.60	2.41	0.65	1.30	0.78
0.0158	140.09	0.56	0.44	0.42	0.75
0.0021	170.37	0.97	0.58	0.56	0.80
0.0082	38.68	0.56	0.50	0.42	1.00
0.0037	88.64	1.53	0.55	0.97	0.58
0.2172	132.94	0.83	0.67	0.42	1.00
0.0343	102.20	0.70	0.63	0.42	0.75
0.0008	2.45	2.23	0.75	1.67	0.90
0.0104	170.95	0.83	0.67	0.42	0.75
0.0073	6.76	0.56	0.57	0.42	0.75
0.1572	21.16	1.25	0.82	0.56	1.00
0.0007	2.82	2.50	0.69	1.67	0.75
0.0011	143.61	1.25	0.36	0.70	0.33
0.0153	1.22	0.70	0.71	0.42	1.00
0.1845	123.62	1.25	0.56	0.56	0.67
0.0065	177.45	1.25	0.56	0.70	0.71
0.0053	173.55	1.11	0.36	0.70	0.71
0.0053	18.58	0.70	0.83	0.28	0.67
0.0016	60.69	0.74	0.57	0.37	0.50
0.0030	39.82	1.11	0.80	0.56	0.80
0.0003	140.52	1.39	0.33	0.83	0.75
0.0012	142.34	2.04	0.58	1.48	0.57
0.0029	23.08	1.53	0.65	0.97	0.64
0.0061	100.79	2.22	0.29	1.67	0.46
0.0026	174.46	0.56	0.80	0.42	1.00
0.0047	16.53	2.04	0.38	1.48	0.53
0.0021	89.10	1.67	0.69	1.11	0.60
0.0022	43.64	2.60	0.82	1.85	0.83
0.0017	164.21	2.22	0.35	1.48	0.62
0.0008	167.88	1.11	0.75	0.56	0.75
0.0014	0.00	1.11	0.62	0.70	0.62
0.0017	108.43	0.83	0.50	0.56	0.67
0.0018	119.79	0.70	0.45	0.56	0.57
0.0030	173.15	1.11	0.55	0.56	0.75
0.0016	164.13	0.83	0.75	0.56	0.80

Table B.3 Numerical values of severe OA wear particles.

Shape parameters				
Area (μm^2)	**Length (μm)**	**Material Volume (μm^3)**	**Void Volume (μm^3)**	**Net Volume (μm^3)**
6.57E+02	48.53	4.50E+03	4.95E-02	4.50E+03
2.22E+03	72.25	1.64E+04	1.67E+01	1.64E+04
1.16E+02	14.56	1.88E+02	1.20E+02	6.86E+01
2.32E+02	19.92	1.16E+03	9.43E+00	1.15E+03
1.18E+02	16.46	6.74E+02	8.82E-01	6.73E+02
2.78E+02	19.80	5.05E+01	8.01E+02	-7.50E+02
8.34E+02	42.51	3.34E+02	1.76E+03	-1.40E+03
8.04E+02	36.95	9.27E+02	6.05E+02	3.21E+02
9.39E+01	16.51	3.44E+02	1.75E-01	3.43E+02
3.07E+02	37.50	6.08E+02	2.63E-01	6.07E+02
1.07E+02	16.38	9.40E+01	8.52E+01	8.81E+00
4.48E+01	9.74	3.19E+01	3.81E+01	-6.20E+00
1.40E+02	17.16	8.53E+01	1.46E+02	-6.10E+01
1.09E+02	14.58	2.52E+02	2.30E+01	2.29E+02
1.38E+02	18.95	3.13E+02	7.19E-02	3.13E+02
1.52E+02	20.02	1.09E+02	1.05E+02	3.68E+00
2.81E+02	23.52	1.44E+02	2.69E+02	-1.30E+02
1.89E+02	22.85	1.57E+02	1.05E+02	5.20E+01
1.88E+02	24.72	2.33E+01	4.17E+02	-3.90E+02
2.12E+01	7.20	4.42E+00	2.45E+01	-2.00E+01
1.06E+03	47.57	1.09E+03	3.32E+02	7.63E+02
3.16E+02	28.17	2.19E+02	5.18E+01	1.67E+02
1.25E+02	15.43	3.65E+02	1.60E+00	3.63E+02
3.79E+01	7.57	5.99E+00	4.73E+01	-4.10E+01
1.91E+02	17.19	2.78E+02	1.81E+00	2.76E+02
1.81E+02	21.62	4.47E-03	7.65E+02	-7.60E+02
1.70E+03	74.49	1.21E+03	6.66E+02	5.42E+02
6.62E+01	14.25	6.79E+01	1.14E+01	5.64E+01
4.40E+01	9.48	3.23E+01	1.48E+01	1.75E+01
1.93E+02	27.38	1.32E+02	7.17E+01	5.99E+01
1.10E+02	18.95	4.32E+01	7.26E+01	-2.90E+01
4.79E+01	9.89	9.13E+00	5.27E+01	-4.40E+01
7.47E+01	11.65	1.77E+02	1.59E+00	1.76E+02
7.31E+01	15.73	8.40E+01	1.08E+01	7.32E+01
3.66E+01	10.51	5.17E+01	1.46E+00	5.02E+01

7.41E+01	12.91	1.81E+02	1.80E+02	1.67E+00
1.87E+01	6.41	2.36E+01	6.80E-01	2.29E+01
2.48E+01	7.15	1.21E+01	1.15E+01	6.79E-01
1.07E+03	49.69	1.22E+03	1.69E+02	1.05E+03
4.56E+01	9.28	3.37E+01	1.26E+01	2.11E+01
5.33E+02	32.78	7.22E+02	5.53E+00	7.17E+02
1.59E+02	15.85	1.25E+02	3.49E+01	9.06E+01
5.83E+01	9.63	8.23E+01	1.54E-02	8.23E+01
6.28E+01	11.33	3.35E+01	2.40E+01	9.55E+00
3.23E+01	8.29	6.02E+00	2.34E+01	-1.70E+01
3.06E+01	7.54	8.12E+01	2.96E-03	8.12E+01
2.12E+01	6.54	1.47E+01	5.90E+00	8.80E+00
6.37E+02	41.94	3.31E+02	8.96E+01	2.41E+02
4.22E+01	8.97	5.85E+01	3.86E-03	5.84E+01
1.42E+01	5.30	1.75E+01	9.70E-01	1.65E+01
6.05E+01	11.43	3.49E+01	1.98E+01	1.51E+01
3.05E+01	7.25	9.30E+01	1.57E-01	9.28E+01
7.02E+01	12.26	5.07E+01	2.47E+01	2.60E+01
1.39E+02	16.05	3.52E+01	9.95E+01	-6.40E+01
2.31E+01	6.83	6.79E+01	1.05E-02	6.79E+01
4.50E+01	9.46	1.84E+00	4.20E+01	-4.00E+01
8.72E+02	36.94	8.13E+02	2.04E+00	8.11E+02
5.22E+01	10.32	1.75E+01	2.64E+01	-8.90E+00
7.07E+01	10.56	1.77E+01	4.86E+01	-3.10E+01
1.27E+02	18.01	4.61E+01	7.41E+01	-2.80E+01
7.07E+01	14.82	4.07E+01	2.48E+01	1.60E+01
3.36E+01	7.58	4.45E+01	5.78E-01	4.39E+01
5.36E+01	9.94	2.74E+01	1.85E+01	8.86E+00
1.13E+01	5.51	4.13E+00	5.05E+00	-9.20E-01
2.44E+02	30.76	1.32E+02	8.84E+01	4.41E+01
5.59E+01	14.25	3.68E+01	2.35E+01	1.34E+01
7.58E+01	11.73	2.43E+01	3.86E+01	-1.40E+01
7.22E+01	11.93	2.38E+01	3.77E+01	-1.40E+01
1.24E+02	17.97	1.44E+02	2.10E-02	1.44E+02
1.50E+01	5.72	1.83E+01	6.18E-03	1.83E+01
1.37E+02	19.91	5.87E+01	8.54E+00	5.02E+01
1.32E+02	15.61	2.02E+02	1.81E+00	2.00E+02
1.45E+01	6.04	5.40E+00	5.84E+00	-4.40E-01
5.17E+02	31.61	9.18E+02	9.13E+02	4.56E+00
1.68E+01	6.64	8.20E+00	4.51E+00	3.69E+00

1.22E+01	5.30	1.07E+01	1.19E+00	9.47E+00
1.47E+01	5.77	8.09E+00	3.54E+00	4.54E+00
4.79E+01	8.85	1.01E+02	4.42E-01	1.01E+02
2.62E+01	7.20	1.79E+01	5.71E+00	1.22E+01
1.60E+01	7.44	1.39E+01	1.17E+00	1.27E+01
8.94E+01	15.90	3.94E+01	2.88E+01	1.06E+01
6.90E+01	11.21	6.39E+01	5.67E+01	7.16E+00
3.25E+02	35.58	3.95E+02	1.97E+00	3.93E+02
2.36E+01	9.99	6.88E+00	1.06E+01	-3.70E+00
1.47E+01	5.00	1.66E+01	4.88E-01	1.61E+01
6.89E+01	11.68	8.92E+01	1.99E+00	8.72E+01
1.25E+01	4.96	1.84E+01	8.18E-04	1.84E+01
3.12E+01	8.23	7.31E+01	4.07E-01	7.27E+01
1.14E+02	14.92	1.42E+02	5.55E-01	1.42E+02
1.97E+01	6.26	4.76E+00	8.57E+00	-3.80E+00
1.32E+01	5.62	1.13E+01	5.15E-03	1.13E+01
1.26E+02	16.44	4.23E+01	4.91E+01	-6.80E+00
1.75E+01	5.69	2.37E+01	3.02E-03	2.37E+01
5.09E+01	14.72	1.37E+02	4.52E-02	1.37E+02
2.01E+01	7.49	8.17E+00	5.52E+00	2.65E+00
1.11E+01	4.54	1.16E+01	7.09E-03	1.16E+01
1.13E+02	21.39	5.26E+01	2.71E+01	2.55E+01
1.30E+01	4.91	1.16E+00	8.35E+00	-7.20E+00
3.93E+01	10.96	3.74E+00	2.72E+01	-2.30E+01
8.07E+01	15.86	6.10E+01	7.57E+00	5.34E+01
1.23E+02	16.54	2.37E+01	5.13E+01	-2.80E+01
1.61E+01	5.68	1.56E+01	2.52E-02	1.56E+01
3.22E+01	10.46	7.83E+00	1.04E+01	-2.60E+00
1.34E+01	4.72	2.38E+00	5.64E+00	-3.30E+00
1.53E+01	6.53	5.77E+00	3.52E+00	2.25E+00
3.76E+01	11.51	4.29E+00	1.92E+01	-1.50E+01
1.70E+01	5.96	1.37E+00	9.27E+00	-7.90E+00
1.82E+01	6.56	2.21E+01	1.48E-01	2.20E+01
1.66E+02	19.89	8.26E+01	0.00E+00	8.26E+01
2.36E+01	8.58	1.24E+01	2.74E+00	9.69E+00
1.96E+01	8.36	2.95E+00	6.70E+00	-3.70E+00
1.26E+01	4.46	2.60E+00	2.86E+00	-2.60E-01
1.16E+01	5.80	2.08E+00	2.72E+00	-6.50E-01
9.02E+00	4.72	5.81E+00	7.54E-02	5.73E+00
1.10E+01	4.61	1.77E+00	2.14E+00	-3.70E-01

Shape parameters				
Roundness	**Form Factor**	**Convexity**	**Elongation**	**Solidity**
0.35	0.07	2.76	0.42	0.79
0.52	0.32	4.86	0.26	0.93
0.66	0.29	1.34	0.15	0.92
0.68	0.41	1.38	0.22	0.95
0.55	0.47	1.68	0.36	0.93
0.76	0.55	1.31	0.07	0.97
0.55	0.19	3.27	0.25	0.92
0.64	0.45	1.64	0.18	0.92
0.42	0.63	1.13	0.51	0.92
0.28	0.32	3.86	0.66	0.93
0.50	0.24	2.69	0.41	0.90
0.57	0.42	1.06	0.19	0.93
0.52	0.17	5.66	0.08	0.86
0.63	0.36	2.57	0.07	0.91
0.48	0.25	1.24	0.35	0.92
0.47	0.57	1.38	0.45	0.98
0.60	0.49	1.18	0.30	0.96
0.46	0.22	2.17	0.40	0.90
0.39	0.26	1.84	0.39	0.89
0.52	0.61	1.24	0.35	0.93
0.59	0.27	1.54	0.32	0.97
0.49	0.32	1.95	0.33	0.93
0.56	0.22	2.24	0.06	0.93
0.75	0.56	1.15	0.04	0.93
0.72	0.36	1.73	0.18	0.94
0.49	0.28	1.38	0.39	0.95
0.38	0.41	2.16	0.48	0.97
0.41	0.21	2.69	0.35	0.87
0.61	0.50	1.22	0.28	0.93
0.33	0.16	1.55	0.58	0.86
0.39	0.28	1.81	0.46	0.89
0.62	0.42	3.03	0.16	0.88
0.67	0.56	1.19	0.05	0.93
0.34	0.23	1.57	0.55	0.87
0.42	0.36	1.59	0.54	0.93
0.56	0.74	0.98	0.34	0.95

0.58	0.66	1.25	0.35	0.95
0.59	0.26	1.37	0.14	0.82
0.55	0.46	2.23	0.24	0.91
0.66	0.66	0.95	0.17	0.92
0.59	0.15	4.17	0.26	0.91
0.67	0.56	1.28	0.00	0.96
0.64	0.76	1.15	0.25	0.94
0.57	0.59	3.06	0.15	0.92
0.57	0.38	1.06	0.29	0.91
0.65	0.50	1.83	0.16	0.91
0.61	0.76	1.04	0.35	0.97
0.46	0.46	1.16	0.47	0.96
0.64	0.71	1.02	0.10	0.93
0.54	0.32	0.98	0.19	0.88
0.52	0.25	2.57	0.21	0.88
0.72	0.72	1.28	0.14	0.95
0.59	0.29	1.42	0.17	0.91
0.59	0.24	1.71	0.09	0.92
0.62	0.30	1.33	0.26	0.92
0.63	0.78	1.04	0.35	0.97
0.66	0.33	1.87	0.08	0.94
0.58	0.56	2.36	0.18	0.87
0.66	0.53	1.03	0.04	0.93
0.49	0.31	1.90	0.40	0.88
0.38	0.30	3.86	0.40	0.80
0.67	0.80	1.02	0.23	0.97
0.64	0.68	1.39	0.28	0.96
0.46	0.62	1.13	0.42	0.88
0.32	0.25	4.57	0.56	0.92
0.32	0.23	2.04	0.50	0.80
0.66	0.63	1.12	0.15	0.95
0.63	0.59	1.11	0.32	0.96
0.48	0.26	1.71	0.38	0.82
0.54	0.48	1.31	0.44	0.93
0.44	0.28	1.11	0.43	0.92
0.62	0.54	1.46	0.17	0.95
0.51	0.66	1.92	0.36	0.94
0.55	0.61	1.20	0.21	0.96
0.43	0.48	1.01	0.23	0.79
0.46	0.41	1.27	0.05	0.82

0.55	0.62	1.59	0.28	0.90
0.73	0.87	1.51	0.23	0.98
0.61	0.61	1.07	0.13	0.92
0.36	0.37	2.31	0.45	0.81
0.44	0.53	1.20	0.44	0.90
0.68	0.50	1.46	0.14	0.92
0.32	0.17	1.44	0.58	0.92
0.29	0.36	1.81	0.67	0.90
0.65	0.54	1.41	0.19	0.92
0.61	0.71	1.20	0.38	0.94
0.63	0.82	1.22	0.24	0.97
0.58	0.42	1.08	0.27	0.90
0.65	0.74	1.30	0.27	0.98
0.62	0.59	1.09	0.28	0.90
0.51	0.74	1.10	0.45	0.98
0.55	0.35	1.58	0.28	0.92
0.68	0.86	1.08	0.29	0.98
0.30	0.19	1.29	0.59	0.87
0.44	0.54	1.69	0.42	0.87
0.68	0.82	1.07	0.22	0.97
0.32	0.20	3.48	0.40	0.87
0.66	0.69	1.03	0.20	0.94
0.41	0.30	1.81	0.38	0.92
0.41	0.38	1.14	0.45	0.94
0.57	0.63	3.31	0.22	0.92
0.58	0.81	1.29	0.35	0.98
0.37	0.37	1.00	0.48	0.86
0.74	0.56	1.23	0.09	0.92
0.44	0.50	2.34	0.36	0.91
0.33	0.24	1.83	0.49	0.90
0.60	0.58	0.94	0.25	0.93
0.51	0.52	1.38	0.28	0.91
0.47	0.32	1.39	0.18	0.93
0.40	0.51	1.24	0.44	0.94
0.35	0.35	0.84	0.51	0.75
0.68	0.64	1.26	0.15	0.89
0.43	0.48	0.94	0.49	0.87
0.52	0.64	1.03	0.35	0.93

0.66	0.81	1.03	0.22	0.96

Amplitude parameters							Hybrid parameter
Sa (μm)	**Sq (μm)**	**Ssk**	**Sku**	**S10z (μm)**	**Sv （μm）**	**Sp （μm）**	**Sdr (%)**
3.79	4647.30	0.25	2.58	25.27	10.44	16.41	14560.00
3.68	4337.30	-0.36	2.01	19.78	9.21	10.98	4389.20
2.72	3426.40	0.91	3.36	19.20	6.00	13.68	18598.00
2.69	3204.80	-0.02	2.18	15.48	7.70	8.32	14725.00
2.69	3351.40	0.19	2.53	16.86	7.75	10.54	8120.90
2.43	2979.90	-0.57	2.64	14.96	8.16	7.05	8493.60
2.17	2518.70	0.10	1.98	11.21	4.96	6.26	8237.20
1.99	2659.30	1.13	4.00	15.18	5.77	10.16	3416.10
1.85	2249.90	-0.01	2.46	11.79	5.14	7.75	6510.50
1.71	2329.80	1.86	6.93	15.31	2.77	12.82	9222.10
1.65	2112.60	0.43	2.96	11.72	5.11	7.33	9376.80
1.53	1955.40	0.36	2.89	9.77	4.31	5.86	7085.90
1.53	2005.30	0.52	3.67	12.60	5.00	8.74	10115.00
1.52	1901.30	0.41	3.33	12.87	5.39	8.78	8191.30
1.47	1909.10	1.20	4.97	11.84	2.99	9.95	8778.40
1.43	1854.20	0.32	3.63	12.14	6.43	6.65	5417.60
1.41	1798.60	0.31	3.79	16.02	4.97	13.69	6097.40
1.38	1792.90	0.70	3.51	10.90	4.10	7.21	6624.70
1.32	1741.10	0.55	4.18	11.91	4.45	8.69	4732.80
1.27	1473.10	0.00	2.15	6.08	2.51	4.28	3833.20
1.20	1520.40	0.62	3.90	12.09	3.79	8.56	3915.60
1.20	1452.30	0.09	2.49	8.73	3.97	5.54	5186.10
1.18	1550.00	0.24	3.78	10.88	4.26	8.18	5677.70
1.10	1383.50	-0.26	3.15	7.83	4.42	4.73	5201.70
1.08	1450.70	1.58	6.24	9.39	1.68	8.22	4038.20
1.08	1384.20	0.15	3.35	8.54	4.14	4.57	5150.40
1.08	1392.50	0.59	4.14	11.09	4.14	7.16	987.91
1.06	1356.80	0.98	4.19	7.75	2.30	6.23	5832.30
1.05	1397.20	0.78	4.16	7.98	2.74	5.83	3440.00
1.02	1331.40	0.35	3.65	8.75	3.01	6.52	4201.40
1.02	1408.00	0.67	5.05	10.47	4.19	7.42	4950.00
1.00	1260.80	0.56	4.07	7.77	3.56	5.64	3165.30
1.00	1350.00	-0.10	4.19	8.49	4.02	5.89	1787.70
0.99	1227.70	0.26	2.99	7.06	2.79	4.97	3056.90

0.98	1108.70	-0.04	1.90	4.63	1.93	3.34	2937.10
0.98	1298.10	0.06	3.94	8.91	4.27	5.69	3528.00
0.95	1131.70	0.52	2.80	5.12	1.58	3.76	3496.80
0.95	1194.20	-0.25	3.01	6.40	3.24	4.26	4062.50
0.94	1199.60	0.22	3.50	9.56	4.31	5.84	694.49
0.92	1171.00	-0.20	2.96	5.61	3.09	3.71	1385.70
0.92	1120.60	0.67	3.50	7.96	1.99	7.40	2409.70
0.92	1131.20	0.30	3.16	7.22	2.74	5.05	1943.00
0.92	1170.30	1.08	4.23	6.08	1.42	5.30	3585.90
0.92	1236.80	1.00	5.30	8.74	3.14	6.94	3547.50
0.90	1163.00	-0.49	3.76	7.04	4.00	5.32	4329.50
0.90	1150.40	0.18	3.06	6.17	2.68	4.17	3286.70
0.89	1111.40	-0.11	2.93	5.87	3.34	3.11	2335.10
0.89	1111.00	0.22	3.01	7.41	2.71	4.86	2651.70
0.88	1080.00	0.66	2.81	4.77	1.39	3.79	2374.00
0.88	1052.90	0.04	3.09	4.20	2.69	3.88	3002.60
0.87	1208.70	0.92	5.71	9.10	3.56	6.68	3994.90
0.87	1138.00	-0.67	3.73	4.98	3.71	2.60	1280.30
0.87	1102.40	-0.74	3.06	6.00	3.58	2.68	3471.00
0.86	1103.70	0.17	3.43	7.35	3.04	4.71	3895.70
0.86	1098.50	0.10	3.52	6.27	3.90	4.58	3509.50
0.85	1029.50	-0.80	2.53	4.16	2.86	1.59	1896.50
0.85	1123.50	1.89	8.42	9.53	1.08	9.32	2086.00
0.85	1188.80	0.47	4.46	7.07	2.54	4.87	2405.70
0.85	1113.00	0.29	3.45	6.25	2.83	3.60	3063.30
0.85	1088.10	0.38	3.73	7.83	2.79	5.52	2990.30
0.85	1091.90	-0.09	3.52	7.46	3.60	4.39	2910.90
0.84	990.59	0.04	1.96	3.94	1.56	2.80	2443.30
0.83	1142.80	-0.25	4.71	7.70	3.48	5.92	3432.40
0.81	1043.90	0.76	4.39	4.66	1.82	4.47	2929.00
0.81	1092.20	-0.03	4.30	8.97	3.22	6.80	3590.00
0.81	1018.90	-0.11	3.37	6.54	3.21	4.31	2844.30
0.81	1102.40	0.56	4.61	7.51	2.83	5.55	3461.60
0.80	1118.40	-0.03	4.34	8.16	3.99	5.48	3744.20
0.79	960.00	0.73	3.69	6.40	1.55	5.25	2432.70
0.79	948.92	0.77	4.27	4.63	1.24	5.11	3237.20
0.78	955.89	-0.30	2.80	6.29	2.93	4.03	1805.10
0.78	981.27	0.32	3.49	6.39	2.04	5.23	2382.30
0.77	923.24	0.01	2.59	4.52	2.45	2.79	2445.00
0.77	972.35	0.17	3.18	6.88	2.72	4.27	1698.40

0.77	916.95	-0.06	2.36	4.18	2.51	1.95	2495.80
0.76	922.48	0.11	2.76	4.75	2.54	3.40	2989.60
0.76	955.20	-0.14	3.19	4.96	3.19	3.52	2905.90
0.75	1105.00	1.01	8.68	6.12	3.09	6.20	949.18
0.75	963.64	-0.76	3.41	5.13	2.77	2.72	2814.80
0.75	848.31	-0.04	1.84	2.98	1.71	1.65	1006.20
0.73	923.19	-0.37	3.09	5.77	2.25	4.18	1860.80
0.73	903.63	0.14	3.15	5.84	3.06	3.06	2199.90
0.73	859.11	0.17	2.14	4.53	1.46	3.41	1304.10
0.72	873.28	0.07	2.46	4.28	2.41	2.74	2152.40
0.72	844.53	-0.14	2.03	3.31	1.39	2.08	1505.50
0.72	954.55	0.60	5.05	6.23	2.45	6.06	943.39
0.72	893.55	0.57	4.47	4.20	1.48	4.96	2127.10
0.71	960.08	-0.25	4.16	6.05	3.27	3.24	3143.70
0.70	929.87	1.26	7.19	7.22	2.11	7.88	1812.30
0.70	875.34	-0.73	3.19	4.14	2.99	1.95	1793.80
0.69	891.22	1.60	7.17	4.44	0.86	4.98	2635.50
0.69	885.21	0.50	3.83	6.07	2.16	4.48	1838.80
0.68	814.63	0.18	2.37	3.51	1.37	2.50	1549.60
0.67	912.80	0.17	4.69	6.62	3.03	4.53	2559.60
0.66	846.00	-0.45	2.71	3.73	2.45	2.16	1370.30
0.65	799.06	0.78	3.29	3.58	1.07	3.05	1974.00
0.65	814.60	-0.64	3.31	5.48	3.46	2.75	1569.50
0.64	817.64	-0.57	3.07	3.88	2.46	1.70	1728.60
0.63	801.14	-0.31	3.19	4.96	2.37	3.69	1936.90
0.62	787.77	-0.16	3.50	5.70	3.40	3.24	1388.60
0.61	754.11	-0.46	2.79	4.32	2.67	1.92	1028.50
0.61	759.39	0.75	3.09	3.24	0.99	2.42	1811.10
0.58	771.72	-1.12	4.32	4.18	3.20	1.95	1064.20
0.58	757.13	-0.93	5.11	3.44	3.24	1.67	1048.70
0.57	707.28	-0.78	2.88	3.09	1.79	1.41	1306.40
0.57	770.60	-0.64	3.82	4.46	2.36	2.54	1836.20
0.56	737.31	-0.81	3.45	3.60	2.30	2.00	1769.50
0.55	679.87	0.15	3.32	3.46	1.89	2.28	1363.00
0.54	708.24	1.92	6.99	4.48	0.66	3.96	783.65
0.51	659.38	-0.48	3.58	3.83	2.35	2.01	1171.60
0.48	640.15	-0.38	3.59	3.44	2.48	2.11	1316.90
0.43	602.32	-0.85	4.33	3.19	2.22	1.45	1172.30
0.42	590.42	-1.52	6.16	2.48	2.31	1.09	1096.40
0.42	559.49	-0.92	6.38	2.90	2.86	1.54	747.71
0.36	541.07	-0.31	4.80	2.37	1.76	1.48	766.27

Functional parameters				
Spk (µm)	**Sk (µm)**	**Svk (µm)**	**Smr1 (%)**	**Smr2 (%)**
5.07	12.74	2.43	10.01	92.12
2.14	10.22	4.52	4.72	76.97
6.02	6.15	1.42	24.47	92.19
2.05	9.60	1.91	5.88	92.88
3.45	7.26	2.39	16.99	84.92
1.56	6.42	3.95	7.20	78.67
1.55	7.50	0.82	9.31	96.13
5.77	4.13	1.44	21.44	89.46
1.75	6.21	1.89	8.61	92.06
5.29	2.89	0.28	26.55	96.97
2.96	4.27	1.63	19.11	87.88
2.60	3.87	1.65	19.37	86.62
3.26	4.36	1.73	14.36	89.79
2.54	5.02	1.18	10.16	92.68
3.33	4.31	0.29	16.18	97.27
2.72	4.14	1.77	13.62	90.74
2.73	4.21	1.59	11.04	87.69
2.81	3.81	1.07	17.18	90.14
2.68	3.79	1.53	13.23	88.38
1.80	2.83	1.64	7.98	70.56
2.32	4.01	0.85	10.39	94.00
1.30	4.08	0.90	9.35	92.31
2.13	3.03	1.72	14.94	83.96
1.43	3.45	1.52	6.92	86.77
2.99	2.53	0.00	21.31	100.00
1.72	3.29	1.28	11.09	88.59
2.17	3.21	1.00	12.04	89.78
2.28	3.07	0.28	15.49	92.91
2.30	2.86	0.99	15.84	87.94
1.93	2.87	1.22	12.42	85.22
2.88	2.65	1.38	12.45	85.94
2.08	3.19	0.81	8.15	90.90
1.83	2.64	1.84	13.33	86.22
1.71	3.18	0.78	8.74	89.96
0.66	2.63	0.88	7.29	78.40
1.85	2.67	1.59	11.90	86.01

1.39	2.92	0.00	14.35	100.00
1.18	2.50	1.40	9.12	79.27
1.59	2.82	0.99	11.16	87.27
0.98	2.83	1.35	10.51	86.95
1.46	2.83	0.33	15.53	96.94
1.34	2.64	1.07	15.21	92.50
2.18	2.69	0.00	14.97	100.00
2.27	2.49	0.82	13.68	87.85
1.36	1.68	1.94	11.85	73.61
1.64	2.54	1.11	12.28	87.20
1.35	2.71	1.16	6.81	86.46
1.38	2.90	0.80	8.98	90.58
1.35	2.77	0.00	15.15	100.00
1.62	1.58	1.45	7.58	63.77
2.32	2.29	1.11	13.25	87.92
0.80	2.45	2.00	12.75	88.61
0.75	1.96	1.88	9.53	76.88
1.49	2.47	1.08	10.29	84.82
1.23	2.49	1.12	14.02	89.42
0.26	1.83	1.86	4.14	73.56
2.39	0.95	0.00	41.35	100.00
2.59	1.44	1.53	13.18	71.61
1.67	2.38	1.09	12.44	85.87
1.52	2.56	0.92	12.02	89.37
1.26	2.63	1.33	10.40	89.23
0.73	3.03	0.10	4.67	94.27
1.64	2.05	1.79	10.86	82.58
1.99	2.49	0.48	9.18	87.32
1.60	2.03	1.51	11.57	82.14
1.30	2.15	1.26	8.64	82.74
1.96	1.99	1.18	13.51	82.94
1.67	1.86	1.78	15.37	84.50
1.31	2.33	0.13	16.94	98.69
1.05	2.28	0.00	18.96	100.00
0.98	2.24	1.04	6.71	82.29
1.21	2.35	0.73	11.13	86.95
0.71	2.54	0.75	7.76	90.71
1.17	2.50	0.78	9.73	89.95
0.66	2.33	0.89	13.38	93.99
0.86	2.29	0.75	10.12	88.19

0.84	2.23	1.01	13.51	88.29
2.10	1.67	1.51	12.80	82.04
0.79	1.88	1.75	7.35	82.04
0.27	2.31	0.48	6.57	87.09
1.07	2.23	1.22	5.42	85.01
1.13	2.47	0.79	7.79	92.83
0.81	2.75	0.06	5.02	98.97
0.71	2.24	0.66	14.04	91.38
0.46	1.85	0.84	10.02	75.01
1.45	1.83	0.81	15.99	83.13
0.94	2.33	0.40	11.96	88.98
1.21	1.62	1.30	18.35	83.67
1.65	1.83	0.67	17.75	93.22
0.57	1.70	1.50	8.35	80.61
1.66	0.94	0.00	43.39	100.00
1.37	1.97	0.60	11.70	84.81
0.71	2.27	0.33	8.85	89.82
1.36	1.81	1.29	13.15	88.61
0.62	1.62	1.12	16.34	79.34
1.18	1.95	0.00	15.65	100.00
0.75	1.29	1.35	10.55	74.25
0.52	1.79	1.16	10.30	83.93
0.90	1.70	0.99	8.81	81.32
0.80	1.80	0.94	13.84	89.44
0.53	1.68	0.88	7.68	80.82
1.16	1.95	0.00	13.14	100.00
0.55	1.26	1.65	8.62	80.77
0.36	1.70	0.94	14.14	85.91
0.42	1.33	1.22	5.36	77.19
0.83	1.42	1.49	11.66	84.91
0.61	1.17	1.32	12.49	76.61
1.04	1.54	0.69	7.20	85.23
1.72	0.39	0.08	38.52	90.65
0.75	0.94	0.86	13.56	67.34
0.70	1.13	0.90	14.43	79.40
0.58	0.95	1.19	12.83	81.70
0.35	1.15	1.38	5.66	87.08
0.71	1.11	1.11	10.75	91.63
0.99	0.54	1.14	16.53	80.40

Spatial parameters					
Sds ($1/\mu m^2$)	**Std (^{o})**	**Scl20 (µm)**	**Str20**	**Scl37 (µm)**	**Str37**
0.1498	163.97	5.28	0.72	3.89	0.74
0.0378	165.97	8.90	0.71	5.84	0.81
0.0267	174.95	2.36	0.77	1.39	0.77
0.0544	15.80	3.06	0.58	2.22	0.76
0.0020	177.94	3.34	0.44	2.50	0.47
0.0647	167.00	3.89	0.76	2.78	0.83
0.2021	39.08	3.75	0.55	2.64	0.63
0.0127	1.31	5.28	0.68	3.61	0.72
0.0192	3.98	1.81	0.32	1.39	0.50
0.0691	163.54	1.95	0.27	1.25	0.45
0.0232	164.08	1.67	0.52	0.97	0.58
0.0077	36.33	1.67	0.71	1.11	0.89
0.0306	156.44	1.95	0.70	1.11	0.73
0.0202	33.01	1.11	0.62	0.56	0.80
0.0296	11.79	0.97	0.78	0.42	0.60
0.0332	90.27	1.81	0.35	1.11	0.38
0.0633	24.35	2.09	0.79	1.11	0.73
0.0423	165.87	2.64	0.86	1.39	0.77
0.0135	159.74	2.41	0.68	1.48	0.73
0.0034	142.63	1.53	0.61	0.97	0.78
0.2311	13.36	3.34	0.51	1.67	0.92
0.0702	1.40	2.22	0.64	1.11	0.73
0.0292	174.93	1.67	0.80	0.83	1.00
0.0080	172.59	1.11	0.67	0.56	0.67
0.0427	6.41	2.09	0.58	1.11	0.67
0.0438	96.99	1.95	0.25	1.25	0.60
0.0252	143.36	4.45	0.48	2.50	0.60
0.0150	8.83	1.39	0.77	0.42	0.60
0.0073	165.48	1.53	0.46	0.83	0.75
0.0426	25.45	1.67	0.41	0.97	0.78
0.0252	15.44	1.39	0.42	0.83	0.55
0.0078	174.38	1.39	0.91	0.97	0.87
0.0011	12.50	2.50	0.39	1.11	0.67
0.0154	17.96	1.25	0.37	0.70	0.62
0.0075	156.03	1.95	0.64	1.25	0.69
0.0150	16.10	1.81	0.81	1.25	0.90
0.0033	0.66	0.83	0.75	0.42	0.75

0.0045	149.61	1.95	0.82	1.25	0.82
0.0166	175.88	3.89	0.64	2.50	0.75
0.0007	0.00	2.50	0.64	1.11	0.80
0.1104	4.63	2.09	0.88	0.83	0.86
0.0322	133.04	1.67	0.50	1.11	0.67
0.0118	32.44	1.11	0.67	0.56	0.80
0.0118	175.01	1.81	0.72	0.97	0.87
0.0062	87.25	0.83	0.75	0.42	0.75
0.0050	176.91	1.53	0.50	0.83	0.55
0.0011	133.05	0.56	0.37	0.37	0.50
0.1327	90.60	1.11	0.35	0.56	0.80
0.0080	150.92	1.39	0.53	0.83	0.67
0.0016	38.40	0.70	0.56	0.42	0.75
0.0124	5.73	1.39	0.83	0.70	0.83
0.0005	88.24	2.50	0.45	1.95	0.50
0.0147	162.49	0.70	0.71	0.42	1.00
0.0311	90.91	0.97	0.58	0.42	1.00
0.0044	1.00	2.09	0.88	1.39	0.83
0.0074	3.60	0.70	0.71	0.42	0.75
0.0633	51.37	1.11	0.75	0.56	1.00
0.0110	177.73	1.81	0.59	1.39	0.77
0.0137	0.90	2.09	0.83	1.25	0.82
0.0267	31.35	1.67	0.67	0.83	0.86
0.0150	27.02	1.81	0.87	0.97	0.87
0.0058	30.28	1.25	0.82	0.56	0.67
0.0103	0.00	1.39	0.77	0.70	0.71
0.0022	150.26	0.83	0.50	0.56	0.67
0.0550	77.11	1.39	0.53	0.56	0.67
0.0111	177.08	1.25	0.69	0.56	0.67
0.0170	0.00	1.67	0.80	0.97	0.78
0.0162	120.29	1.53	0.48	0.70	0.56
0.0243	8.44	1.11	0.53	0.56	1.00
0.0025	39.34	0.83	0.55	0.42	0.60
0.0245	11.71	1.11	0.67	0.56	0.67
0.0289	173.38	0.97	0.70	0.42	0.75
0.0031	0.61	1.11	0.53	0.70	0.63
0.0978	100.81	1.53	0.69	0.83	0.75
0.0024	25.04	0.97	0.47	0.56	0.80
0.0022	160.61	0.70	0.56	0.42	0.60
0.0025	178.09	0.70	0.56	0.42	0.75
0.0005	148.52	0.83	0.50	0.56	0.67

0.0047	113.41	1.11	0.36	0.42	0.43
0.0022	154.89	1.67	0.55	1.11	0.62
0.0191	37.58	0.97	0.58	0.56	0.67
0.0136	11.62	1.67	0.80	0.83	0.86
0.0567	65.25	0.83	0.55	0.56	0.67
0.0042	40.62	0.70	0.83	0.42	1.00
0.0021	30.32	1.39	0.45	0.97	0.87
0.0009	115.51	0.83	0.60	0.56	1.00
0.0021	7.36	1.25	0.60	0.83	0.67
0.0063	57.64	1.53	0.46	0.83	0.43
0.0247	176.23	1.25	0.53	0.83	0.86
0.0037	22.51	1.67	0.75	1.11	0.80
0.0023	90.59	0.83	0.60	0.42	0.60
0.0245	144.06	1.39	0.48	0.83	0.60
0.0028	3.62	0.56	0.36	0.42	0.50
0.0104	73.78	1.39	0.50	0.83	0.50
0.0012	67.90	1.11	0.32	0.56	0.50
0.0018	31.41	0.70	0.71	0.42	0.75
0.0217	155.45	1.39	0.56	0.56	1.00
0.0024	88.26	1.25	0.64	0.83	0.60
0.0072	93.05	0.83	0.55	0.42	0.75
0.0163	65.95	1.81	0.43	1.25	0.47
0.0214	111.39	1.11	0.30	0.70	0.50
0.0024	168.47	1.25	0.50	0.56	0.67
0.0045	44.32	1.67	0.48	1.25	0.64
0.0013	39.96	1.67	0.57	1.11	0.62
0.0026	168.95	0.97	0.44	0.56	0.57
0.0083	124.29	0.83	0.46	0.42	0.50
0.0030	5.80	0.83	0.60	0.28	0.50
0.0022	5.63	0.97	0.64	0.42	0.75
0.0098	92.85	1.85	0.56	0.74	0.57
0.0038	107.16	0.97	0.39	0.56	0.67
0.0034	10.97	0.70	0.50	0.42	0.75
0.0022	175.38	0.70	0.71	0.42	0.60
0.0018	1.96	1.39	0.45	0.83	0.67
0.0018	91.01	1.25	0.50	0.83	0.50
0.0012	9.56	0.42	0.60	0.28	0.67

Table B.4 Numerical values of OA wear particles found in a patient without OA classification.

Shape parameters				
Area (μm^2)	**Length (µm)**	**Material Volume (μm^3)**	**Void Volume (μm^3)**	**Net Volume (μm^3)**
4.83E+02	27.92	3.11E+03	3.10E+03	8.42E+00
2.20E+02	24.39	1.01E+03	2.37E+01	9.86E+02
6.69E+02	43.65	1.61E+03	1.37E+03	2.35E+02
3.06E+02	30.87	1.93E+02	-3.80E+02	5.71E+02
6.05E+02	44.61	1.95E+03	1.94E+03	9.54E+00
8.20E+01	15.40	3.15E+02	7.56E-02	3.15E+02
3.49E+02	40.88	6.46E+02	6.02E+02	4.36E+01
4.60E+02	41.27	1.01E+03	1.01E+03	1.00E-01
1.57E+01	5.71	1.62E+01	5.29E+00	1.09E+01
2.79E+01	7.03	6.85E+01	6.84E+01	1.05E-01
2.09E+01	6.37	3.15E+01	2.87E+01	2.85E+00
2.03E+02	19.67	6.45E+01	-9.50E+01	1.60E+02
2.25E+01	7.06	6.00E+00	-1.30E+01	1.87E+01
2.74E+02	24.88	1.15E+02	-7.30E+01	1.88E+02
3.55E+01	8.87	1.77E+01	-4.80E-01	1.81E+01
8.04E+02	42.79	4.37E+02	1.07E+02	3.30E+02
6.15E+01	12.49	5.27E+01	1.58E+01	3.70E+01
4.39E+02	41.73	4.40E+02	3.62E+02	7.72E+01
6.16E+01	11.59	1.49E+02	1.48E+02	4.65E-01
2.39E+02	31.68	8.76E+01	-4.50E+01	1.33E+02
4.61E+01	9.94	3.18E+01	1.17E+01	2.01E+01
2.76E+01	7.66	8.62E+00	1.65E+01	-7.80E+00
7.04E+01	14.09	1.08E+01	-4.80E+01	5.85E+01
2.07E+01	6.34	8.40E+00	-4.10E-01	8.81E+00
4.84E+01	9.46	1.23E+01	2.79E+01	-1.60E+01
1.98E+01	5.93	3.06E+00	1.28E+01	-9.70E+00
2.81E+01	8.43	1.85E+01	5.04E+00	1.34E+01
2.20E+01	7.21	3.26E+01	6.56E-01	3.19E+01
8.27E+01	15.31	2.43E+01	-1.30E+01	3.78E+01
3.04E+01	8.87	8.67E+00	-4.10E+00	1.27E+01
1.38E+01	4.68	2.14E+00	7.84E+00	-5.70E+00
1.42E+02	17.18	4.39E+01	-1.30E+01	5.73E+01
4.13E+01	10.26	3.85E+00	-2.90E+01	3.31E+01
5.91E+01	14.64	5.64E+01	5.19E+01	4.52E+00
7.30E+01	10.86	2.03E+01	2.69E+01	-6.60E+00
1.23E+02	21.69	8.95E+01	8.20E+01	7.57E+00

4.17E+01	12.37	1.73E+01	9.96E+00	7.33E+00
9.35E+00	4.39	1.14E+01	1.23E-01	1.13E+01
1.85E+01	5.46	6.25E+00	5.37E+00	8.81E-01
4.00E+01	9.66	1.70E+01	7.84E+00	9.20E+00
2.24E+01	7.17	3.63E+01	3.47E-01	3.60E+01
1.35E+01	4.89	1.09E+01	6.66E-01	1.03E+01
3.23E+01	8.20	2.63E+01	2.35E+01	2.85E+00
3.84E+01	9.89	8.29E-01	-2.50E+01	2.54E+01
6.78E+01	14.97	2.60E+01	1.15E+01	1.45E+01
4.49E+01	14.41	5.66E+01	5.54E+01	1.21E+00
1.08E+01	4.91	7.86E+00	7.33E+00	5.29E-01
1.83E+01	7.73	4.32E+00	4.96E+00	-6.40E-01
2.80E+01	7.41	1.19E+01	3.96E+00	7.94E+00
1.58E+01	5.04	6.84E+00	2.21E+00	4.63E+00
8.12E+01	13.74	1.31E+01	2.47E+01	-1.20E+01
3.13E+01	10.88	1.07E+01	4.35E+00	6.34E+00
3.80E+01	7.36	4.03E+00	1.14E+01	-7.40E+00
4.31E+01	10.66	1.75E+00	2.34E+01	-2.20E+01
8.27E+01	11.65	1.66E+01	1.08E+01	5.78E+00
3.86E+01	8.22	3.31E+00	7.26E+00	-4.00E+00

Shape parameters				
Roundness	**Form Factor**	**Convexity**	**Elongation**	**Solidity**
0.66	0.44	2.64	0.15	0.96
0.46	0.57	1.01	0.50	0.96
0.43	0.37	1.45	0.44	0.92
0.40	0.22	2.67	0.44	0.87
0.39	0.29	2.40	0.35	0.93
0.44	0.58	1.14	0.52	0.96
0.26	0.23	3.22	0.58	0.94
0.34	0.18	2.78	0.46	0.86
0.61	0.63	1.09	0.23	0.92
0.68	0.41	1.39	0.10	0.88
0.66	0.64	1.35	0.22	0.92
0.66	0.52	1.19	0.15	0.94
0.57	0.59	1.10	0.36	0.94
0.52	0.42	1.97	0.26	0.90
0.57	0.61	1.14	0.29	0.94
0.49	0.49	1.49	0.28	0.91
0.49	0.37	1.57	0.29	0.93
0.30	0.15	16.11	0.28	0.70

0.52	0.24	1.70	0.02	0.87
0.29	0.18	6.57	0.50	0.84
0.51	0.50	1.18	0.19	0.89
0.60	0.47	1.50	0.17	0.90
0.45	0.37	1.46	0.41	0.93
0.63	0.69	1.05	0.30	0.96
0.59	0.46	3.49	0.03	0.85
0.66	0.76	1.22	0.17	0.93
0.46	0.49	1.86	0.39	0.83
0.51	0.53	0.94	0.26	0.95
0.44	0.21	1.68	0.25	0.83
0.43	0.19	1.30	0.28	0.78
0.71	0.68	1.17	0.14	0.95
0.56	0.46	0.95	0.19	0.95
0.49	0.25	1.82	0.29	0.84
0.34	0.33	1.22	0.48	0.73
0.75	0.81	1.18	0.15	0.96
0.31	0.13	3.34	0.41	0.80
0.35	0.50	1.16	0.58	0.96
0.60	0.58	0.88	0.18	0.92
0.76	0.88	1.11	0.21	0.98
0.48	0.28	1.81	0.15	0.86
0.54	0.70	1.00	0.39	0.94
0.72	0.78	1.01	0.25	0.97
0.60	0.65	1.22	0.22	0.91
0.48	0.52	1.60	0.41	0.94
0.38	0.31	1.48	0.40	0.81
0.27	0.22	4.20	0.53	0.64
0.55	0.49	1.26	0.27	0.89
0.39	0.58	1.06	0.58	0.96
0.64	0.56	1.47	0.20	0.94
0.79	0.91	1.02	0.16	0.98
0.51	0.27	2.53	0.26	0.77
0.34	0.25	2.28	0.60	0.81
0.86	0.87	1.08	0.05	0.97
0.47	0.62	0.97	0.41	0.91
0.75	0.55	2.16	0.11	0.93
0.69	0.41	1.96	0.11	0.93

Aμplitude parameters							Hybrid parameter
Sa (μm)	**Sμ(μm)**	**Ssk**	**Sku**	**S10z（μm）**	**Sv (μm)**	**Sp (μm)**	**Sdr (%)**
4.04	4527.80	-0.19	1.74	19.92	8.70	12.08	6717.60
2.99	3518.10	-0.07	1.94	13.84	5.75	8.54	5752.00
2.49	3134.10	-0.37	2.79	17.22	8.98	9.56	6838.70
2.42	2823.60	-0.02	2.13	13.86	6.02	8.31	4878.20
1.67	2195.20	0.82	3.50	12.29	4.15	8.25	4820.20
1.65	2081.00	0.57	2.99	10.41	3.92	6.93	4405.00
1.44	1962.20	0.96	4.33	12.01	4.77	7.55	4431.00
1.36	1771.60	1.05	5.46	12.91	3.32	10.77	3528.60
1.29	1632.60	0.41	3.09	7.88	3.71	5.38	5580.50
1.15	1490.90	0.92	3.93	7.94	3.11	5.98	3547.30
1.13	1429.70	-0.10	2.90	7.12	3.67	3.78	2641.40
1.09	1394.90	-0.02	3.38	9.74	3.94	7.14	2711.60
1.06	1286.30	-0.01	2.65	6.26	2.76	4.12	3056.90
1.05	1375.30	0.52	3.85	9.76	4.24	6.52	2879.80
0.99	1223.20	-0.58	2.68	5.70	3.39	2.68	2370.30
0.95	1204.20	0.46	3.82	8.73	2.60	6.57	1634.60
0.94	1113.40	-0.43	2.49	6.08	2.70	3.77	1394.70
0.94	1225.50	0.62	5.43	10.60	3.08	8.31	2131.40
0.93	1169.30	-0.19	2.92	6.77	3.35	3.86	2145.30
0.93	1147.10	-0.08	3.05	7.66	2.92	5.27	2666.70
0.90	1021.00	-0.03	2.03	4.77	2.56	3.20	1561.90
0.88	1101.40	0.05	3.12	5.64	2.84	5.09	2313.90
0.88	1139.20	-0.53	3.61	7.12	3.92	3.72	2222.70
0.83	1009.50	0.38	2.32	3.99	1.50	2.70	2153.00
0.81	1036.30	-0.16	2.96	5.37	2.50	3.19	2610.00
0.75	972.74	-0.64	3.69	5.24	3.53	2.87	1619.30
0.74	860.06	-0.24	2.14	3.73	1.95	1.96	1481.50
0.73	933.39	-0.60	3.10	4.43	2.30	2.58	1818.10
0.73	922.78	0.68	3.80	5.60	1.74	5.16	1916.30
0.72	934.06	-0.91	3.72	4.65	3.31	1.74	1651.80
0.71	879.27	-0.58	2.85	4.02	2.76	1.68	974.79
0.69	1000.40	-0.88	4.91	6.94	4.01	3.64	1255.40
0.67	869.51	-0.33	3.51	5.14	2.89	2.65	1588.60
0.67	872.73	-0.05	3.42	5.22	2.50	3.29	1295.60
0.66	865.64	-0.38	3.93	5.44	2.43	3.17	1669.30
0.65	783.18	0.63	2.80	3.89	0.96	3.30	1035.00
0.64	799.85	0.05	2.71	4.16	2.37	2.54	1244.40
0.63	777.18	-0.08	2.38	3.02	1.46	2.07	1151.90

0.62	774.56	-0.23	2.65	3.64	2.36	1.64	1044.90
0.61	811.23	-0.81	4.07	4.62	2.77	2.16	1450.60
0.61	791.27	-1.00	3.62	4.16	2.46	2.55	1072.10
0.60	793.41	-0.88	4.08	3.85	3.15	2.14	1443.20
0.60	777.22	-0.39	3.76	4.60	2.79	2.73	1153.00
0.59	805.44	-1.55	4.78	3.75	2.96	1.16	1016.30
0.58	780.33	-0.16	4.24	5.30	2.64	3.79	1361.80
0.56	715.65	-0.60	3.58	4.06	2.20	2.60	1111.60
0.55	680.66	-0.09	3.26	3.42	1.50	2.60	1326.30
0.51	694.40	-0.74	3.76	3.64	2.25	1.64	1023.30
0.50	703.58	-0.49	4.75	4.07	2.95	2.08	757.80
0.48	658.71	-1.16	5.07	2.88	2.62	1.51	756.71
0.47	615.89	0.46	3.58	3.62	1.82	2.02	764.37
0.46	576.24	-0.59	4.78	3.92	2.70	1.86	629.36
0.39	487.40	0.03	3.12	2.70	1.59	1.46	426.07
0.33	512.69	-0.43	6.76	3.61	2.64	1.82	574.61
0.31	438.23	-0.78	4.65	2.88	2.09	1.51	283.68
0.27	395.48	-0.69	4.13	2.38	1.47	1.13	288.84

Functional parameters				
Spk (µm)	**Sk (µm)**	**Svk (µm)**	**Smr1 (%)**	**Smr2 (%)**
2.64	9.41	4.73	5.01	67.12
2.51	7.83	2.62	10.58	72.74
2.53	7.51	4.13	8.15	85.31
2.19	7.40	1.98	6.67	86.43
4.09	3.46	1.54	22.59	85.14
3.45	3.34	1.76	25.61	87.60
3.99	3.69	1.46	15.90	89.36
3.04	4.29	0.64	12.04	93.57
2.09	3.69	1.15	15.48	89.77
2.41	3.26	0.74	17.93	94.85
1.39	3.34	1.75	10.88	88.84
1.94	2.54	1.77	10.91	76.72
1.57	2.79	1.14	8.20	77.14
2.10	3.06	1.13	14.26	90.16
0.75	2.16	1.88	11.41	74.10
1.67	3.03	0.73	10.01	89.12
0.78	1.70	1.76	9.34	66.29
2.11	2.80	1.00	8.90	86.20
1.15	2.52	1.23	9.71	80.44
1.29	2.66	1.17	8.12	83.23
0.75	2.56	0.69	5.64	80.90
1.18	2.86	0.91	8.59	88.11

1.08	2.45	1.54	8.99	83.69
1.12	2.74	0.05	11.26	93.15
1.21	2.06	1.21	12.05	80.74
0.90	1.86	1.61	10.53	82.42
0.52	1.68	0.97	10.55	71.61
0.73	2.05	1.56	7.06	84.13
1.46	2.24	0.33	11.67	89.97
0.46	1.74	1.59	11.16	79.54
0.80	1.79	1.30	6.16	79.25
1.17	1.48	2.13	11.79	82.40
0.94	1.81	1.13	10.53	83.38
1.10	1.74	1.02	12.85	84.22
0.99	1.67	1.37	9.02	82.62
1.07	1.75	0.00	21.68	100.00
0.73	1.82	0.62	15.90	85.59
0.88	1.91	0.67	6.27	84.29
0.52	1.83	0.74	11.45	85.48
0.76	1.51	1.54	9.60	83.98
0.54	1.32	1.71	5.96	79.66
0.63	1.26	1.40	13.04	77.94
0.72	1.70	1.08	11.05	86.34
0.27	1.04	2.04	6.85	78.08
0.95	1.37	1.14	16.97	83.57
0.59	1.40	1.10	8.82	81.13
0.91	1.39	0.97	6.20	79.97
0.75	1.04	1.28	11.43	77.29
0.90	1.15	1.42	16.86	87.57
0.40	1.24	1.47	11.71	87.02
1.34	0.71	0.81	14.04	66.73
0.78	1.19	0.83	4.67	82.74
0.66	1.08	0.37	8.74	80.16
0.92	0.50	0.87	19.96	80.52
0.54	0.66	0.89	12.39	81.57
0.62	0.43	0.89	16.37	80.23

Spatial parameters					
Sds ($1/\mu m^2$)	**Std (°)**	**Scl20 (nm)**	**Str20**	**Scl37 (nm)**	**Str37**
0.0355	177.35	5.00	0.73	3.71	0.77
0.0127	128.66	2.97	0.37	2.41	0.62

0.0531	174.11	3.71	0.41	2.78	0.48
0.0227	11.60	3.89	0.42	2.78	0.60
0.0455	174.65	4.26	0.79	2.60	0.78
0.0059	107.97	2.41	0.36	1.85	0.63
0.0265	168.67	3.15	0.81	1.85	0.83
0.0353	168.17	3.52	0.73	2.22	0.75
0.0011	25.97	2.22	0.75	1.48	0.73
0.0016	1.54	2.04	0.73	1.30	0.78
0.0012	1.28	2.41	0.76	1.48	0.73
0.0163	172.22	2.22	0.80	1.48	0.89
0.0013	93.74	1.67	0.35	0.93	0.42
0.0206	0.62	2.41	0.72	1.11	0.75
0.0030	88.68	1.85	0.37	1.11	0.50
0.0498	12.06	2.41	0.45	1.11	0.67
0.0032	163.29	2.04	0.37	1.48	0.53
0.0329	7.01	1.30	0.70	0.74	0.80
0.0041	87.62	2.04	0.48	1.30	0.70
0.0182	175.05	0.93	0.83	0.37	0.67
0.0033	19.22	2.41	0.72	1.48	0.89
0.0017	19.50	0.74	0.50	0.56	1.00
0.0051	152.51	1.11	0.75	0.56	0.75
0.0012	97.27	1.48	0.47	0.93	0.63
0.0041	2.09	0.74	0.67	0.37	0.67
0.0013	30.58	1.48	0.57	0.74	0.57
0.0013	65.44	0.93	0.56	0.56	0.60
0.0016	89.92	1.85	0.50	1.11	0.55
0.0061	170.13	0.93	0.71	0.56	1.00
0.0019	56.43	1.67	0.26	1.11	0.67
0.0009	144.40	1.85	0.45	1.30	0.54
0.0112	90.25	2.04	0.26	1.48	0.40
0.0024	133.42	0.74	0.40	0.56	0.75
0.0034	16.56	1.30	0.58	0.74	0.80
0.0056	162.48	0.93	0.71	0.37	0.67
0.0076	99.96	1.48	0.67	0.56	0.60
0.0027	115.09	0.56	0.25	0.37	0.67
0.0005	85.50	1.67	0.56	1.11	0.55
0.0012	159.95	0.93	0.71	0.56	0.75
0.0027	156.53	0.74	0.67	0.37	1.00
0.0017	0.00	2.04	0.69	1.48	0.67
0.0012	154.56	1.85	0.53	1.11	0.67
0.0020	84.77	0.56	0.23	0.37	1.00
0.0021	1.49	1.67	0.26	1.30	0.41
0.0040	7.58	0.74	0.67	0.37	1.00
0.0026	0.00	0.74	0.67	0.37	1.00

0.0008	90.00	1.85	0.63	1.11	0.67
0.0009	138.12	0.56	0.50	0.37	0.67
0.0016	24.88	1.30	0.64	0.74	0.57
0.0010	142.00	1.48	0.42	1.11	0.67
0.0060	36.97	0.56	0.75	0.37	1.00
0.0021	0.00	1.48	0.73	0.93	0.83
0.0023	132.26	0.93	0.42	0.56	0.75
0.0021	26.44	0.56	0.75	0.37	1.00
0.0050	67.53	1.30	0.33	0.74	0.57
0.0016	170.67	0.74	0.80	0.37	0.67